Universität Ulm

Abteilungen Angewandte Physiologie und Neurologie

Abteilungsleiter: Prof. Dr. F. Lehmann-Horn

Prof. Dr. A. C. Ludolph

Functional Characterization of Voltage-gated Sodium Channels associated with human Idiopathic Epilepsies

Dissertation Zur Erlangung des Doktorgrades der Humanbiologie der Medizinischen Fakultät der Universität Ulm

Vorgelegt von:

Yunxiang Liao

aus

Guilin, V.R.China

Ulm, 2009

Amtierender Dekan: Prof. Dr. Klaus-Michael Debatin

1. Berichterstatter: Prof. Dr. Holger Lerche

2. Berichterstatter: Prof. Dr. Harald Bode

Tag der Promotion:

26. Juni 2009

TABLE OF CONTENTS

1. INTRODUCTION 1

1.1. VOLTAGE-GATED SODIUM CHANNELS 1
1.1.1. Diversity of voltage-gated sodium channel α subunits 3
1.1.2. Function of voltage-gated sodium channels in the brain 4
1.1.3. The auxiliary β subunits 6
1.2. IDIOPATHIC EPILEPSY 8
1.2.1. Generalized epilepsy with febrile seizures plus 8
1.2.2. Benign familial neonatal-infantile seizures 9
1.3. FEATURES OF CORTICAL NEURONS 9
1.4. AIMS 10

2. MATERIALS AND METHODS 12

2.1. MOLECULAR AND CELL BIOLOGY METHODS 12
2.1.1. Mutagenesis 12
2.1.2. Cell culture and transfection 12
2.1.2.1. Subcultivating and maintainance of tsA-201 cell line 12
2.1.2.2. Cryopreservation 13
2.1.2.3. Transient cell transfection 14
2.1.2.4. Primary mouse neuronal culture 15
2.2. ELECTROPHYSIOLOGY 16
2.2.1. Patch-clamp technique 16
2.2.1.1. Setup 16
2.2.1.2. Experimental procedure 17
2.2.1.3. Glass electrodes 21
2.2.1.4. Ag/AgCl electrodes 21
2.2.1.5. Whole cell measurements from tsA-201 cells 22
2.2.1.6. Current clamp recordings in primary cultured neurons 22
2.2.2. Reagents and solutions 23
2.2.3. Voltage-clamp protocols and data analysis 23
2.2.3.1. Voltage dependence of activation 23
2.2.3.2. Steady state fast inactivation 24
2.2.3.3. Inactivation time constants and persistent current 24
2.2.3.4. Recovery from fast inactivation 25
2.2.3.5. Steady state slow inactivation 25
2.2.3.6. Entry into slow inactivation 26
2.2.3.7. Recovery from slow inactivation 26
2.2.3.8. Subtraction of leak and capacitive currents 26
2.2.4. Statistics 26
2.3. IMMUNOCYTOCHEMISTRY 26

3. FUNCTIONAL MODIFICATION OF $Na_V1.1$ CHANNEL BY ß1 AND ß2 SUBUNITS AND FUNCTIONAL CHARACTERIZATION OF THE $GEFS^+$ ASSOCIATED MUTATION R1648H 28

3.1. B SUBUNITS MODIFY THE GATING OF THE $Na_V1.1$ WT CHANNEL 28
3.2. FUNCTIONAL DEFECTS CAUSED BY THE R1648H MUTATION 30
3.3. CO-EXPRESSION OF B SUBUNITS REFINES THE EFFECTS OF R1648H MUTATION ON $Na_V1.1$ CHANNEL GATING 33

4. THREE NOVEL MUTATIONS IN *SCN2A* ASSOCIATED WITH BFNIS 37

4.1. ALTERNATIVE SPLICING OF $Na_V1.2$ 40
4.2. FUNCTIONAL CHARACTERIZATION OF MUTATION M252V 42
4.3. FUNCTIONAL DETERMINATION OF MUTATION V261M 44
4.4. ELECTROPHYSIOLOGICAL PROPERTIES OF A263V MUTANT CHANNEL 47

5. MORPHOLOGICAL, ELECTROPHYSIOLOGICAL AND IMMUNOCYTOCHEMICAL IDENTIFICATION OF PRIMARY CULTURED RAT CORTICAL NEURONS 52

5.1. MORPHOLOGICAL DIVERSITY OF MEASURED CORTICAL NEURONS 53
5.2. IMMUNOCYTOCHEMICAL IDENTIFICATION OF CORTICAL NEURONS 54
5.3. ELECTROPHYSIOLOGICAL PROPERTIES OF CULTURED CORTICAL NEURONS 54

6. DISCUSSION 59

6.1. FUNCTIONAL CONSEQUENCES OF A GEFS+ CAUSING *SCN1A* MUTATION 59
6.2. DIFFERENTIAL MODULATING EFFECTS OF B SUBUNITS ON *SCN1A* WT AND R1648H MUTANT CHANNEL FUNCTION 60
6.2.1. Modulation of SCN1A WT channel gating by β subunits 61
6.2.2. Attenuation of α-β1 interaction by the R1648H mutation 61
6.2.3. The β2 subunit modulates R1648H channel functions 62
6.2.4. Co-expression of both β1 and β2 subunits partially repair defects caused by the R1648H mutation 62
6.3. COMPARISON OF NEONATAL AND ADULT SPLICE VARIANTS OF $Na_V1.2$ CHANNELS 63
6.4. FUNCTIONAL CONSEQUENCES OF THREE NOVEL BFNIS MUTATIONS IN *SCN2A* 64
6.4.1. The mutants in domain I S5 affect sodium channel inactivation 64
6.4.2. All mutations predict an increase in neuronal excitability 66
6.4.3. Remission of seizures during development 66
6.5. CLASSIFICATION OF CORTICAL NEURONS 68

SUMMARY 70

REFERENCES 72

INDEX OF FIGURES

Figure 1.1: Molecular structure of voltage-gated sodium channels. 2
Figure 1.2: A phylogenetic tree of rat voltage-gated sodium channel α subunits. 3
Figure 1.3: The three main conformational states of voltage-gated sodium channels. 5
Figure 1.4: Preliminary map of β1 subunit functional domains 7
Figure 2.1: Schematic representation of transfection technology based on chemical reagents. 14
Figure 2.2: Schema of a common electrophysiological set-up 18
Figure 2.3: Four simple conceptual variations of the Patch clamp technique. 20
Figure 3.1: Typical whole-cell sodium current recordings of $Na_v1.1$ WT channels and R1648H mutant channels with or without β subunits. 28
Figure 3.2: Co-expression of β1 or/ and β2 subunits modulate the voltage dependence of activation and inactivation of Nav1.1 WT 29
Figure 3.3: Co-expression of β1 or/ and β2 subunits modulate the kinetics of $Na_v1.1$ WT channel gating 30
Figure 3.4: Co-expression of β1 or/ and β2 subunits modulate the voltage dependence of activation and inactivation of R1648H mutant channel. 31
Figure 3.5: Co-expression of β1 and/or β2 subunits modulates the kinetics of R1648H mutant channel gating. 33
Figure 3.6: Co-expression of β subunits modified the voltage dependence of the time course of fast inactivation 35
Figure 3.7: Co-expression of β subunits modified the persistent sodium current levels in different test potentials 36
Figure 4.1: Pedigrees of the three novel SCN2A mutations associated with BFNIS. 39
Figure 4.2: Three novel BFNIS mutations. 39
Figure 4.3: Electrophysiological properties of SCN2A channels. 40
Figure 4.4: Representative WT and M252V whole-cell SCN2A sodium currents 42
Figure 4.5: Electrophysiological properties of M252V mutant channel. 43
Figure 4.6: Typical sodium current recording of the V261M neonatal channel 45
Figure 4.7: Electrophysiological properties of V261M mutant channel. 46
Figure 4.8: Typical sodium current recording of the A263V neonatal channel 48
Figure 4.9: Electrophysiological properties of A263V mutant channel. 50
Figure 4.10: Entry into and voltage dependence of slow inactivation of the three mutant channels 51
Figure 5.1: Morphological reconstruction of measured neurons and identification of their immunoreaction for GAD_{67} 52
Figure 5.2: Three morphological classes of cortical neurons 53
Figure 5.3: A GAD_{67} negative DIV22 cortical pyramidal neuron. A: reconstruction of the GAD_{67} negative cortical neuron 55
Figure 5.4: An accommodating spiking GAD_{67} positive cortical basket neuron 56
Figure 5.5: A stuttering spiking GAD_{67} positive cortical bitufted neuron at DIV 24 58
Figure 6.1: Immunohistochemical staining of Nav1.2 and Nav.16 in mouse hippocampus during development 68

INDEX OF TABLES

Table 3.1: Electrophysiological properties of *SCN1A* WT and the R1648H mutant channels 32
Table 3.2: Kinetics of *SCN1A* WT and R1648H mutant channel gating 34
Table 4.1: Clinical features of patients with M252V or V261M mutation. 38
Table 4.2: Electrophysiological properties of *SCN2A* WT neonatal and adult channels 41
Table 4.3: Electrophysiological properties of *SCN2A* WT and the mutant channels 44
Table 4.4: Steady-state slow inactivation parameters of SCN2A WT and the mutant channels 49
Table 5.1: Electrophysiological properties of recorded cortical neurons 56

LIST OF ABBREVIATIONS

AC	Accommodating
AIS	Axon initial segment
AMP	Adenosine monophosphate
AP	Action potential
Asn	Asparagine
Asp	Aspartic acid
BFNIS	Benign familial neonatal-infantile seizures
BST	Bursting
C	Capacitance
cDNA	Complementary deoxyribonucleic acid
DAPI	4', 6-diamidino -2-phenylindole
DIV	Days in vitro
DMEM	Dulbecco's modified essential medium
DMSO	Dimethyl sulfoxide
EEG	Electroencephalogram
EGTA	Ethylene glycol tetra-acetic acid
Em	Equilibrium potential
GABA	γ-aminobutyric acid
GAD	Glutamate decarboxylase
GEFS+	Generalized epilepsy with febrile seizures plus
GFP	Green fluorescent protein
HBSS	Hank's buffered salt solution
HEBS	HEPES buffered saline
HEPES	N-2-Hydroxyethylpiperazine-N'-2-ethanesulfonic acid
I	Current amplitude
Ig	Immune globulin
IS	Irregular spiking
k	Slope factor of the Boltzmann function
MEM	Modified Eagle's Medium
NAC	Non-accomodating
$Na_v1.1$-$Na_v1.9$, Na_x	Voltage-gated sodium channel α-subunit isoforms

PBS	Phosphate buffered saline
PCR	Polymerase chain reaction
PFA	Paraformaldehyde
R	Resistance
RNA	Ribonucleic acid
RP	Resting potential
SMEI	Severe myoclonic epilepsy of infancy
STUT	Stuttering
TTX	Tetrodotoxin
V	Voltage
V_{rev}	Reversal potential
WT	Wild type

1. Introduction

Ion channels are transmembrane proteins with a specific selectivity to particular ions, which allow ions to flow passively across the cell membrane along their concentration gradient. The opening and closing, called gating of channels is controlled by voltage or binding of ligands or other processes. They play important roles for controlling rapid changes of membrane potential during action potential and contribute to synaptic transmission and postsynaptic potentials of the target cells, alter many metabolic processes within cells. With help of gene cloning and sequencing, numerous ion channel genes have been identified to date. The patch-clamp technique enables the recording of the ion flow through a single open channels and the determination of ion channel functions. In addition, X-ray crystallography has provided a detailed view of the three-dimensional structure of some ion channels. A number of Chemical and genetic disorders may disrupt ion channel function, thereby leading to human diseases (Lehmann-Horn and Jurkat-Rott, 1999; Lerche et al., 2005). Molecular electrophysiological studies of the genetic disorders of ion channels, the so called channelopathies, elucidate the pathophysiology of these diseases, and can help improve therapy. Furthermore, naturally occurring mutations have delivered important hints to the biophysical mechanism of ion channel family.

1.1. Voltage-gated sodium channels

Voltage-gated sodium channels are heteromeric complexes consist of a large glycosylated α subunit (approximately 260 kDa) associated with at least one auxiliary β subunit (Fig. 1.1). The pore forming α subunit contains four homologous domains termed I-IV, each of which has six transmembrane segments called S1-S6. The voltage sensor is located in the S4 segment, which contain four to eight positively charged amino-acid residues (Yu and Catterall, 2003). The p-loop between S5 and S6 is embedded into the transmembrane region of the channel, forming the ion-selective filter at the extracellular end of the pore. The cytoplasmic linker between domain III and IV is acknowledged to serve as inactivation particle contributing to fast inactivation (Patton et al., 1992). Voltage-gated sodium channels are widely expressed in the excitable cells of mammalian

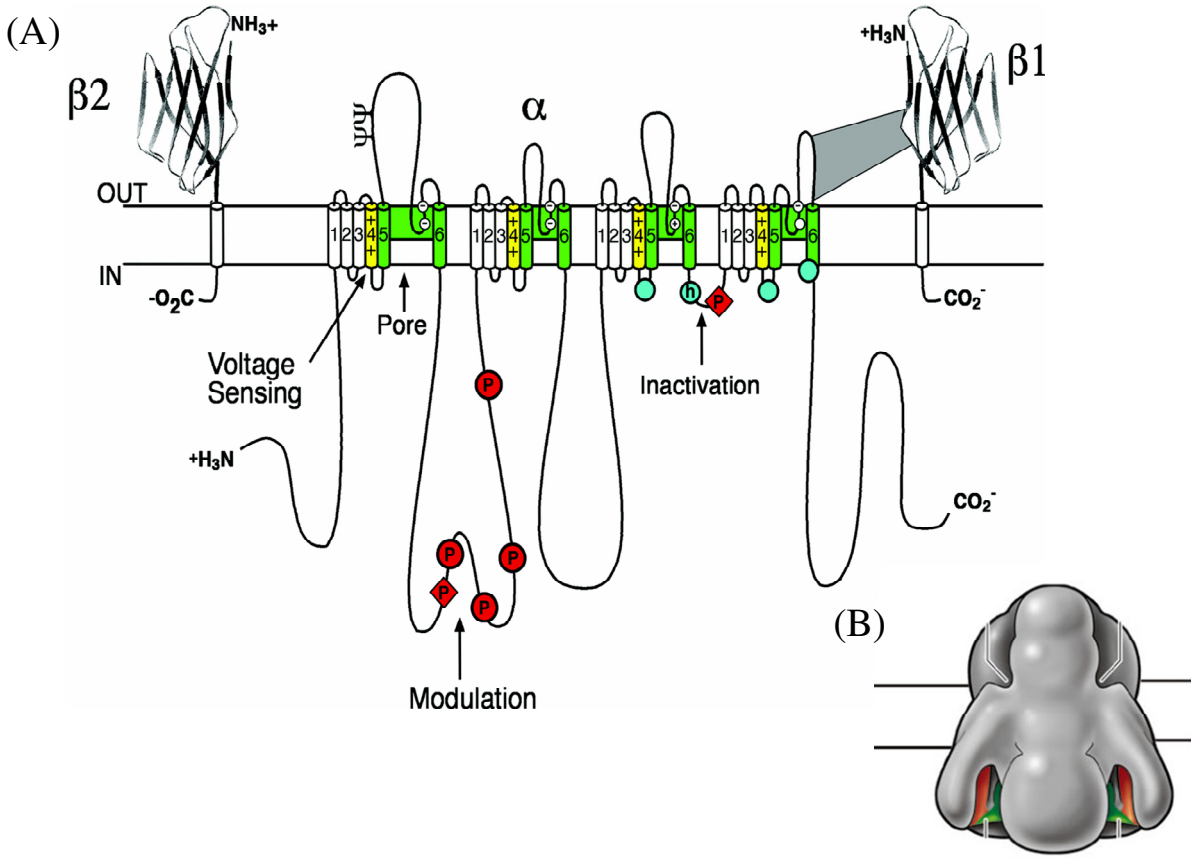

Figure 1.1: Molecular structure of voltage-gated sodium channels. (A) Schematic representation of the sodium-channel subunits. The α subunit of the $Na_v1.2$ channel is illustrated together with the β1 and β2 subunits; the extracellular immunoglobulin-like folds domains of the β subunits interact with the loops in the α subunits as shown. Roman numerals indicate the domains of the α subunit; S5 and S6 (shown in green) are the pore lining segments and the S4 helices (yellow) make up the voltage sensors. Blue circles in the intracellular loops of domain III and IV indicate the inactivation gate IFM motif and its receptor (h, inactivation gate); P, phosphorylation sites (in red circles, sites for protein kinase A; in red diamonds, sites for protein kinase C); Ψ, probable N-linked glycosylation site. The circles in the re-entrant loops in each domain represent the amino acids that form the ion selectivity filter (the outer rings have the sequence EEDD and inner rings DEKA). (B) The three-dimensional structure of the voltage-gated sodium channel α subunits at 20 Å resolution, compiled from electron micrograph reconstructions (Yu and Catterall, 2003).

nervous system, heart and skeletal muscles. They play essential roles in the initiation and propagation of action potentials in neurons and other electrically excitable cells such as myocytes and endocrine cells (Hille, 2001).

1.1.1. Diversity of voltage-gated sodium channel α subunits

Nine α subunits ($Na_v1.1$-$Na_v1.9$) of voltage-gated sodium channels have been functionally characterized so far and a tenth closely related isoform (Na_x) may function as a sodium channel as well (Goldin et al. 2000). At least 20 exons encode each of the nine sodium channel α-subunit proteins. The nine mammalian sodium channels can be divided into three groups according to the chromosomal localization of their encoding genes (Fig. 1.2; Plummer et al., 1999). The first group consists of $Na_v1.1$, $Na_v1.2$, $Na_v1.3$ and $Na_v1.7$, whose encoding genes are clustered together on chromosome 2 in humans and mice. These channels share a number of common characteristics, including expression in the nervous system and the sensibility to the nanomolar concentrations of tetrodotoxin (TTX).

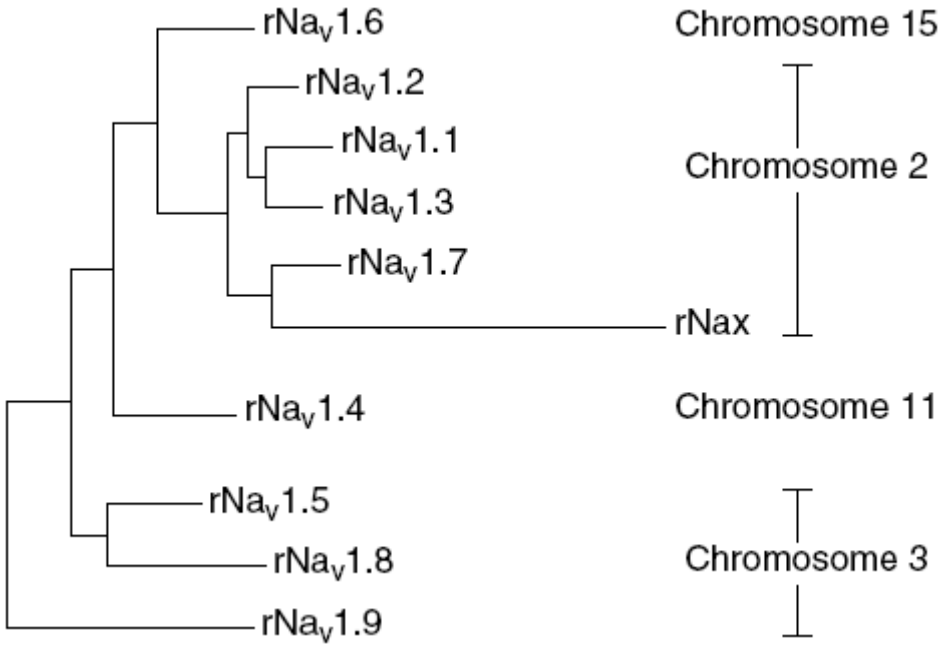

Figure 1.2: A phylogenetic tree of rat voltage-gated sodium channel α subunits. The human chromosomes on which the human ortology of each rat gene is found are shown on the right (Yu and Catterall, 2003).

Genes encoding $Na_v1.5$, $Na_v1.8$ and $Na_v1.9$ are clustered on chromosome 3 in humans. These channels are all considered as 'TTX-resistant' (micromolar concentrations of TTX are needed to block these channels.). The final two isoforms, $Na_v1.4$ and $Na_v1.6$ belong to the third group, although the genes encoding them are located on separate chromosomes.

They share similar properties with the channels whose genes are located on chromosome 2, such as TTX sensitivity. The gene encoding $Na_v1.6$ locates on human chromosome 15. $Na_v1.6$ is one of the most important channels in the nervous system. $Na_v1.4$ is primarily expressed in adult skeletal muscle and its encoding gene locates on human chromosome 17.

In addition, post-transcriptional processing, alternative splicing and RNA editing also generate more diversity in sodium channels. Alternative splicing has been reported for six isoforms which are present in the mammalian nervous system, $Na_v1.1$, $Na_v1.2$, $Na_v1.3$ (Schaller et al., 1992; Gustafson et al,. 1993; Lu and Brown, 1998; Kasai et al., 2001;), $Na_v1.5$ (Zimmer et al., 2002; Raymond et al., 2004), $Na_v1.6$ (Plummer et al., 1997), $Na_v1.7$ (Belcher et al., 1995; Raymond et al., 2004). Various factors, including age, the tissue of origin and the presence of modulator agents such as dibutyryl cyclic AMP, modulate the proportion of differentially spliced transcripts (Gustafson et al., 1993; Plummer et al., 1997; Dietrich et al., 1998; Oh and Waxman, 1998). The alternative splice isoforms of exon 6, so called exon 6N and exon 6A, causing a single amino acid change (Asn to Asp) at position 209, located in the extracellular loop between the S3 and S4 of domain I, result in developmentally regulated alternative splicing of human $Na_v1.2$ (Kasai et al., 2001).One of the splice variants is predominantly expressed neonatally (N), while the other is expressed only in adult age (A). However, the functional consequence of the splice variants is still poorly understood.

1.1.2. Function of voltage-gated sodium channels in the brain

Voltage-gated sodium channels have three main conformational states, a closed, an open, and an inactivated state (Fig. 1.3). The channels stay in the closed state at the resting membrane potential and can be activated and inactivated rapidly in a voltage dependent manner. Upon membrane depolarization, the voltage sensors, locate in the S4 segments, move outward opening the ‘activation gate’ of the channel on a time scale of milliseconds by a yet unknown mechanism. With sustained depolarization the channels are inactivated by the IFM motif, namely the inactivation particle, which folds into the channel therefore blocks the inner mouth of the pore (Hodgkin and Huxley, 1952; Vassilev et al., 1988, 1989; Eaholtz et al., 1994). The outward movement of the S4 segment in domain IV triggers fast inactivation of the sodium channel by closure of the intracellular inactivation gate, which is

called coupling of activation to inactivation (Chen et al., 1999).Upon membrane repolarization, inactivated channels remain refractory to further openings for a certain period determined by the time needed for substantial (~80%) recovery from inactivation, normally a couple of. milliseconds.

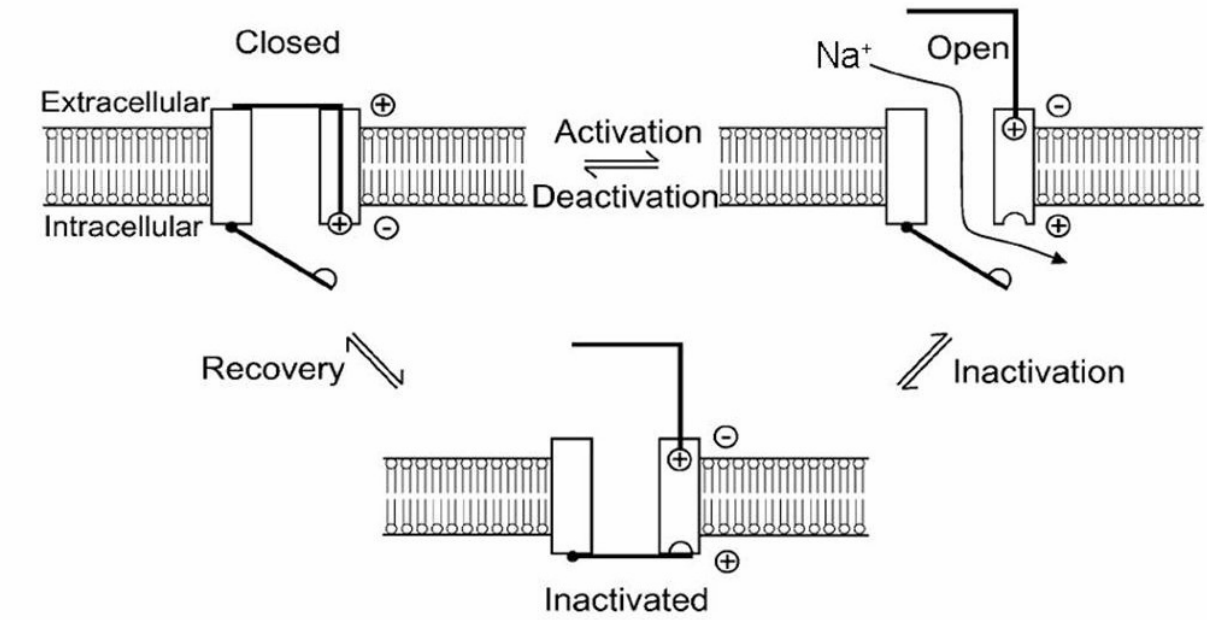

Figure 1.3: The three main conformational states of voltage-gated sodium channels. From a closed state at the hyperpolarized resting membrane potential, the voltage-gated sodium channels open upon depolarization during an action potential via outward movement of the voltage sensors that open the activation gate. The channels inactivate spontaneously via closing of an inactivation gate, when depolarization is maintained. From the inactivated state they can only recover upon repolarization of the cell membrane before they are ready for another opening (Lerche et al., 2001).

Inactivation closes the channel and prevents it from reopening until recovery, which one parameter to determine the frequency of action potential firing. Prolonged depolarizations (seconds to minutes) result in slow inactivation, which is a separate process that does not involve the inactivation particle. Recovery from slow inactivation needs several seconds, which could prevent sodium channels from becoming fully available too fast after a single or short train of action potentials (Mickus et al., 1999; Ellerkmann et al., 2001).

The molecular mechanism of slow inactivation is not yet well determined. One hypothesis is that it results from a structural rearrangement of the pore, similar to the mechanism for C-type inactivation in potassium channels (Liu et al., 1996). Although various studies demonstrated conflicting data concerning this hypothesis, it is suggested that the mouth of the pore does not close during slow inactivation (Ong et al., 2000; Struyk et al., 2002). Several regions like the pore (Balser et al., 1996), the voltage sensors (Mitrovic et al., 2000; Struyk et al., 1999), S4-S5 loops (Cummins et al., 1996; Hayward et al., 1997), S5 (Bendahhou et al., 1999) and S6 (Hayward et al., 1997) segments have been reported being involving in slow inactivation process.

1.1.3. The auxiliary β subunits

Biochemical studies revealed that the brain voltage-gated sodium channels are composed of a pore-forming α subunit and auxiliary β subunits (Catterall, 2000). The voltage-gated sodium channel β subunit family includes four members, β1, β2, β3, β4, and a splice variant of β1 designated β1a. β1 and β3 are more closely related (~45% sequence identity) to each other, whereas β2 and β4 are more similar to each other (35% identity).

β 1 and β2 subunits were originally identified as proteins copurifying with a brain α subunits of voltage-gated sodium channel with a subunit stoichiometry of 1:1:1 (Catterall, 2000). The two β subunits share similarities in the structure, a large extracellular Ig-like domain, a single transmembrane domain, and a short cytoplasmic tail (Fig. 1.4; Isom et al., 1992, 1995). The β1 subunit is a protein of 23 kDa, which noncovalently associates with the α subunit. It has four cysteines in its extracellular domain, which contribute to the Ig-like folding. The β2 subunit has 21 kDa. It contains five extracellular cysteines and forms a disulfide bond to the α subunit.

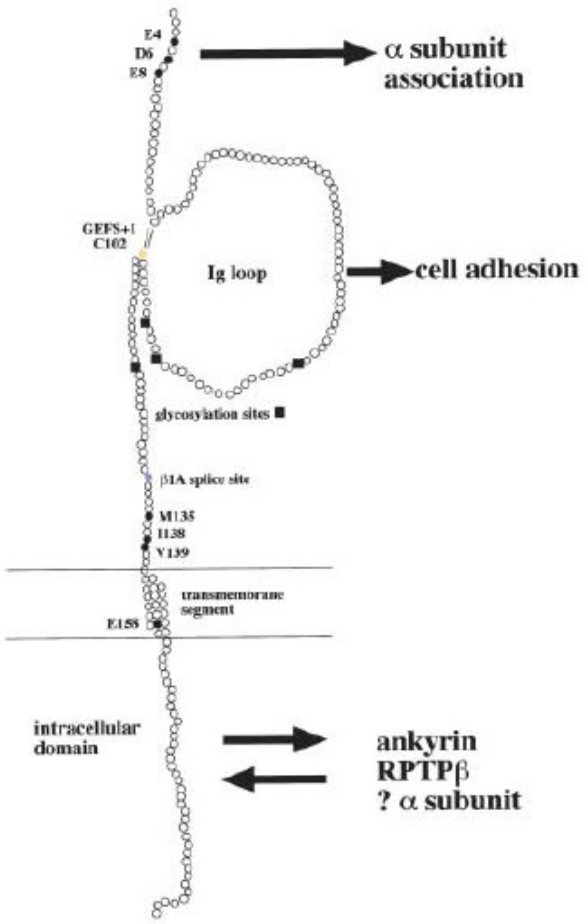

Figure 1.4: Preliminary map of β1 subunit functional domains (Isom, 2001).

The β subunits appear to be multifunctional. First, they modulate the voltage-gated sodium channel gating. Co-expression of the β1 and β2 subunits shift sodium channel into a fast gating mode by accelerating the rates of activation and inactivation (Isom et al., 1992, 1995). Functional studies have proved that the extracellular Ig-like fold of β1 is critical for modulation (Chen and Cannon 1995; Makita et al., 1996; Mc Cormick et al., 1998; Mc Cormick et al., 1999). The loops on the extracellular side of transmembrane segment IS5-S6 and IVS5-S6 have been pointed as important regions for interaction between α and β1 subunit (Makita et al., 1996; Qu et al., 1999). Interactions of the extracellular loop with transmembrane segment IVS6 serve to modulate channel activation and coupling to fast inactivation via an unknown mechanism. Other studies have also revealed an intracellular interaction domain of α and β1 subunits (An et al., 1998; Malhotra et al., 1999; Meadows et al., 2001). Second, they serve as cell adhesion molecules that mediate cell-cell interactions in the nervous system and other tissues. The interactions of β1 and β2 with ankyrin, tenascin-R and neurofascin may be responsible for targeting sodium channel

complexes to specialized area, such as nodes of Ranvier and the axon initial segment. They may also stabilize the high density of sodium channels in these regions (Srinivasan et al., 1998; Malhotra et al., 2000; Ratcliffe et al., 2001).

1.2. Idiopathic epilepsy

Epilepsies are currently classified as symptomatic, cryptogenic and idiopathic forms. Up to 40% of all epilepsies are idiopathic. They are not preceded or secondarily caused by other disorders, but mainly due to genetic predispositions. Clinical features include typical seizures, such as absences or myoclonic seizures, with various abnormalities of the electroencephalogram (EEG), such as 3-4 Hz generalized spike and wave discharges or generalized polyspikes. Genetic defects have been identified in several different syndromes, such as generalized epilepsy with febrile seizures plus (GEFS+), severe myoclonic epilepsy of infancy (SMEI) and benign familial neonatal-infantile seizures (BFNIS), which are caused by mutations in sodium channel encoding genes.

1.2.1. Generalized epilepsy with febrile seizures plus

Febrile seizures, which affect approximately 3-5% of children under 6 years of age, are the most common seizure disorder occurring in children. A fraction of the affected children generate epilepsy in their later life. Generalized epilepsy with febrile seizures plus (GEFS+; OMIM604233) is a dominantly inherited epilepsy syndrome characterized by childhood febrile seizures and often progressing to afebrile seizures (Scheffer and Bercovic, 1997; Singh et al., 1999).

The identification of a β1 subunit mutation in a large Australian family with GEFS+ revealed the first association between genetic defects in sodium channels and epilepsy (Wallace et al., 1998). The missense mutation C121W is located in the extracellular Ig-like domain of the β1 subunit, which disrupts a disulfide bridge changing the secondary structure of the extracellular loop and resulting in a loss of β1 subunit function.

Subsequently, linkage analysis localized a second GEFS+ locus to a cluster of genes encoding brain sodium channel α subunits on chromosome 2q24 (Baulac et al., 1999;

Moulard et al., 1999). Sequencing of *SCN1A* disclosed two missense mutations, T875M in one family and R1648H in the other (Escayg et al., 2000). Both mutations are located in the voltage sensor. Since then many more *SCN1A* mutations related to GEFS+ have been reported since then.

1.2.2. Benign familial neonatal-infantile seizures

Afebrile seizures occurring in early ages normally indicate serious underlying structural brain disease or metabolic disorders, often with a bad prognosis (Chevrie and Aicardi, 1978; Matsumoto et al. 1983). Benign familial neonatal-infantile seizures (BFNIS; OMIM 607745) is a mild, autosomal dominant epilepsy synptome, which is characterized by focal afebrile seizures often secondarily generalized without brain abnormalities or other etiological factors; seizures occur usually in the first week of life, and in most cases remit spontaneously within weeks, latest in one year. Age of onset and associated genetic defects are important factors to distinguish this syndrome from benign familial neonatal seizures (BFNS), which has a very narrow age of onset within the first days of life and is associated with potassium channel mutations; second, BFNS has to be separated from benign familial infantile seizures (BFIS), which characteristically begin at between 3 and 12 months of age. For BFIS, there are 2 loci identified on chromosome 19q12-q13.11 (Guipponi et al., 1997) and 16p12-q12 (Caraballo et al., 2001), but disease causing genes are still unknown. Missense mutations in *SCN2A*, encoding the $Na_v1.2$ α subunit, have been identified in BFNIS patients (Sugawara et al., 2001; Heron et al., 2002; Kamiya et al., 2004; Berkovic et al., 2004).

1.3. Features of cortical neurons

The extreme numerous neurons in the mammalian cerebral cortex have a various morphology. Two important types are pyramidal neurons and interneurons. Approximately 70-80% of the cortical neurons are pyramidal neurons, which release the excitatory transmitter glutamate. They have a pyramidal shaped cell body and are located mainly in layer III and V. These neurons provide the main output pathway of the cerebrum and their axons project to other important neurons of the nervous system, such as the peripheral motor neurons to mediate voluntary movements. The remaining 20-30% of the cortical

neurons are interneurons, which use the inhibitory neurotransmitter γ-aminobutyric acid (GABA). The interneurons have diverse morphological, physiological, molecular and synaptic characteristics (De Felipe, 1993; Cauli et al., 1997; Kawaguchi and Kubota, 1997; De Felipe, 2002). They are located in all layers.

Several types of GABA-ergic interneurons have been distinguished based on their morphological properties. About 50% of all inhibitory interneurons have a basket-like appearance around pyramidal cell soma, termed 'basket cell'. They target the somata and proximal dendrites of pyramidal neurons as well as of other interneurons and adjust the gain of the integrated synaptic response. Chandelier cells are multipolar or bitufted neurons, targeting the axons of other neurons. They have been found in layers II-VI. Martinotti cells locate in the same layer. They have a bitufted morphology with a more elaborate dendritic tree than most interneurons, which project their axons towards layer I. Bipolar cells in layer II-VI have a spindle or ovoid somata and narrow bipolar or bitufted dendrites that extend vertically towards layer I and down to layer VI. Bitufted cells are similar to bipolar cells, but have wider horizontal axonal spans. They target dendrites.

The physiology of pyramidal neurons is relatively uniform and was described as "regular spiking" (Connors and Gutnick, 1995) whereas the interneurons respond differently to depolarizing stimulations. Interneurons can be divided into five groups according to their steady-state response: non-accomodating (NAC); accommodating (AC); stuttering (STUT); irregular spiking (IS) and bursting (BST). NACs fire without frequency adaptation to the depolarizing current injection. In contrast, ACs adapt the firing frequency and therefore do not reach such high firing rates as NACs. STUT cells fire high-frequency clusters of action potentials with unpredictable periods of silence. The firing of action potentials in IS cells occurs randomly and shows marked accommodation. BST cells fire a brief cluster of action potentials followed by interburst hyperpolarizations.

1.4. Aims

The present thesis is divided into three parts:

1) The aim of the first part was to investigate the functional defects caused by a GEFS+ mutation in the *SCN1A* gene, predicting the amino acid exchange R1648H

in the $Na_v1.1$ channel and the modification of channel gating by the β1 and β2 subunits.

2) The aim of the second part was to evaluate the functional consequences of three novel *SCN2A* mutations predicting the amino acid changes in S5 of domain I, in which no disease-associated mutations had been identified thus far.

3) The goal of the third part was to classify cultured rat cortical neurons by their morphology, electrophysiological feature and GAD_{67} immunoreaction. This classification should help to use such cells later as an expression system for epilepsy-associated mutations.

2. Materials and Methods

2.1. Molecular and cell biology methods

2.1.1. Mutagenesis

Mutagenesis and cloning procedures were performed by other coworkers in our laboratory. Therefore only a short description of the procedures is provided.

The construct of the coding sequence (cDNA) of the human voltage gated sodium channel $Na_v1.1$ inserted in the pCDM8 plasmid vector was kindly provided by Dr. Mantegazza (Milan). The cDNA of the human voltage gated sodium channel $Na_v1.2$ (neonatal and adult isoforms) inserted in the pcDNA3.1 plasmid vector was a gift from Dr. Steven Petrou (Melbourne). Site-directed mutagenesis to engine the mutations into pCDM8-h$Na_v1.1$ and pcDNA3.1-h$Na_v1.2$ was performed by overlap polymerase chain reaction (PCR) mutagenesis methods. The human voltage gated sodium channel auxiliary subunits hβ1 and hβ2 were cloned into plasmids containing the marker genes GFP (pCLH-hβ1-EGFP) or CD8 (pCLH-hβ2-CD8), respectively. All mutant cDNAs were resequenced fully before they were used in electrophysiological experiments.

2.1.2. Cell culture and transfection

2.1.2.1. Subcultivating and maintainance of tsA-201 cell line

The tsA-201 cell line is a variant of the human embryonic kidney cell line HEK-293 that expresses the simian virus 40 large T antigen, which allows episomal replication of transfected plasmids containing the SV40 origin of replication. This leads to an amplification of transfected plasmids and extended temporal expression of the desired gene products. TsA-201 cells contain only few endogenous sodium channels. Therefore they are commonly used for heterologous expression of Na^+ channels and their functional characterization using the whole cell patch clamp technique. Standard cell culture procedures for adherent cell lines were applied: cells were maintained in 25ml sterile flasks (Integra Bioscience or Greiner, Frickenhausen) in 50% Dulbeco´s MEM + 50% HAMS nutrition mixture (GIBCO Brl, Paisley, Scotland or PAA Laboratories, Linz, Austria) supplemented with 10% (v/v) fetal bovine serum (Lonza, Switzerland) in controlled 5%

CO_2 atmosphere at 37°C (Cell incubator IG 150, Jouan, Unterhachingen, Germany). The culture was maintained regularly to prevent overgrowth and accelerated cell death from exhausted medium. The cell line was subcultured at least two times per weak. Before splitting, cells were gently washed with Ca^{2+} and Mg^{+} free PBS solution (PAA Laboratories, Linz, Austria) for stabilizing the pH of the medium and attenuating the following resuspension by weakening the cell-cell and cell-dish connections. In order to create a cell suspension, new growing medium was added to the flask, washing the sides of the flask to ensure that all of the cells become suspended. Pipetting (with 5 ml plastic pipette Greiner, Frickenhausen, Germany) is necessary to break up cell clumps or to aid in the removal of attached cells. Cells were distributed into clean, sterile flasks supplemented with fresh medium, in the ratio 1:3. The culture was examined microscopically for reattachment and active growth. Cells were used for transfections until passage 40.

2.1.2.2. Cryopreservation

Cryopreservation is a technique of freezing cells and tissues at very low temperatures such as (typically) -197°C, at which the biological material remains genetically stable and metabolically inert. Intracellular water must be replaced with other compounds that will not form crystals when frozen. For this purpose, the culture was expanded to allow for adequate cell density for the desired volume to freeze. The optimum time of performing the cryopreservation procedure is approximately 2-4 days after subculturing, in a period of active proliferation, during which the number of cells increases exponentially. The cells were detached from the substrate and resuspended in a complete growth medium and a cell count was performed to determine the number of viable cells. The cells were centrifuged at 300 rpm for 10 minutes. The amount of freezing media – 10% DMSO (Dimethyl sulfoxide: a cryoprotectant, that can prevent the cells dying as they are frozen) in fresh complete medium - was calculated as total cell concentration through the desired cell density. The cell pellet was resuspended using the cryopreservation medium, was pipetted up and down to ensure a single-cell suspension. After dispensing into the desired number of vials for cryopreservation, the vials were transferred at -20°C for one hour then to a -80°C freezer (in a styropor box) for 24 hours, afterwards to liquid nitrogen storage (-197°C).

When needed, thawing was performed as quickly as possible (at 37°C or by hand), the cryopreservation medium was immediately diluted by transfering the cells into a 25 cm^2 culture flask with appropriate fresh, cold (4°C) culture medium. The cells were then placed in a 37°C incubator; the medium was exchanged after 24 hours. The thawed culture required usually one week to adjust to the culture conditions before splitting.

2.1.2.3. Transient cell transfection

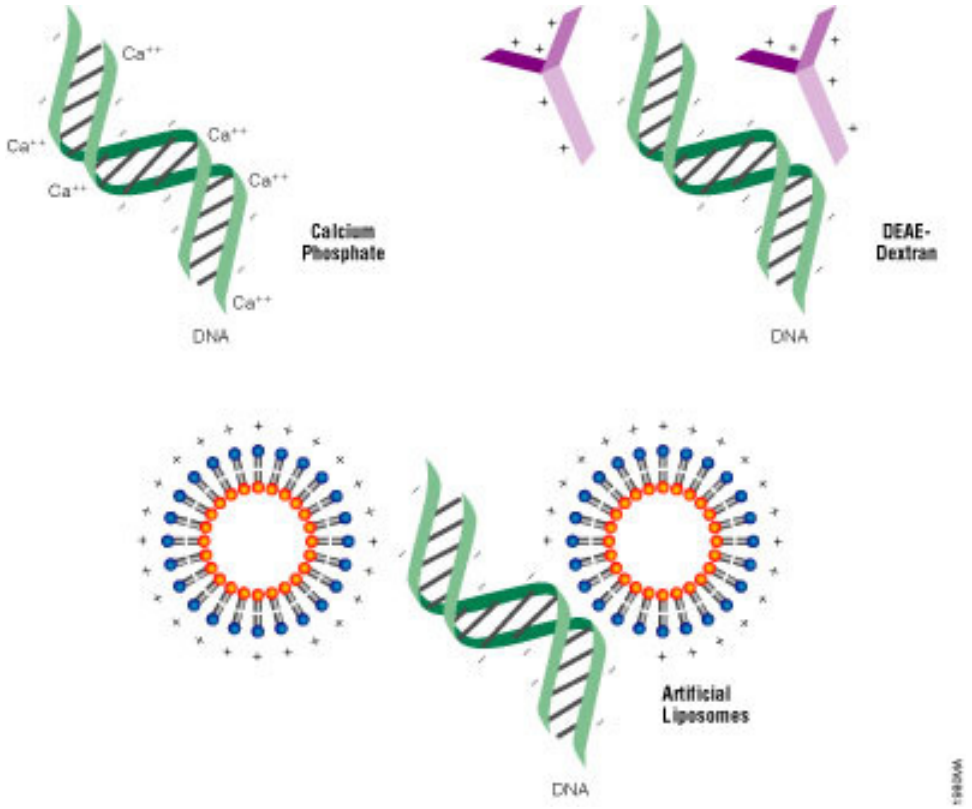

Figure 2.1: Schematic representation of transfection technology based on chemical reagents.

Transfection is a method to introduce foreign DNA into a recipient eukaryote cell and its integration into the recipient cell chromosomal DNA. Applications of a transient transfection do not insert the DNA into the nuclear genome; therefore the foreign DNA is lost in the later stage when the cells undergo mitosis. The standard calcium-phosphate method (Jordan et al., 1996) was performed in this study for transient transfections. This technique, originally developed by Graham and Van der Eb (1973) has been used for more than 20 years for the transfer and expression of genetic information in mammalian cells in culture. The principle is simple: the negatively charged phosphate and the positively

charged calcium will form fine precipitates, with the purified DNA. These DNA-$CaPO_4$ precipitates are then brought into eukaryotic cells via endocytosis or phagocytosis (cell-eating). The efficiency of this type of transfection is however variable, since highly effective precipitates can be generated in a very narrow range of physical-chemical conditions. Sterile 60 mm dishes (Greiner, Flickenhausen, Germany) filled with 5 ml cell culture medium and a cell density of around 50% were prepared the day before transfection. 5 µg of cDNA encoding the WT or mutant sodium channel α-subunit was cotransfected with 3 µg plasmid containing CD8 cDNA in order to recognize transfected cells using microbeads with CD8-antibodies. For co-transfection experiments, 6 µg of cDNA in total encoding the WT or mutant sodium channel α-subunit, β1 and/or β2-subunit was cotransfected in a 1:1 or 1:1:1 molar ratio. The whole amount of cDNA was mixed with 250 µl sterile $CaCl_2$ solution and added dropwise to 250 µl 2xHEBS solution (in mM: 274 NaCl, 40 HEPES, 2 KCl, 10 Dextrose, and 1.4 Na_2HPO_4, pH: 7.05). After 20 min incubating at room temperature, the mixture was added to the cells, supplemented with fresh cell culture medium. Transfection was stopped after 12 hours by gently washing the cells with PBS and resuspending like mentioned before. Different amounts of the suspension (from 100 µl up to 300 µl) were distributed in 3.5 cm cell culture dishes for further electrophysiological experiments.

2.1.2.4. Primary mouse neuronal culture

All animal experiments were conducted in accordance with the guidelines of the German National Board for Laboratory Animals. Hippocampal and cerebral cortical neurons were isolated from embryonic day 17 BALB/c mice brains. Pregnant dams were sacrificed by carbon dioxide. Embryos were quickly taken out and decapitated. Using micro surgical dissection methods, hippocampus and cerebral cortex were isolated. Tissues were washed 3 times with 4°C Hank's BSS without Mg, Ca (PAA Laboratory GmbH, Austria), before 15 minutes treatment with 2.5% trypsin. Then the tissues were rinsed 3 times in HBSS solution, and 1% Deoxyribonuclease I (Invitrogen, Carlsbad, CA) was added for removing DNA of the dead neurons from preparation. Single neurons were obtained by mechanical dissociation using a cell strainer (Becton Drive, USA). The dissociated neurons were plated at a density of 80,000 or 60,000 per well in 24 well cell culture multiwell plates (Greiner bio-one). Each well contains a 13 mm diameter glass cover slip which is coated with Poly-D-Lysine solution (5 mg Poly-D-Lysine in 100 ml HBSS, filtered by 0.45 µm

filter), and approximately 500 µl DMEM with Fetal Bovine Serum (Biochrom AG), L-Glutamine (Gibco) and Penicillin/Streptomycin (Gibco) in a volume ratio of 10:1:0.1:0.1. After allowing the neurons to settle over night in a 37°C incubator with 5% CO_2 supply, the solution was replaced with Neurobal culture medium (Invitrogen, Carlsbad, CA) supplemented with B27 (Invitrogen, Carlsbad, CA), glutamine and penicillin/streptomycin in a volume ratio of 50:1:0.5:0.5. During the culture maintenance, Neurobal plus medium was half exchanged every week for sustaining the osmorality.

2.2. Electrophysiology

2.2.1. Patch-clamp technique

The function of ion channels is to conduct ions; hence any investigation on how they work implies current measurements. The recordings of inherent electrical activity in frogs in the nineteenth century start the historical route to present-day patch clamping. Following the development of the principle of voltage clamp by Cole (1949) for the squid giant axon, the application of voltage clamp in cells was described at the end of 1970s by Neher and Sakmann (1976) using microelectrodes and improved by Hamill et al. (1981). The voltage clamp technique, in which the voltage across a cell membrane is controlled by a feedback circuit that balances (and therefore measures) the net current, has been the best biophysical tool for the study of voltage-sensitive channels for half a century. Information about the electrophysiological properties of these proteins is obtained by applying a basic set of voltage clamp protocols. These are based on charging, the voltage across the membrane from a holding potential to several test potentials, and on recording the transient current. Analysis of these currents, from the point of view of their time course and their voltage dependence provide information on underlying molecular mechanisms of channel gating.

2.2.1.1. Setup

An Axopatch 200B amplifier (Molecular Devices, Union City, CA, USA) was used to perform continuous single electrode voltage clamp and current clamp in the whole-cell configuration. The amplifier head-stage was mounted on a motorized mini manipulator (LN Unit Junior, Luigs & Neumann Feinmechanik und Elektrotechnik GmbH, Germany) and fixed on an inverted stereo microscope Axiovert 10 (Zeiss, Germany).

A common electrophysiology setup is shown in figure 2.2 A.

The recording chamber, the microscope and the micromanipulators were placed on an anti-vibration table – a heavy granite plate placed on active (pneumatic) support for the patch clamp setup. A faraday cage was built around the experimental setup and all metal parts near the head-stage were grounded, using the virtual ground input of the amplifier.

In all experimental configurations, the voltage clamp amplifier output was digitized by a Digidata 1320A digitizer (Axon Instruments, Union City, USA) connected to a personal computer (PC) running Clampex 6.0 (Axon Instruments, Union City, USA) acquisition software under Microsoft Windows (Microsoft Corp. Redmond, USA). The current responses to the voltage stimuli or the voltage responses to the current stimuli were recorded on the hard drive and additionally a hard copy record was done for every protocol. Data analysis was performed on a PC using a combination of Clampfit (Molecular Devices, U.S.A.), Origin (Microcal, Northampton, U.S.A.) and Excel (Microsoft) software.

2.2.1.2. Experimental procedure

Using the patch-clamp technique, we are able to *clamp* the *voltage* of the whole cell membrane and to record the currents passing through the cellular surface membrane. This is the current that the patch-clamp amplifier supplies to hold the voltage steady (clamped). The electrical events at the cellular level are measured via an electrode connected to the patch-clamp amplifier (Fig. 2.2 A, B). Amplifier 1 is configured as a current-voltage converter, the feedback amplifier 2 compares the two voltage inputs received, i.e. the voltage from the first amplifier (voltage at the top of the pipette electrode) with the

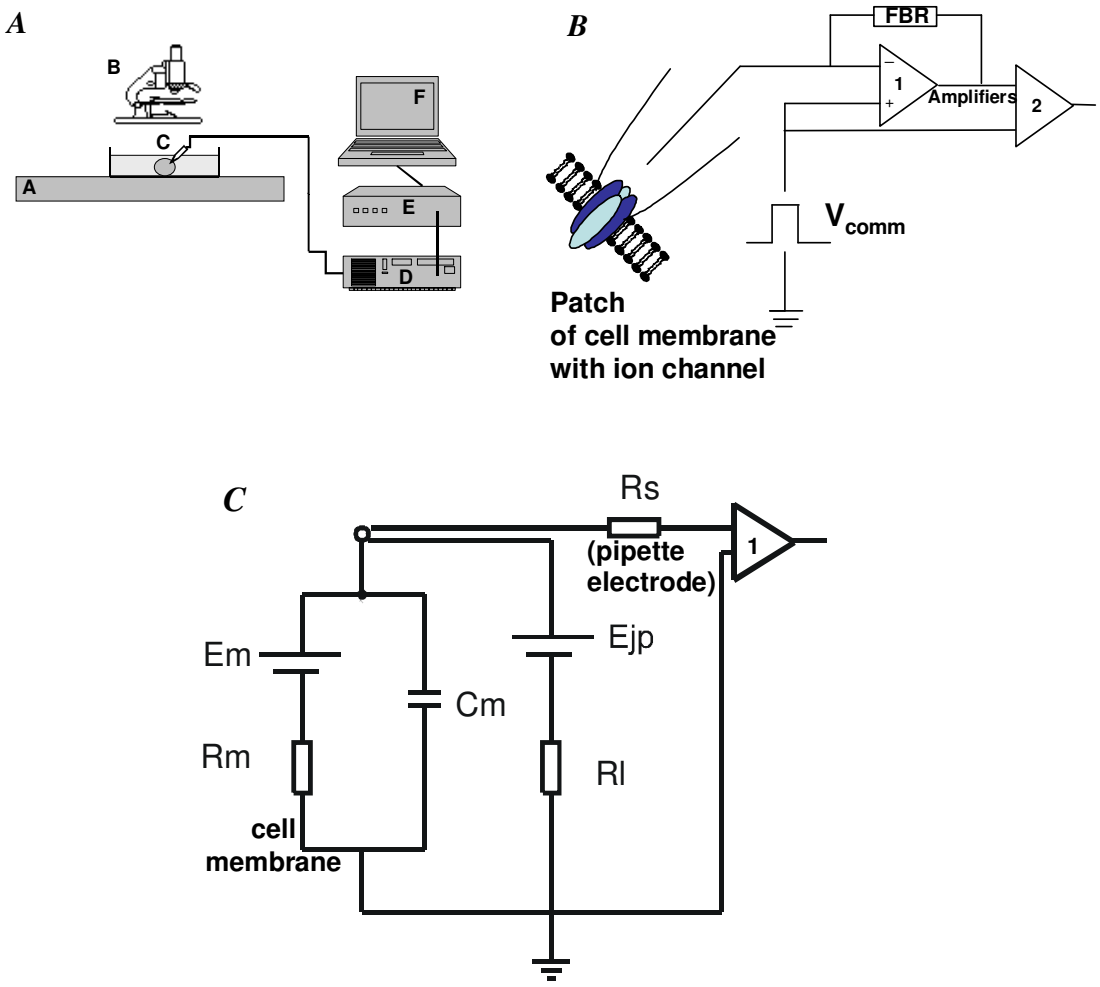

Figure 2.2: (A) Scheme of a common electrophysiological setup. The probe is placed on a massive antivibration table A under an optical microscope B. The glass microelectrode is connected to a feedback amplifier D. The amplified and filtered signal is digitized by the AD converter E. The digitized signal is visualized and stored on a PC F running specific software. (B) The high gain operational amplifier is connected in the circuit so that the current flowing through the ion channel is measured as a voltage drop across the feedback resistor (FBR). The FBR has a resistance of 50 GΩ allowing very small currents (10-12 A) to be measured. (C) Circuit diagram of patch-clamp recordings that includes a shunt through the seal between the pipette and membrane. The cell is presented by the whole cell resistance (Rm), capacitance (Cm), and the cell equilibrium potential (Em) that corresponds to the membrane potential of the intact cell. The seal contact is represented by a shunt resistance (Rl) and the liquid junction potential between the pipette and extracellular solutions (Ejp). The series resistance (Rs) represents mainly the pipette resistance.

command voltage (the desired voltage for clamping the membrane) and generates the output by subtraction. The electrode is introduced in a borosilicate glass pipette with a fine tip, filled with an ionic buffered solution. The glass pipette is brought under microscopic

control in contact with the cellular membrane. A tight contact between the glass electrode and the cell membrane is achieved by placing the pipette onto the cell and then applying negative pressure. This results in a resistance of the pipette in tight contact with the cellular membrane higher than 1 GΩ, a so-called gigaseal. Measurements in several configurations can be performed: whole-cell recordings, allowing measurements through all cellular membrane, cell-attached, inside-out and outside-out configurations for measurements of the currents through the patch in the tip of the pipette.

In order to have an accurate recording of the current passing through the ion channels expressed in the membrane, two major points have to be taken into account: the necessity of a very good control of the membrane potential (i.e. a very good clamp) and the extraction of the measured current from all current that is passing through the feedback resistor i.e. separating capacitive transients and leak current from the actual ionic current.

Clamping the membrane at the desired value requires:

- Compensation of the liquid junction potential (Fig. 2.2 C).

  Whenever solutions with two different ionic compensations come into contact, a liquid junction potential develops between them due to different ionic distribution at their boundary. The liquid junction potential for the solution used for the measurements of Na^+ channels in this thesis was 7mV. It was compensated prior to patch formation.

- Compensation of the error due to the so-called series resistance.

  The main source of error in clamping the membrane at a certain voltage arises from additional resistances between the pipette electrode and the membrane (R_s, Fig. 2.2 C). These are from the pipette itself and the rests of the membrane patch that has been broken to achieve the whole-cell configuration. This resistance, in *series* with the membrane resistance (Fig. 2.2 C), causes a voltage drop $V_s = I*R_s$, where I is the pipette current. Compensation of the series resistance error is achieved by adding to the command signal a voltage signal proportional to the membrane current, which is scaled appropriately. In whole cell experiments, compensation of 70~90% of the series resistance was used, which corresponds to a maximal voltage error of 5 mV for current sizes ranging from 1 to 15 nA.

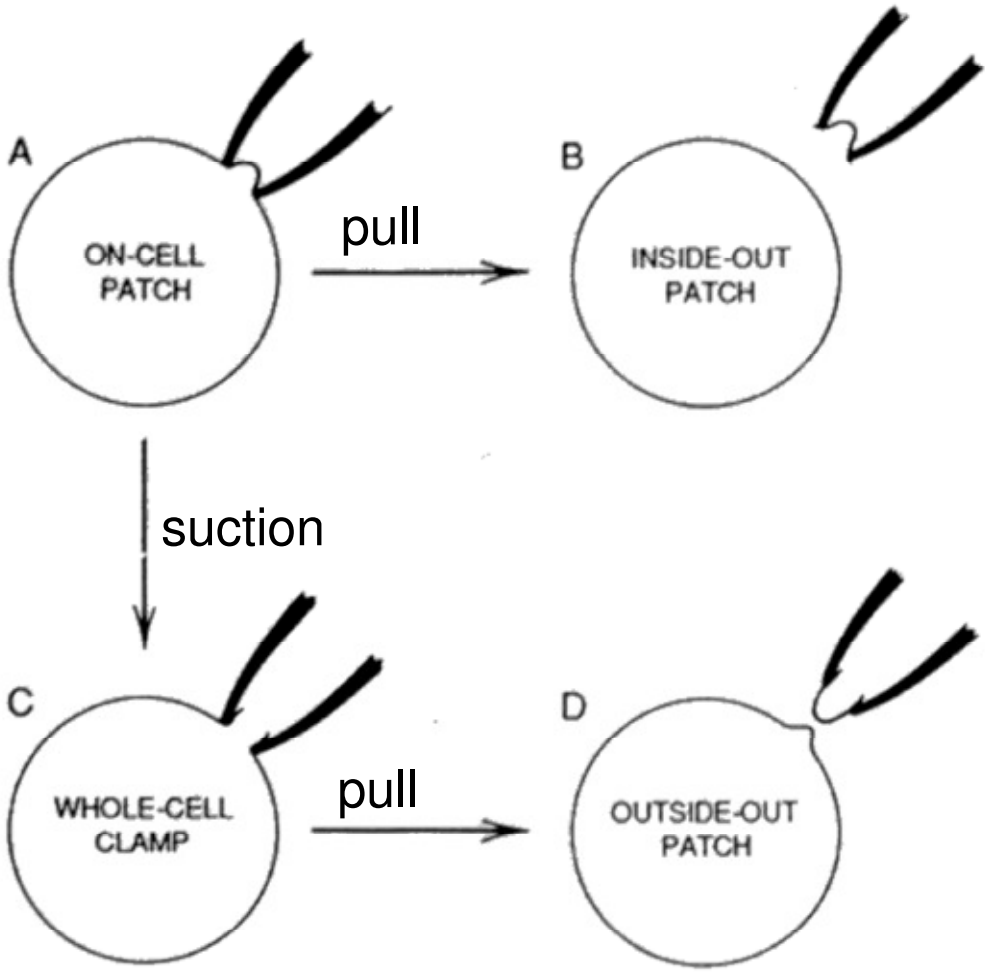

Figure 2.3: Four simple conceptual variations of the Patch clamp technique *(Corey, 1983).*

Recording of the currents flowing only through the ion channel pores implied:

- Subtraction of the leak currents

The current measured during a voltage-clamp experiment are a sum of channel current and leak current. The *leak* current may reflect ion permeation through lipid bilayers or through poorly defined pathways involving unspecified membrane proteins. Higher is the shunt resistance (R_l, Fig. 2.2 C) – seal resistance of GΩ order – smaller will be the leak current.

- Cancellation of the capacitive currents

Capacitive currents appear when the voltage is stepped between two values, due to charging of the membrane lipid bilayer (slow transients) and of the glass pipette walls (fast transients) that are equivalent electrically with two capacitors. Fig. 2.2 C shows a

simplified circuit of a cell with capacitance C_m and membrane resistance R_m. Voltage clamp is performed by an amplifier with amplification μ through an electrode with resistance R_S. Application of a square voltage impulse results in capacitance current, which can be described by the simple equation $I_{IN} = \frac{R_S x C_M}{\mu}$. This current can interfere with the currents flowing through ion channels and additionally can lead to saturation of the amplifiers of the recording circuits. Cancellation of this capacitive current is achieved by supplying the command stimulus with the additional current, required to charge the cell directly to the desired value.

The patch-clamp protocols designed included a P/4 leak current and capacitive transient subtraction protocol.

2.2.1.3. Glass electrodes

Glass microelectrodes were pulled on a horizontal two stage DMZ Universal Puller (Zeitz Instruments, Augsburg, Germany) from thin wall borosilicate glass pipettes with filament (1.5 mm OD, 1.17 mm ID; Science Products, Hofheim, Germany). The microelectrodes for patch-clamp recordings were fire polished. The resistances of whole cell patch clamp electrodes ranged between 1 and 1.5 MΩ.

2.2.1.4. Ag/AgCl electrodes

Ag/AgCl electrodes were prepared by chemically chloriding silver wire pieces (l=5 cm, d=300 µm, Science Products, Hofheim, Germany). The electrodes were let to soak for about 10 minutes in a chloriding solution until a dull, dark coating was achieved. The chloriding solution was composed of iron chloride and dilute hydrochloric acid (600 ml distilled H_2O, 300 mg $FeCl_3$, 300 ml HCl). The electrode was rechlorided before every experimental day and occasionally during experiments, to avoid a drift of the pipette potential due to a loss of chloride coating.

2.2.1.5. Whole cell measurements from tsA-201 cells

Cell culture dishes of 3.5 cm diameter were used as a recording chamber. In order to recognize transfected cells, they were incubated with 0.5 ml PBS with 1 µg/µl CD8-antibody coated beads (Dynabeads M-450, Dynal, Oslo, Norway) for 2-3 minutes prior measuring. Only cells marked with beads and green fluorescence (when pCLH-hβ1-EGFP was co-expressed) were chosen for measurements. Usually more than 80% of the cells with those markers showed recordable sodium current. Whole-cell recordings were performed after allowing equilibration between the pipette and the intracellular solutions for 10 minutes (from the membrane rupture). Non-transfected tsA-201 cells can have endogenous sodium currents of usually less than 200 pA. Therefore, only transfected cells with sodium currents larger than 1 nA were taken for evaluation. Series resistance compensation was used and only recordings with a voltage error less than 5 mV were evaluated.

2.2.1.6. Current clamp recordings in primary cultured neurons

Primary cultured rat cortical neurons grew on a poly-D-Lysine coated, 13mm diameter coverslip with a density of 60,000/well. After the neurons had grown in vitro for at lest 14 days, they were transported into a cell culture dish of 3.5 cm diameter filled with bathing solution for whole-cell measurements at room temperature. One neuron per coverslip was chosen for recordings. The whole-cell configuration was obtained at 0 mV in the voltage-clamp mode and program switched immediately into fast current clamp mode. Resting membrane potentials were measured just after the patched membranes were ruptured by suction. After 10 minutes at the resting potential, allowing dialysis between the pipette (containing Biocytin) and the extracellular solutions, a holding potential of -70 mV was adjusted by injecting stepwise hyperpolarizing currents. Currents in a range of -40 to +150 pA (duration: 500-2000 ms) were injected in stepwise for estimating the input resistance and evoking action potentials. The action potential rate-of-rise was determined from the first time derivative of the membrane potential (d*V*/dt), with the spike threshold defined as the membrane potential at which d*V*/dt equals 50 Vs^{-1}. In the phase plane plot, the spike potential was displayed against the first time derivative. Spike width was measured at half maximal spike amplitude, which was defined as the peak relative to the holding potential. Data were low pass filtered at 5 kHz and sampled at 20 kHz. After recording, the pipette was kept attached to neurons for another 15 minutes for sufficient Biocytin diffusion. After obtained an outside-out configuration, neurons were maintained in the recording chamber

for another 30 minutes then fixed at 4°C in 4% PFA for 15 minutes. Immunocytochmistry using antibodies against Biocytin and GAD was performed to determine the morphology and type of the neurons from which recordings had been obtained.

2.2.2. Reagents and solutions

Most reagents were ordered from Sigma-Aldrich (Deisenhofen, Germany). The used solutions are listed below in mM. For whole-cell recordings in tsA-201 cells, the pipette solution contained (in mM): 105 CsF, 35 NaCl, 10 EGTA, 10 HEPES, pH = 7.4. The bathing solution contained (in mM):150 NaCl, 2 KCl, 1.5 $CaCl_2$, 1 $MgCl_2$, 10 HEPES, pH = 7.4. The pH was adjusted to 7.4 using CsOH. For whole-cell recording in primary neurons, the pipette solution contained (in mM): 153.33 KCl, 1 $MgCl_2$, 10 HEPES, 5 EGTA, pH=7.3 with KOH. Biocytin (Molecular Probes, U.S.A.) was added into the pipette solutions in a final concentration of 2 mg/ml for labeling the recorded neuron. The bathing solution contained (in mM): 142 NaCl, 8.09 KCl, 6 $MgCl_2$, 10 Glucose, 10 HEPES, pH=7.4 with NaOH. The osmolarity of the solutions was approximately 300 Osm/kg.

2.2.3. Voltage-clamp protocols and data analysis

2.2.3.1. Voltage dependence of activation

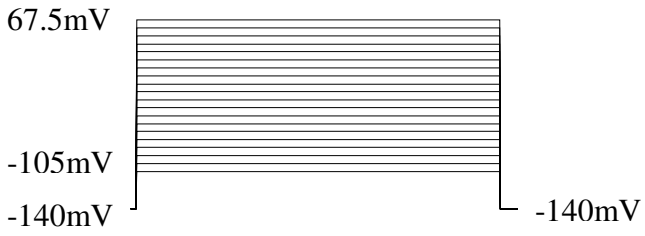

The activation curve (conductance-voltage relationship) was derived from the current-voltage relationship by measuring the peak current at various step depolarizations from a holding potential of –140 mV, and the obtained data was fitted by a Boltzmann function:

g/g_{max} (V) = 1/(1+exp[(V-$V_{1/2}$)/k_V]),

with g = I/(V-V_{rev}) being the conductance, g_{max} the maximal conductance, V_{rev} the Na^+ reversal potential, $V_{1/2}$ the voltage of half-maximal activation, and k_V a slope factor.

2.2.3.2. Steady state fast inactivation

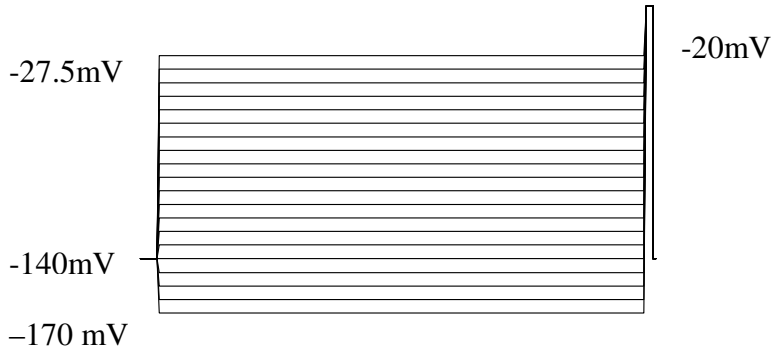

Steady-state inactivation was determined using 300 ms-conditioning pulses to various potentials followed by the test pulse to -20 mV at which the size of the peak current reflected the percentage of non-inactivated channels. Inactivation curves were fitted by a standard Boltzmann function:

I/I_{max} (V) = 1/(1+exp[(V-$V_{1/2}$)/k_V]),

with I_{max} being the maximal current amplitude, $V_{1/2}$ the voltage of half-maximal inactivation, and k_V a slope factor.

2.2.3.3. Inactivation time constants and persistent current

The time course of inactivation was best fit by a second order exponential function yielding two time constants of inactivation.

$$I(t) = A_f \exp[-(t - t_0)\tau_f] + A_s \exp[-(t - t_0)/\tau_S] + C$$

The weight of the second slower time constant was relatively small (0-25%). To describe the defects of inactivation in the results section, only the fast time constant was therefore used, which was termed τ_h. Persistent Na^+ currents (I_{ss}, for 'steady-state' current), were determined at the end of 70 ms-lasting depolarizing pulses to 0 mV and are given relative to the initial peak current (I_{peak}).

2.2.3.4. Recovery from fast inactivation

Recovery from fast inactivation was recorded from a holding potential of -140 mV. Cells were depolarized to -20 mV for 100 ms to inactivate all Na^+ channels and then repolarized to various recovery potentials -80/–100/-120 mV for increasing durations. The time course of recovery from inactivation, which was termed $\tau_{rec,}$ was best fitted to a first or second order exponential function with an initial delay.

2.2.3.5. Steady state slow inactivation

Entry into, recovery from and steady-state slow inactivation were characterized using cumulative protocols (Alekov et al., 2001). For steady-state slow inactivation 30 s-conditioning pulses starting at –140 mV and stepping by 10 mV increasingly to 10 mV were used, which each were followed by a 20 ms-hyperpolarization to –140 mV (to let the channels recover from fast inactivation) and the 5 ms-test pulse to -20 mV. Curves were fitted to a standard Boltzmann function:

$I/I_{max}=1/(1+exp[(V-V_{0.5})/k_V])$,

as for fast inactivation (see above).

2.2.3.6. Entry into slow inactivation

To measure the entry, cells were held at –140 mV, depolarized to 0 mV for increasing duration, repolarized for 100 ms to –100 mV to let the channels recover from fast inactivation, and then depolarized again shortly for 3 ms to determine the fraction of slow inactivated channels without inducing further slow inactivation. The time course of slow inactivation was well fitted by a first order exponential function.

2.2.3.7. Recovery from slow inactivation

Recovery from slow inactivation was measured for different time points at -120 mV after a 30 s-conditioning pulse to 0 mV. Curves were fitted by a second order exponential function.

2.2.3.8. Subtraction of leak and capacitive currents

The protocols used to characterize electrophysiological properties of the Na^+ channels generally included a protocol to subtract leak and capacitive currents. Four hyperpolarizing prepulses from a holding potential of -120mV, with a fourth of the amplitude of the test pulse (P/4) were applied before each test pulse. At these voltages no Na^+ channel opens. The sum of the recorded currents during the P/4 prepulses is subtracted from the current recorded during the test pulse. The leak current depends linearly on the voltage; therefore the sum of the four prepulse elicited currents equals the leak current during the test pulse.

2.2.4. Statistics

All data are shown as means ± standard error of the mean (S.E.M.) if not indicated otherwise. Independent Student´s *t*-test was used to test for statistically significant differences. Statistically significance requires the p value less than 0.05.

2.3. Immunocytochemistry

Immunocytochemistry is a common method to target proteins in the intact cells using specific primary antibodies. There are many methods to perform immunological staining including direct and indirect methods. In indirect staining, which was performed in this study, the antigen reacts directly with a primary antibody which binds directly to the antigen, followed by a fluorescence labeled secondary antibody which binds to the primary antibody.

Primary cultured neurons grown on a 13 mm diameter glass cover slip were fixed at 4°C with 4% PFA and incubated for 2 hours in block medium (PBS with 0,2% Triton-X100 and 3% normal goat serum) at room temperature. After a PBS washing step, neurons were incubated with a monoclonal antibody against glutamate decarboxylase (GAD_{67}) (Chemicon, Millipore, International), dilution: 1:1000 at 4°C over night, on the next day the preparation was incubated with secondary Alexa 488-conjugated goat anti mouse antibodies (1:500) (Molecular Probes, U.S.A.) and cy3-conjugated Streptavidin (Jackson ImmunoResearch Laboratories, Inc. U.S.A.) dilution (1:1000) for 1 hour at room temperature. Neurons were exposed to 4', 6-diamidino -2-phenylindole (DAPI, dilution 1:5000) for 2 minutes, in order to stain the nuclei. Cells were mounted with Vecta Shield mounting medium (Vector Laboratories, U.S.A.) and visualized on an Axiovision 2 plus microscope (Zeiss, Germany).

3. Functional modification of $Na_v1.1$ channel by ß1 and ß2 subunits and functional characterization of the $GEFS^+$ associated mutation R1648H

The aim of this study was to investigate the differential functional modulation of $Na_v1.1$ WT and R1648H mutant sodium channel gating by β1 and β2 subunits, and the functional defects caused by the $GEFS^+$ associated mutation R1648H. The WT or R1648H mutant α subunit alone or together with β1 and/or β2 subunits was transiently transfected in tsA- 201 cells and electrophysiologically characterized. Families of whole-cell current elicited by various voltage steps from a holding potential of -140 mV are shown in Fig. 1. In order to determine the functional modification by β1 and β2 subunits, the kinetics and voltage dependence of activation, fast inactivation and slow inactivation of sodium channels were investigated.

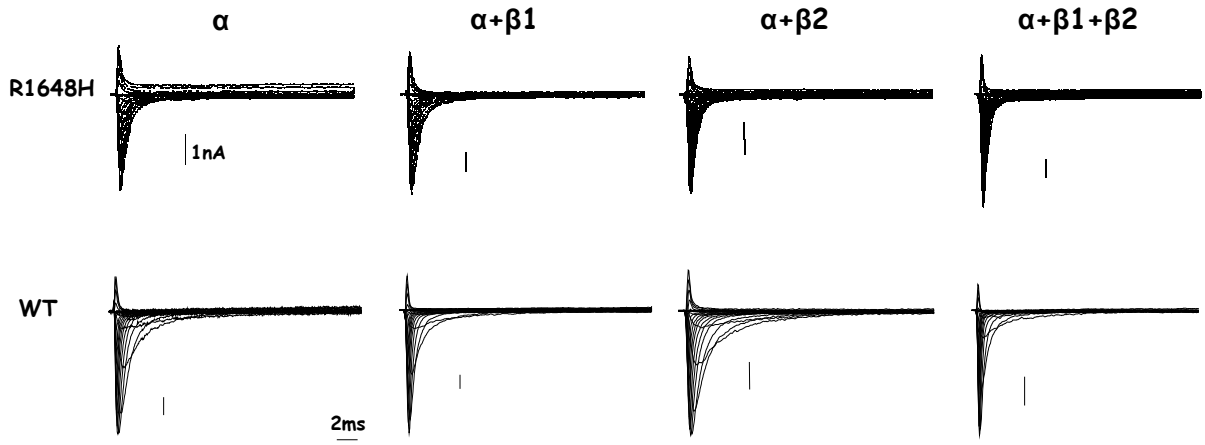

Figure 3.1: Typical whole-cell sodium current recordings of $Na_v1.1$ WT channels and R1648H mutant channels with or without β subunits. Sodium currents elicited by various membrane potentials between -105 and +67.5 mV stepping from a holding potential of -140 mV.

3.1. β subunits modify the gating of the $Na_v1.1$ WT channel

$Na_v1.1$ (encoding gene: *SCN1A*) WT Sodium channels containing α subunits alone or co-expressed with β subunits activated and inactivated rapidly in tsA-201 cells (Fig. 3.1), as previously observed in mammalian cells (Scheuer et al., 1990; West et al., 1992; Ukomadu

et al., 1992). Co-expression of β1 or β2 subunits did not significantly alter the $V_{1/2}$ of sodium channel activation and inactivation. Co-expressing with β1 subunit increased the slope of the voltage dependence of both activation (-6.2±0.1 vs. -4.8±0.4, n=10, 9, p<0.01, Tab. 3.1, Fig.3.2 A) and inactivation (5.6±0.3 vs. 4.8±0.1, n=10, 8, p<0.05, Tab. 3.1, Fig. 3.2 B), whereas co-expression with both β subunits steepened only the slope of voltage dependence of steady-state activation (-6.2±0.1 vs. -4.6±0.4, n=10, 7, p<0.001, Tab. 3.1, Fig. 3.2 A).

The time course of fast inactivation and recovery from fast inactivation was not significantly altered by the β2 subunit, but co-expression with the β1 subunit accelerated the fast inactivation time course (0.26±0.00 ms vs. 0.19±0.01 ms, n=8, 8, p<0.01, Tab.3.2, Fig.3.3 B). Co-expression of both β subunits accelerated both fast inactivation time course (0.26±0.00 ms vs. 0.20±0.01 ms, n=8, 7, p<0.01, Tab. 3.2, Fig.3.3 B) and recovery from fast inactivation (6.1±0.3 ms vs. 3.4±0.4 ms, n=5, 6, p<0.001, Tab. 3.2, Fig. 3.3A). Thus, co-expression of either β1 alone or both β subunits regulated the kinetics of $Na_v1.1$ WT channel gating into a faster manner, which could increase neuronal excitability. Co-expression of β1 and/or β2 subunits did not affect the level of persistent sodium currents remaining after 70 ms of the test pulse.

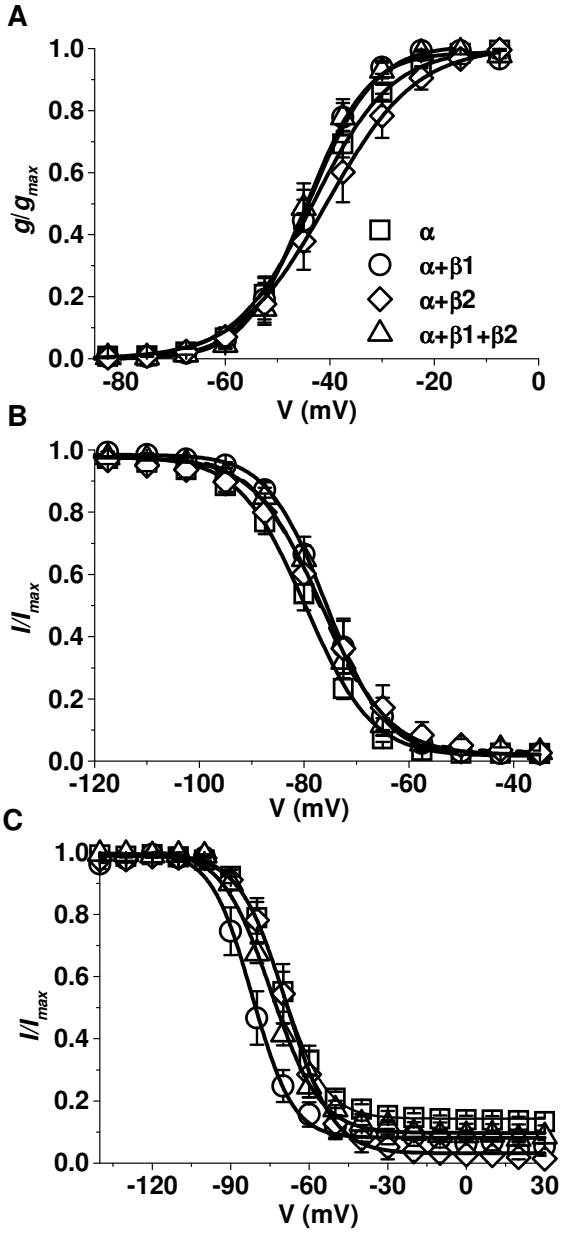

Figure 3.2: Co-expression of β1 or/ and β2 subunits modulate the voltage dependence of activation and inactivation of Nav1.1 WT. α subunits alone: square; α+β1 subunits: circle; α+β2: diamonds;

α+β1+β2: triangle. *A*: voltage dependence of activation; *B*: voltage dependence of steady-state inactivation; *C*: voltage dependence of slow inactivation.

The voltage dependence of steady-state slow inactivation was shifted in the hyperpolarizing direction when co-expressed with β1 subunit (-70.7±2.3 mV vs. -81.4±1.9 mV, n=7, 6, p<0.01, Tab. 3.1, Fig. 3.2C). This stabilization of the slow inactivated state indicated by -10mV shift in the voltage dependence would decrease the number of excitable channels. When co-expressed with both β subunits, no significant change in voltage dependence of slow inactivation was observed.

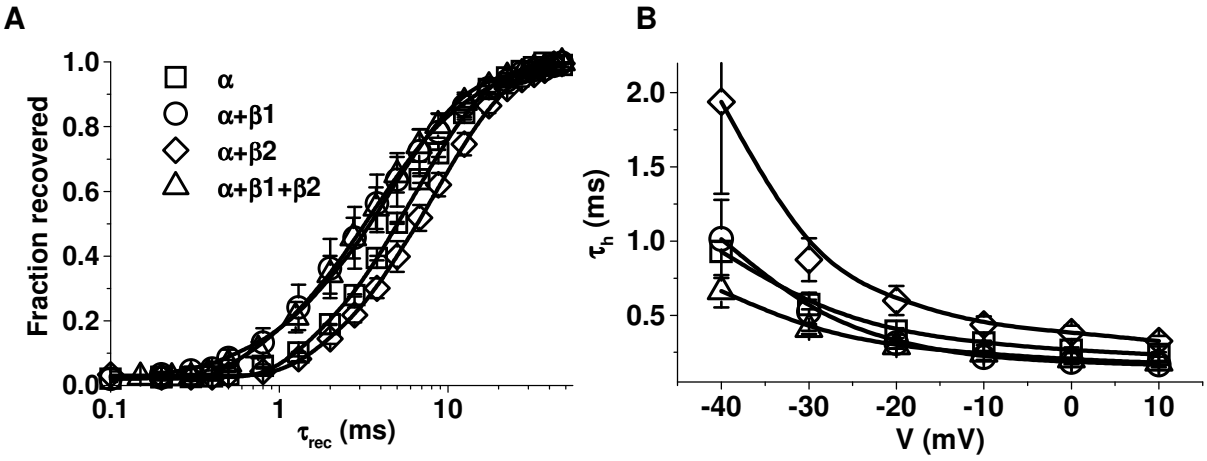

Figure 3.3: Co-expression of β1 or/ and β2 subunits modulate the kinetics of $Na_v1.1$ WT channel gating. α subunits alone: square; α+β1 subunits: circle; α+β2: diamonds; α+β1+β2: triangle. *A*: recovery from fast inactivation; *B*: voltage dependence of fast inactivation time constant.

3.2. Functional defects caused by the R1648H mutation

The R1648H mutation, which is located in the S4 voltage sensor of domain IV, was identified in $Na_v1.1$ (gene: *SCN1A*) in a family with $GEFS^+$ (Escayg et al., 2000). This mutation has been first functionally characterized at the corresponding site in the human skeletal muscle sodium channel, $Na_v1.4$, when the α subunit alone was transiently expressed in tsA-201 cells (Alekov et al., 2001). Later, R1648H was introduced into the human brain sodium channel $Na_v1.1$ and co-expressed with β1 and β2 subunits in tsA-201 cells (Lossin et al., 2002). Since these two studies revealed a striking difference in

persistent Na^+ current (no persistent current in $Na_v1.4$ compared with the WT, significant persistent current in mutant Nav1.1 compared to WT channels), R1648H was studied here in $hNa_v1.1$, exploring the effects of both beta subunits. Electrophysiological properties were studied using whole-cell patch clamp technique.

When the α subunit was expressed alone, the R1648H mutant channel did not affect the $V_{1/2}$ of channel steady-state activation and fast inactivation. However, it significantly decreased the slope of the voltage dependence of both activation (-6.2±0.1 vs. -7.3±0.2, n=10, 8, p<0.001, Tab.3.1, Fig.3.4A) and fast inactivation (5.6±0.3 vs. 7.4±0.2, n=10, 7, p<0.001, Tab.3.1). When co-expressed with the β1 subunit, the differences in slope factor were similar (Tab.3.1) and the voltage dependence of fast inactivation was shifted to more depolarized potentials. When co-expressed with β2 subunit or co-expressed with both β subunits, only the slope factor of the inactivation curve was increased (Tab.3.1). The co-expression with both β subunits also shifted the voltage dependence of fast inactivation to positive potential. These changes in activation and inactivation could lead to an increased window current increasing the neuronal excitability.

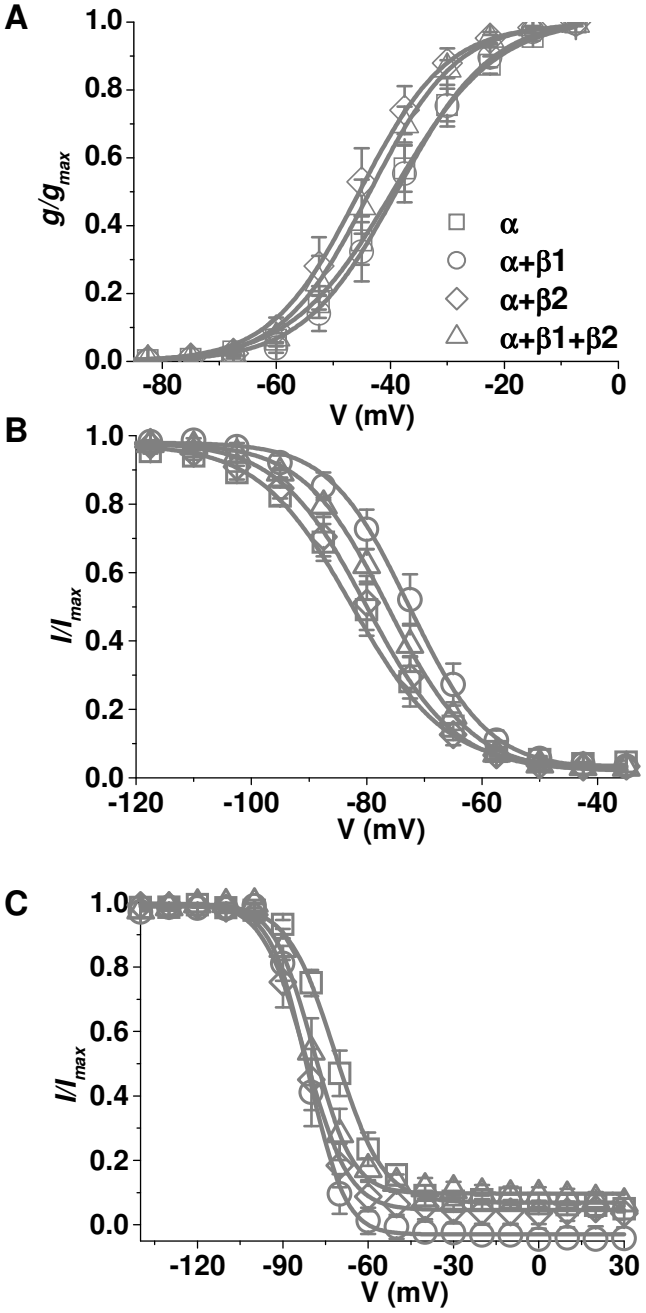

Figure 3.4: Co-expression of β1 or/ and β2 subunits modulate the voltage dependence of activation and inactivation of R1648H mutant channel. α subunits alone: square; α+β1 subunits: circle; α+β2: diamonds; α+β1+β2: triangle. *A*: voltage dependence of activation; *B*: voltage dependence of steady-state inactivation; *C*: voltage dependence of slow inactivation.

Compared with WT channels, the R1648H mutant channel displayed a slowed time course of fast inactivation with or without co-expression of β subunits (Tab.3.2) and a marked decrease of its voltage dependence. The loss of voltage dependence, which has been shown in other DIVS4 mutations, may indicate an uncoupling of inactivation from activation (Chahine et al., 1994; Lerche et al., 1996; Mitrovic et al., 1996). Recovery from fast inactivation at -100 mV was significantly accelerated for R1648H mutant channels with or without β subunits (Tab.3.2). The persistent sodium current at 0 mV after a 70 ms test pulse was significantly increased for R1648H mutant channels with or without β subunits (Tab.3.2). These gain-of-function defects could lead to a hyperexcitability of neurons.

Table 3.1: Electrophysiological properties of *SCN1A* WT and the R1648H mutant channels

	$V_{1/2\ activ.}$ (mV)	k	n	$V_{1/2\ inactiv.}$ (mV)	k	n	$V_{1/2\ SI}$ (mV)	k	n
WT α	-43.5±1.3	-6.2±0.1	10	-79.7±1.3	5.6±0.3	10	-70.7±2.3	7.6±0.4	7
α+β1	-44.6±1.3	-4.8±0.4**	9	-75.7±2.0	4.8±0.1*	8	-81.4±1.9**	6.8±0.3	6
α+β2	-42.9±1.6	-6.2±0.6	5	-78.6±1.8	5.7±0.4	5	-68.7±2.5	8.0±0.5	5
α+β1+β2	-44.3±1.6	-4.6±0.4***	7	-77.1±1.0	5.5±0.4	6	-74.6±1.2	8.5±0.8	3
RH α	-39.9±2.3	-7.3±0.2###	8	-82.6±2.2	7.4±0.2###	7	-71.5±2.0	7.3±0.6	6
α+β1	-39.1±2.7	-6.1±0.2**#	8	-72.7±2.3**	6.2±0.3**#	8	-81.2±2.0*	5.3±0.3	3
α+β2	-45.6±2.8	-6.1±0.3**	9	-80-0±2.3	7.0±0.3##	7	-81.9±2.3*#	6.5±0.5	3
α+β1+β2	-43.6±2.0	-5.8±0.4**	9	-76.3±1.7*	6.7±0.3#	9	-79.3±2.9	5.8±0.3##	4

Values for $V_{1/2}$, the voltage of half-maximal activation and inactivation, and the slope factor k_V were derived from Boltzmann fits to activation and inactivation curves (see Materials and Methods). Significance levels are indicated as follows:*/# p<0.05, **/ ## p<0.01, ***/ ### p<0.001. Where * corresponds to a comparison with the α subunit, and # corresponds to a comparison with the WT channel.

Only when co-expressed with the β2 subunit, the voltage dependence of slow inactivation was shifted towards hyperpolarized potentials for the R1648H mutation (-68.7±2.5 mV vs. -81.9±2.3 mV, n=5, 3, p<0.05, Tab.3.1). When co-expressed with both β subunits, the slope of the slow inactivation curve for R1648H mutant channels was steepened (8.5±0.8 vs. 5.8±0.3, n=3, 4, p<0.01, Tab. 3.1).

3.3. Co-expression of β subunits refines the effects of R1648H mutation on $Na_v1.1$ channel gating

The β1 and β2 subunits modified gating defects in $Na_v1.1$ channel caused by the R1648H mutation in various aspects. According to their modulating effects on $Na_v1.1$ WT channel gating, co-expression with β subunits steepened the voltage dependence of activation and inactivation for R1648H mutant channels, which resulted in no difference or less difference between WT and mutant channels (Tab.3.1). This effect was mainly due to co-expression of the β1 subunit. Whereas no significant difference was found in voltage dependence of steady-state slow inactivation between the WT and the R1648H mutant channel, when only the α subunit was expressed, co-expression of the β1 subunit resulted in a hyperpolarizing shift of approximately 10 mV for both WT and R1648H mutant channel (Tab.3.1). However, a hyperpolarizing shift caused by co-expression with the β2 subunits was only displayed in the R1648H mutant channel, which led to a significant difference between the WT and the mutant channel.

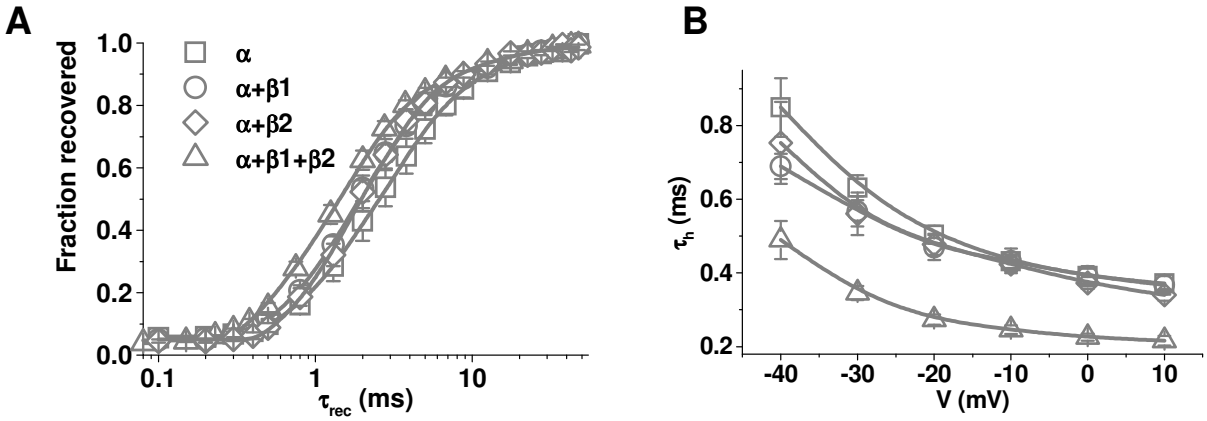

Figure 3.5: Co-expression of β1 and/or β2 subunits modulates the kinetics of R1648H mutant channel gating. α subunits alone (square), α+β1 subunits (circle), α+β2 (diamonds), α+β1+β2 (triangle) A: recovery from fast inactivation B: voltage dependence of the fast inactivation time constant τ_h.

Compared with the WT channel, the time constant of fast inactivation of the R1648H mutant channel is less voltage-dependent. This has been described for other mutations in the IV/S4 domain and may indicate an uncoupling of inactivation from activation (Chahine et al., 1994; Lerche et al., 1996; Mitrovic et al., 1999). The largest difference of the

inactivation time course was displayed when only the β1 subunit was co-expressed and the difference was minimal when both β subunits were co-expressed.

Table 3.2: Kinetics of *SCN1A* WT and R1648H mutant channel gating

	τ_h at 0mV (ms)	n	$\tau_{rec.}$ at -100mV (ms)	n	I_{ss} at 0mV (in %)	n
WT α	0.26±0.00	8	6.1±0.3	5	1.3±0.2	8
α+β1	0.19±0.01**	8	5.0±1.1	6	1.0±0.1	6
α+β2	0.33±0.02	5	8.6±1.0	5	1.8±0.3	4
α+β1+β2	0.20±0.01**	7	3.4±0.4***	6	1.3±0.2	4
RH α	0.39±0.02###	7	3.5±0.6##	7	3.2±0.4###	6
α+β1	0.39±0.03###	5	2.1±0.2#	7	3.4±0.2###	3
α+β2	0.37±0.02	6	2.2±0.4##	6	2.8±0.2#	3
α+β1+β2	0.23±0.01***#	6	1.4±0.1***###	7	2.8±0.3#	6

Fast inactivation time constants were determined by fitting a second order exponential function to the data points, only the fast time constant is shown here. The time constant of recovery from fast inactivation was determined by fitting a first order exponential function with an initial delay to the data points. The steady-state non-inactivating sodium current is shown here in % of the peak current (see Materials and Methods). Significance levels are indicated as follows: */# $p<0.05$, **/## $p<0.01$, ***/### $p<0.001$.Where * corresponds to a comparison with the α subunit, and # corresponds to a comparison with the WT channel.

The R1648H mutation enhanced the persistent sodium current after 70 ms in different test potentials (Tab. 3.2, Fig. 3.6). When the α subunit was expressed alone or co-expressed with the β1 subunit, the mutant channel displayed the most pronounced persistent current compared to the WT. Co-expression with the β2 or both β subunits resulted in a less marked persistent current level at all test potentials.

Co-expression of both β1 and β2 subunits lowered the level of differences in the time course of fast inactivation and persistent current between WT and R1648H mutant channels, which were the most prominent defects caused by R1648H mutation.

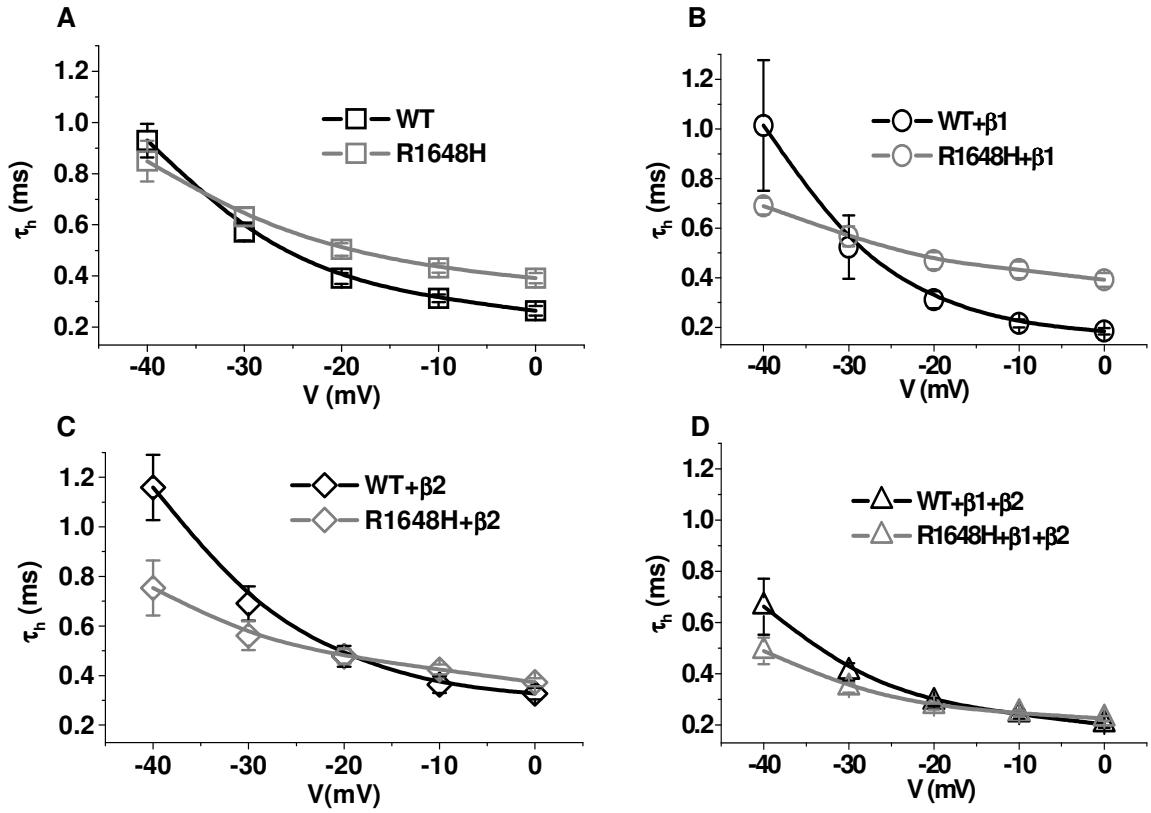

Figure 3.6: co-expression of β subunits modified the voltage dependence of the time course of fast inactivation. *SCN1A* WT (black), R1648H mutant channel (grey) A: α subunits alone B: α+β1 C: α+β2 D: α+β1+β2

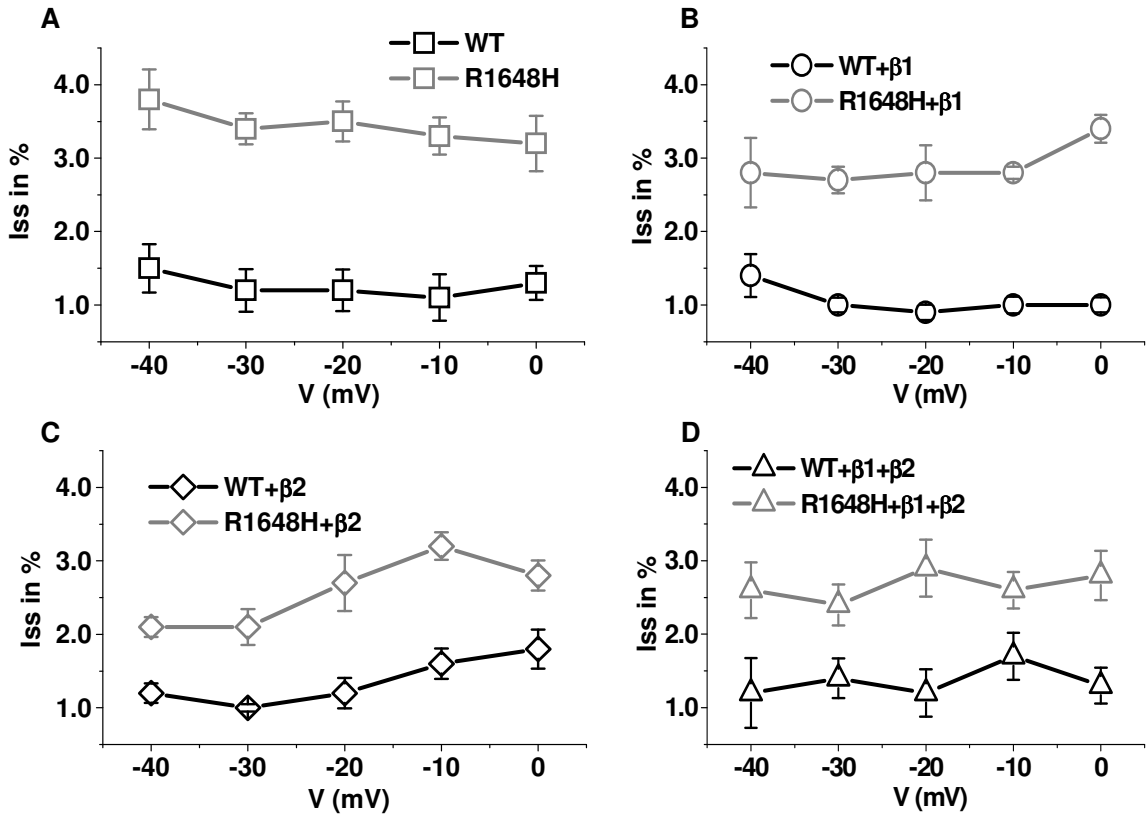

Figure 3.7: co-expression of β subunits modified the persistent sodium current levels in different test potentials. *SCN1A* WT (black), R1648H mutant channel (grey) A: α subunits alone B: α+β1 C: α+β2 D: α+β1+β2

4. Three novel mutations in *SCN2A* associated with BFNIS

In the present study, three novel *SCN2A* mutations associated with benign familial neonatal infantile seizures (BFNIS), M252V, V261M, A263V, were functional investigated. The clinical investigations were done by our collaborators (Deprez et al., group of Prof. P. De Jonghe in Antwerp and Anttonen et al., group of Prof. A-E Lehesjoki in Helsinki).

The M252V mutation was present in the proband of a Bulgarian BFNIS family. His sister and maternal grandfather, who both had BFNIS, and his asymptomatic mother also carried the mutation (Fig. 4.1). The M252V mutation was absent from 200 Bulgarian control individuals. The V261M mutation was found in a Finnish patient with BINS. The unaffected parents of the patient did not carry the mutation and paternity was confirmed demonstrating that the mutation arose *de novo* (Fig. 4.1). The mutation was also not present in 210 Finnish control individuals. The clinical phenotypes of the patients carrying these mutations are summarized in the Tab. 4.1 (Deprez et al.).

The mutation A263V was carried by a patient with typical neonatal seizures and later generating episodic ataxia. The patient's epilepsy started at the age of two days as repeated tonic seizures when he was observed to be neurologically abnormal with poor muscular tonus. The seizures continued in infancy as frequent tonic-clonic seizures. On phenobarbital and phenytoin he was seizure-free since age 1.25 years. Some tonic-clonic seizures have later occurred. His development progressed favorably being mentally at nearly normal level with dyspractic problems. At the age of 1.5 years he started to have intermittent periods of poor balance, stumbling and falling, without disturbance of consciousness or positive motor symptoms lasting from some minutes to one hour. Occasionally he also has tremor or muscle-twitch-like movements. During attacks the muscle strength and deep tendon reflexes are normal. On video-EEG recording during the attack either no epileptiform activity or slight abnormality in frontocentral areas was observed together with myoclonia. Interictal EEG has been normal or slightly abnormal with spikes in fronto-central midline. No abnormalities were observed in blood chemistry, metabolic screens, ENMG and spinal MRI. In latest MRI at the age of 5 years mild cerebellar atrophy was observed. Sodium valproate, acetazolamide, oxcarbamazepine, gabapentin, clobazam, levetiracetam and topiramate have been tried with no effect on the symptoms. Acute medication with diazepam, anti-inflammatory drugs and sumatriptan has

not been helpful. He continuously experiences one to three attacks per month (Anttonen et al.).

Table 4.1: Clinical features of patients with M252V or V261M mutation.

	M252V	**V261M**
Gender	male	male
Nationality	Bulgarian	Finnish
Status at birth	normal	normal
Family history		
-Consanguinity	no	no
-Epilepsy	sister and maternal grandfather: infantile seizures	no
First seizure		
-Onset age	day 6	day 2
-Type	multiple generalized seizures	unilateral jerks
-Fever-associated	no	no
-Other features	eye deviation, sweating and blushing	no
Other seizures	no	yes
-Type		apneas, atypical absences
Age of remission	day 7	3 mo
EEG	normal	multispike bursts, irritative activity, no focal findings
Epilepsy later in life	no	no
Other features		
-Psychomotor development	normal	normal
-Other abnormalities	no	no
Age last examination	3 y	1 y
Current age	4.5 y	5 y
Familial diagnosis	BFNIS	BINS

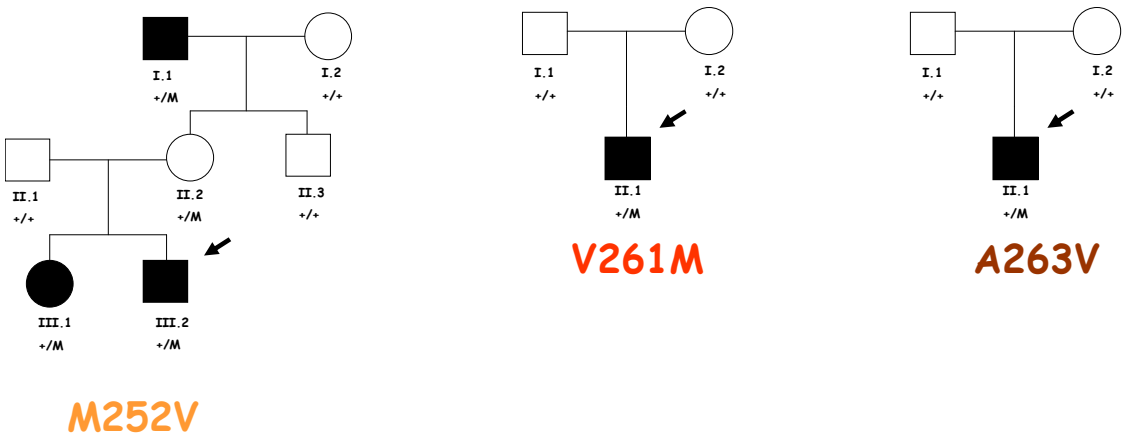

Figure 4.1: Pedigrees of the three novel *SCN2A* mutations associated with BFNIS. The arrows indicated the probands. Filled symbols: individuals with epileptic seizures during the first year of life. The genotype is indicated by (+) for wild type, by (M) for the mutation.

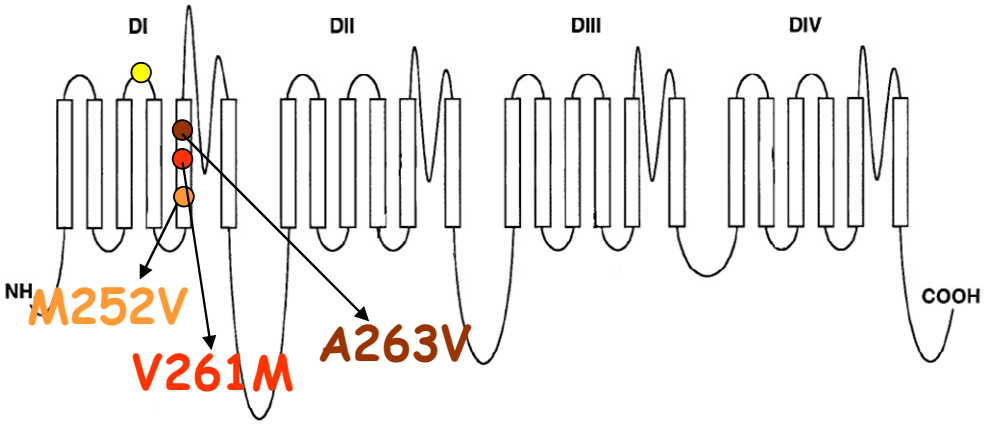

Figure 4.2: Three novel BFNIS mutations. The position of three identified BFNIS mutations is displayed on the schematic membrane topology of the $Na_v1.2$ channel α subunit. The single amino acid difference between the neonatal and the adult splice variant is shown in a yellow circle.

These three novel *SCN2A* mutations associated with benign familial neonatal infantile seizures (BFNIS) are all located in the segment 5 of domain I (Fig. 4.2). Developmentally regulated neonatal and adult isoforms of the sodium channel $Na_v1.2$ have been identified in the human brain (Kasai et al., 2001). Molecular analysis of the $Na_v1.2$ neonatal and adult isoforms has revealed multiple nucleotide differences, but only a single difference at the amino acid level. The functional difference between these two isoforms remains still unclear. The present study focuses on the following goals: first, to investigate the function

of both the $Na_v1.2$ neonatal and adult isoforms. Sodium channel $Na_v1.2$ α subunits were transiently transfected into tsA-201 cells with or without β subunits. Their electrophysiological properties were studied by the whole-cell patch clamp technique. The second aim is to determine the functional consequences caused by three novel BFNIS mutations. Mutations were introduced into the human *SCN2A* cDNAs in both the neonatal und adult splice forms. Then WT or mutant plasmids with their two auxiliary β subunits were transiently transfected into tsA-201 cells for electrophysiological measurements.

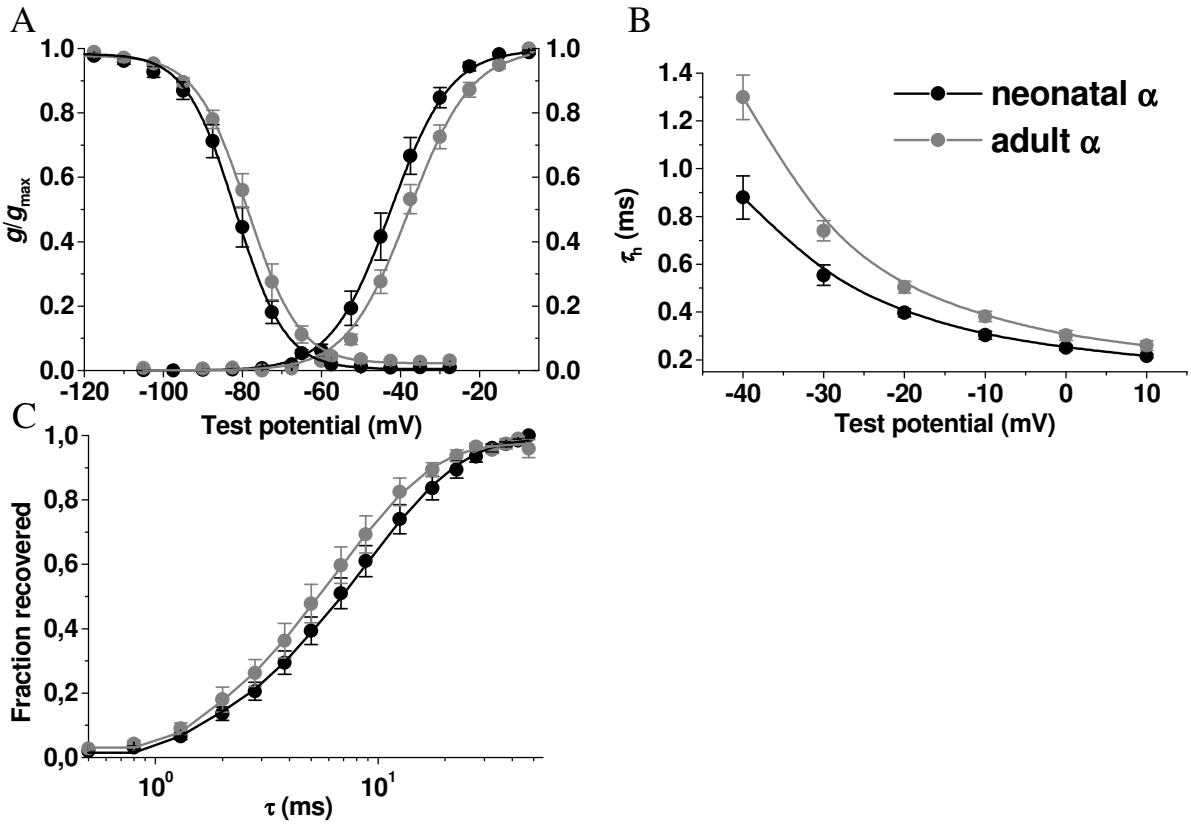

Figure 4.3: Electrophysiological properties of *SCN2A* channels. A: voltage dependence of sodium channel steady-state activation and inactivation (*SCN2A* neonatal channel: black circle, adult channel: grey circle). *B*: voltage dependence of fast inactivation time constants. *C*: recovery from fast inactivation at a membrane potential of -100 mV.

4.1. Alternative splicing of $Na_v1.2$

When only the α subunits were expressed, no difference was found in the average current density between neonatal and adult channels (Tab. 4.2). However, compared to the

neonatal $Na_v1.2$ channels, the voltage dependences of channel activation and steady state fast inactivation for adult channels were slightly shifted towards more depolarized potentials.

Table 4.2: Electrophysiological properties of *SCN2A* WT neonatal and adult channels

	SCN2A WT α subunit alone					with β 1 and β 2 subunits			
	Neonatal	**n**	**Adult**	**n**		**Neonatal**	**n**	**Adult**	**n**
$V_{1/2\ activ.}$ (mV)	-42.6±1.9	13	-37.7±1.4	10		-41.9±1.3	15	-43.3±1.4#	12
k	-5.5±0.3	13	-6.9±0.2**	10		-4.8±0.3	15	-5.6±0.4#	12
$V_{1/2\ inactiv.}$ (mV)	-81.7±1.5	11	-78.7±1.5	7		-75.5±1.1##	11	-77.9±1.4	9
k	5.6±0.2	11	5.8±0.3	7		5.1±0.1	11	4.5±0.1##	9
τ_{rec} at -100mV (ms)	9.4±1.4	9	6.6±1.2	4		4.8±0.4##	10	6.6±0.7	9
Iss at 0 mV	1.1±0.2%	5	0.7±0.2%	8		0.9±0.1%	6	0.8±0.1%	7
τ_h slow at 0mV (ms)	3.66±0.72	8	4.8 ±1.4	10		4.78 ±1.14	10	3.96±0.83	10
τ_h fast at 0mV (ms)	0.25±0.01	8	0.30±0.02	10		0.24±0.01	11	0.24±0.01	10
current density (A/F)	-334.6±95.3	11	-362.4±102.9	10		-806.2±173.1#	16	-800.8±207.5	17

Values for $V_{1/2}$, the voltage of half-maximal activation and inactivation, and the slope factor k_V were derived from Boltzmann fits to activation and inactivation curves. Fast inactivation time constants were fitted to a second order exponentials function. The time constant of recovery from fast inactivation was fitted to a first order exponential function with an initial delay (see Materials and Methods). Significance levels are indicated as follows: */# $p<0.05$, **/## $p<0.01$. Where *corresponds to a comparison with neonatal channels. # corresponds a comparison with the α subunit.

The fast inactivation time course for the neonatal $Na_v1.2$ channels was significantly accelerated compared to adult channels at potentials between -40 and -10 mV (Fig. 4.3 B), suggesting that adult channels inactivate more slowly than neonatal channels. The rates of recovery from fast and slow inactivation for adult channels were increased compared to neonatal channels, although the differences were not significant (Tab. 4.2 and Fig. 4.3 C).

Nevertheless, differences between the two $Na_v1.2$ splice variants were minimized when co-expressed with their auxiliary β subunits. Co-expression with two β subunits shifted the inactivation curve of the neonatal channel towards depolarization, accelerated recovery from steady-state fast inactivation and slowed recovery from slow inactivation. For adult channels, co-expression of β subunits altered the voltage dependences of channel activation,

fast and slow inactivation. No significant difference was found between neonatal and adult channels in current density, voltage dependences or kinetics of channel gating (Tab. 4.2).

In summary, some minor differences would be detected between neonatal and adult isoforms, when recording currents derived from α subunits, but not in the presence of β subunits.

4.2. Functional characterization of mutation M252V

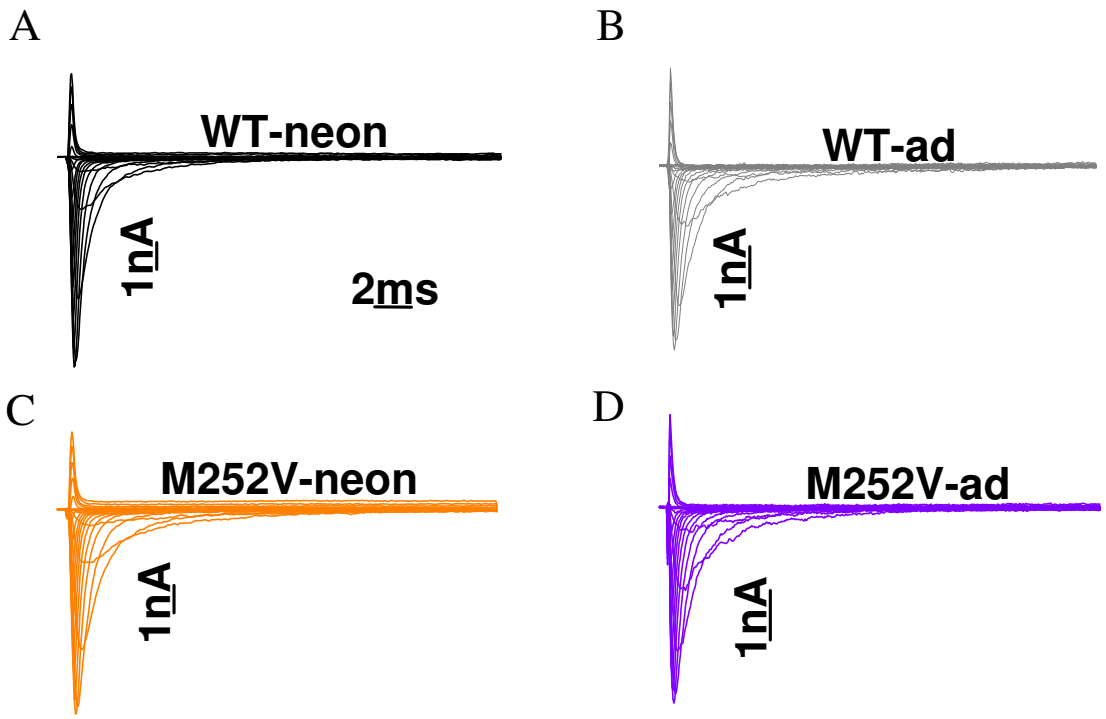

Figure 4.4: Representative WT and M252V whole-cell *SCN2A* sodium currents. *A*: typical sodium current recording of the WT neonatal channel; *B*: WT adult channel; *C*: M252V neonatal channel; *D*: M252V adult channel. Sodium currents elicited by various depolarization steps ranging from -105 to +67.5 mV, from a holding potential of -140 mV.

Typical whole-cell sodium current recordings for WT and M252V mutant channels (in the background of neonatal or adult splice variants) elicited by various depolarizing voltage steps from a holding potential of -140 mV are shown in Fig. 4.4. All clones exhibited robust, rapidly activating and inactivating inward currents. The most obvious result was on the enhanced persistent sodium current that was preferentially observed for the mutant M252V in background of the neonatal splice variant (0.8±0.0% vs. 1.8% ± 0.1%, n=8, 12, $p<0.001$, Fig. 4.5 A). The smaller difference between Wt and mutant channels did not

reach statistical significance in the background of the adult splice variant. This non-inactivating sodium current was evident during a longer test depolarization (70 ms) and could be reversibly and completely blocked by the application of 10 nM TTX, thus excluding a leak current.

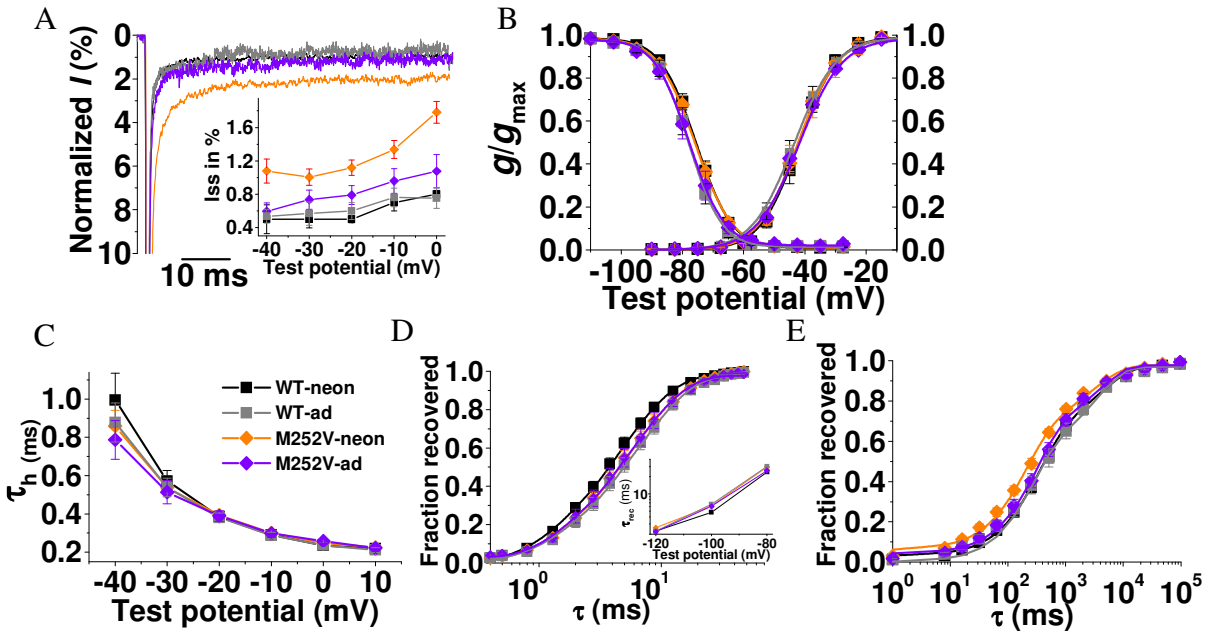

Figure 4.5: Electrophysiological properties of M252V mutant channel. *A:* Representative *SCN2A* WT and M252V mutant TTX sensitive sodium currents. Currents were recorded at the end of a 70-ms depolarization to 0 mV from a holding potential of -140 mV and normalized to the peak current amplitude. The voltage dependence of the persistent current is shown in the inset. *B*: voltage dependence of steady-state sodium channel activation and inactivation. Values of membrane potential for half-maximal activation, inactivation and slope factors are shown in Table 4.3. *C*: voltage dependence of fast inactivation time constants for WT and M252V mutant channels. *D*: recovery from fast inactivation at a membrane potential of -100 mV. The inset shows the voltage dependence of τ_{rec}. *E*: recovery from slow inactivation at a membrane potential of -120 mV.

No significant difference was observed in the voltage dependences of channel activation and inactivation between WT and the M252V mutant channels in either neonatal or adult splice variants (Tab. 4.3, Fig. 4.5 B). The mutation had no significant effect on the kinetics of channel fast inactivation (Tab. 4.3, Fig. 4.5 C and D).

Steady state and entry into slow inactivation were not significantly influenced by the M252V mutation. The time course of recovery from slow inactivation of WT and the

M252V mutant channels is showed in Fig. 4.4 E. When expressed in neonatal splice variants, the M252V channels began to recover from slow inactivation at the first ms, whereas the WT channels recovered very little. The time constant for recovery from slow inactivation, was significantly decreased compared to WT channels (373.0±32.0 vs. 218.6±27.7 ms, n=7, 7, p<0.01, Tab. 4.3, Fig. 4.5 E).

Defects caused by the M252V mutation were only found in its neonatal form: enhanced persistent current and accelerated recovery from slow inactivation. These gain-of-functions observed for the neonatal splice variant could lead to a neuronal hyperexcitability, which may explain seizures occurring in an early stage of development.

Table 4.3: Electrophysiological properties of *SCN2A* WT and the mutant channels

	$V_{1/2\ activ.}$ (mV)	k	n	$V_{1/2\ inactiv.}$ (mV)	k	n	τ_h at 0mV (ms)	n	τ_{rec} at -100mV (ms)	n
WT neon	-41.9±1.3	-4.8±0.3	15	-75.5±1.1	5.1±0.1	11	0.24±0.01	11	4.8±0.4	10
M252V neon	-42.3±1.2	-5.2±0.2	15	-75.9±1.1	5.3±0.2	12	0.25±0.01	13	6.2±0.6	13
V261M neon	-41.0±0.9	**-6.4±0.5##**	11	-77.8±0.6	5.2±0.2	9	0.25±0.02	10	**3.4±0.2##**	11
A263V neon	-40.4±1.0	**-6.8±0.3###**	15	-74.0±1.1	**6.4±0.4##**	12	**0.33±0.02###**	11	6.1±0.6	13
WT ad	-43.3±1.4	-5.6±0.4	12	-77.9±1.4	4.5±0.1	9	0.24±0.01	10	6.6±0.7	9
M252V ad	-42.3±1.8	-5.5±0.4	11	-77.8±1.7	4.8±0.2	10	0.26±0.01	10	6.1±0.8	8
V261M ad	-41.8±1.3	**-6.7±0.2#**	10	-79.5±1.1	**5.8±0.2###**	10	**0.33±0.03##**	8	**4.6±0.3#**	10
A263V ad	**-36.4±1.4##**	**-6.3±0.2**	13	**-71.2±1.5##**	**5.2±0.1###**	13	**0.42±0.03###**	9	5.5±0.8	10

Values for $V_{1/2}$, the voltage of half-maximal activation and inactivation, and the slope factor k_V were derived from Boltzmann fits to activation and inactivation curves. Fast inactivation time constants were fitted with a second order exponentials function with an initial delay, only the fast time constants were shown here. The time constant of recovery was fitted with a first order exponential function with an initial delay (see Materials and Methods). # corresponds a comparison with the WT channel. Significance levels are indicated as follows: # p<0.05, ## p<0.01, ### p<0.001

4.3. Functional determination of mutation V261M

Typical whole cell sodium channel recordings from the mutation V261M in the background of neonatal or adult splice variants are displayed in Fig. 4.6 A and B. In contrast to the M252V mutant channel, a nearly 2-fold enhanced persistent sodium current were observed not in neonatal but in adult V261M mutant channel compared to the WT (0.8±0.1% vs. 1.4±0.3%, n=7, 7, p<0.05, Fig. 4.6 C and D).

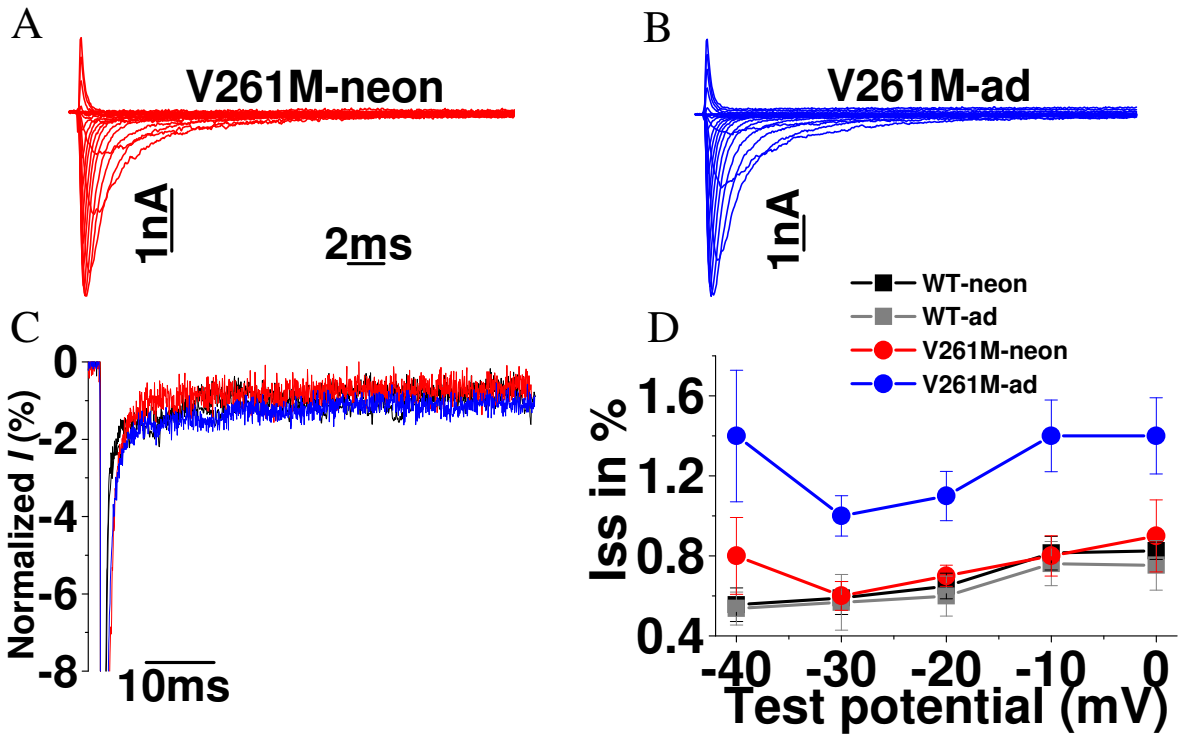

Figure 4.6: A: typical sodium current recording of the V261M neonatal channel; *B*: V261M adult channel. Sodium currents elicited by various depolarization steps ranging from -105 to +67.5 mV, from a holding potential of -140 mV. *C*: Representative *SCN2A* WT and V261M mutant TTX sensitive sodium currents. Currents were recorded at the end of a 70-ms depolarization to 0 mV from a holding potential of -140 mV and normalized to the peak current amplitude. *D*: The voltage dependence of the persistent current.

The $V_{1/2}$ of steady-state activation and inactivation were not significantly shifted by either the neonatal or adult mutant V261M channels. However, the mutation increased slightly but significantly the slope factor of the voltage dependence of activation (when expressed in neonatal splice variants: -4.8±0.3 vs. -6.5±0.4, n=15, 11, $p<0.01$; adult, -5.6±0.4 vs. -6.7±0.2, n=12, 10, $p<0.05$, Tab.4.3, Fig. 4.7 A). The adult mutant channel also increased the slope factor of the voltage dependence of steady-state inactivation (4.5±0.1 vs. 5.8±0.2, n=9, 10, $p<0.001$, Tab.4.3, Fig. 4.7 B).

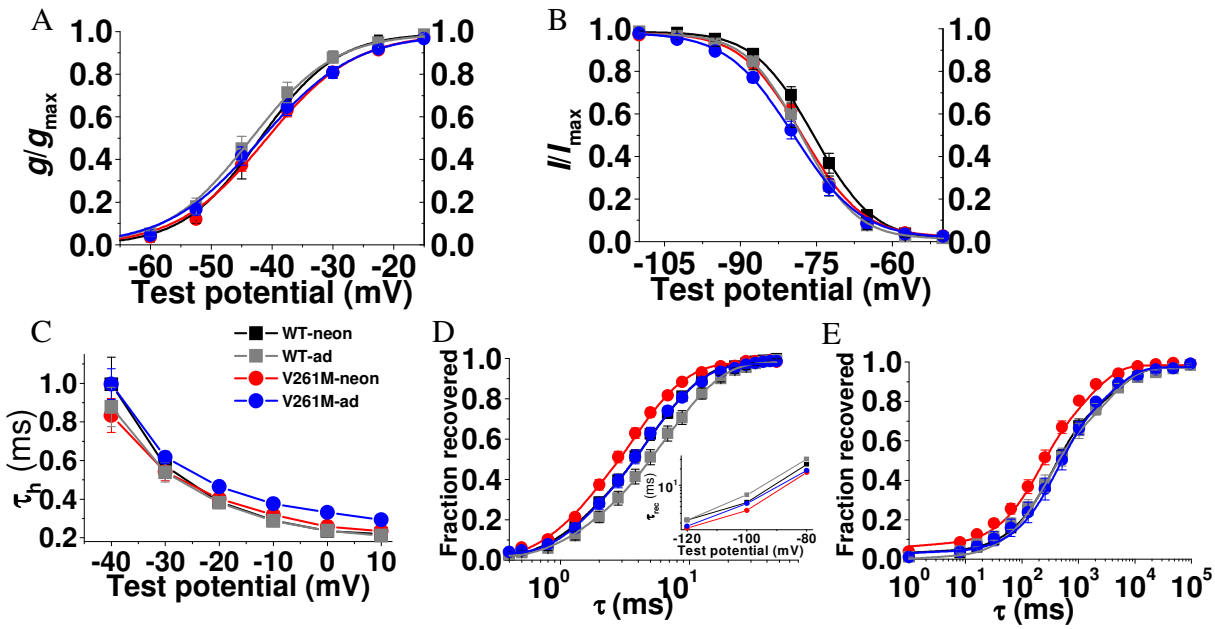

Figure 4.7: Electrophysiological properties of V261M mutant channel. *A*: voltage dependence of steady-state sodium channel activation. *B*: voltage dependence of steady-state sodium channel inactivation. Values of membrane potential for half-maximal activation, inactivation and slope factors are shown in Table 4.3. *C*: voltage dependence of fast inactivation time constants for WT and V261M mutant channels. *D*: recovery from fast inactivation at a membrane potential of -100 mV. The inset shows the voltage dependence of τ_{rec}. *E*: recovery from slow inactivation at a membrane potential of -120 mV.

The time constant of fast inactivation was slightly slowed by mutation V261M in the adult splice variant (0.24±0.01 vs. 0.33±0.03 ms, n=10, 8, p<0.01, Tab. 4.3, Fig. 4.7 C). In both splice variants the mutation accelerated the time course of recovery from fast inactivation at all three test potentials (At -100 mV: neon, 4.8±0.4 vs. 3.4±0.2 ms, n= 10, 11, p<0.01; adult, 6.6±0.7 vs. 4.6±0.3 ms, n=9, 10, p<0.05, Tab. 4.3, Fig. 4.7 D).

The voltage dependence and entry into slow inactivation were not altered by the mutation (Tab. 4.3, Fig. 4.9 C, and D).Recovery from slow inactivation for V261M mutant channels in the background of neonatal splice variant began earlier than the WT channels, and the time constant was significant faster (373.0±32.0 vs. 194.3±31.6 ms, n=7, 7, p<0.01, Tab. 4.4, Fig. 4.7 E).

An enhanced persistent sodium current, an accelerated recovery from fast inactivation, a slowed inactivation were the main functional defects observed for the V261M mutation. These gain-of-function mechanisms can well explain a hyperexcitability of neurons expressing these channels. Since these defects were not only observed in neonatal but also in adult channels, partially even more pronounced in adult channels, the age-dependence of this seizure syndrome can not be explained by differences in these splice variants, hypothesized for M252V in the previous chapter.

4.4. Electrophysiological properties of A263V mutant channel

Mutation A263V is also localized in S5 of domain I in $Na_v1.2$, i.e. at the same site as the previous two mutations. The patient carrying the A263V mutation has a more severe epileptic syndrome and generated myoclonic seizures in his 18th month of life.

A263V neonatal and adult channels displayed generally similar defects, although the positive shifts in voltage dependence of both steady-state activation (-43.3±1.4 vs. -36.4 ±1.4, n=12, 13, $p<0.01$, Tab.4.3, Fig.4.9 A) and fast inactivation (-77.9±1.4 vs. -71.2± 1.5, n=9, 13, $p<0.01$, Tab.4.3, Fig.4.9 A) were only observed in adult mutant channels, but not in neonatal channels. The decreased steepness of the voltage dependences of activation and inactivation for A263V mutant channels (Tab.4.3, Fig.4.9 A) led to increased window current, and raised the channel availability in the subthreshold voltage range to elicit an action potential.

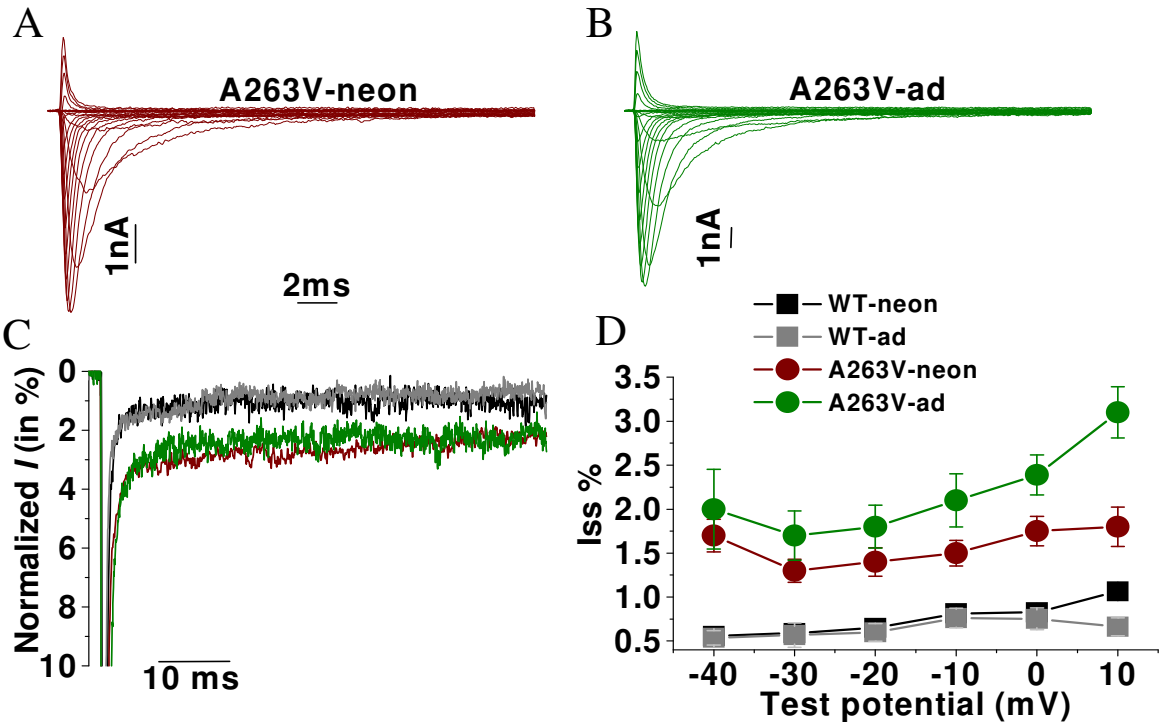

Figure 4.8: A: typical sodium current recording of the A263V neonatal channel; *B*: A263V adult channel. Sodium currents elicited by various depolarization steps ranging from -105 to +67.5 mV, from a holding potential of -140 mV. *C*: Representative *SCN2A* WT and A263V mutant TTX sensitive sodium currents. Currents were recorded at the end of a 70-ms depolarization to 0 mV from a holding potential of -140 mV and normalized to the peak current amplitude. *D*: The voltage dependence of the persistent current.

Table 4.4: Steady-state slow inactivation parameters of *SCN2A* WT and the mutant channels

	Entry into SI (s)	n	$V_{1/2\ SI}$ (mV)	k (mV)	n	τ_{srec} (ms)	n
WT neon	2.7±0.4	7	-78.4±1.7	6.8±0.3	10	373.0±32.0	7
M252V neon	3.5±0.4	7	-77.0±1.9	7.4±0.3	7	**218.6±27.7##**	7
V261M neon	2.8±0.2	7	-77.8±1.2	6.8±0.2	7	**194.3±31.6##**	7
A263V neon	2.7±0.2	8	-76.5±1.2	7.0±0.2	10	**172.4±56.3##**	7
WT ad	3.1±0.3	7	-80.0±1.9	6.9±0.3	9	304.6±58.4	9
M252V ad	4.0±0.3	7	-77.8±1.7	**8.0±0.3#**	9	335.2±57.8	9
V261M ad	2.5±0.4	5	-81.7±1.7	7.3±0.4	5	423.9±112.4	5
A263V ad	3.9±0.5	4	-77.5±1.6	**8.2±0.4#**	7	360.7±105.9	4

The time course of slow inactivation was fitted to a first order exponential function. Values for $V_{1/2}$, the voltage of half-maximal inactivation, and the slope factor k were derived from Boltzmann fits to inactivation curve. The time constant of recovery was fitted with a second order exponential function with an initial delay, only the fast time constant was shown here (see Materials and Methods). # corresponds to a comparison with the WT channel. Significance levels are indicated as follows: # $p<0.05$, ## $p<0.01$, ### $p<0.001$.

A263V mutant channels demonstrated the most pronounced persistent sodium current in both splice variants after a 70 ms among the studied 3 *SCN2A* mutations in this work (neonatal: 0.8±0.0 vs. 1.8±0.2, n=8, 10, $p<0.01$; adult, 0.8±0.1 vs. 2.4±0.2, n=7, 6, $p<0.001$, Fig. 4.8 C and D). The time course of fast inactivation of A263V mutant channel was significantly slowed comparing to $Na_v1.2$ WT channels (Tab.4.3, Fig. 4.9 B). The time course of recovery from fast inactivation was not significantly affected by the A263V mutation.

Defects caused by the A263V mutation in slow inactivation were similar to these caused by the V261M mutation. The voltage dependence and the entry into slow inactivation were not altered (Tab. 4.3, Fig. 4.10 E, F), but the in the neonatal splice variant was accelerated (τ_{rec}: 373.0±32.0 vs. 172.4±56.3 ms, n=7, 7, $p<0.01$, Tab. 4.3, Fig. 4.9 D).

In summary, major defects caused by the A263V mutation were the following: an increased window current, an enhanced persistent current and a slowed fast inactivation. These gain-of-functions were displayed in both, neonatal and adult channels, emphasizing that a differential mutational effect in neonatal and adult splice variant can not account for an age-dependent seizure expression.

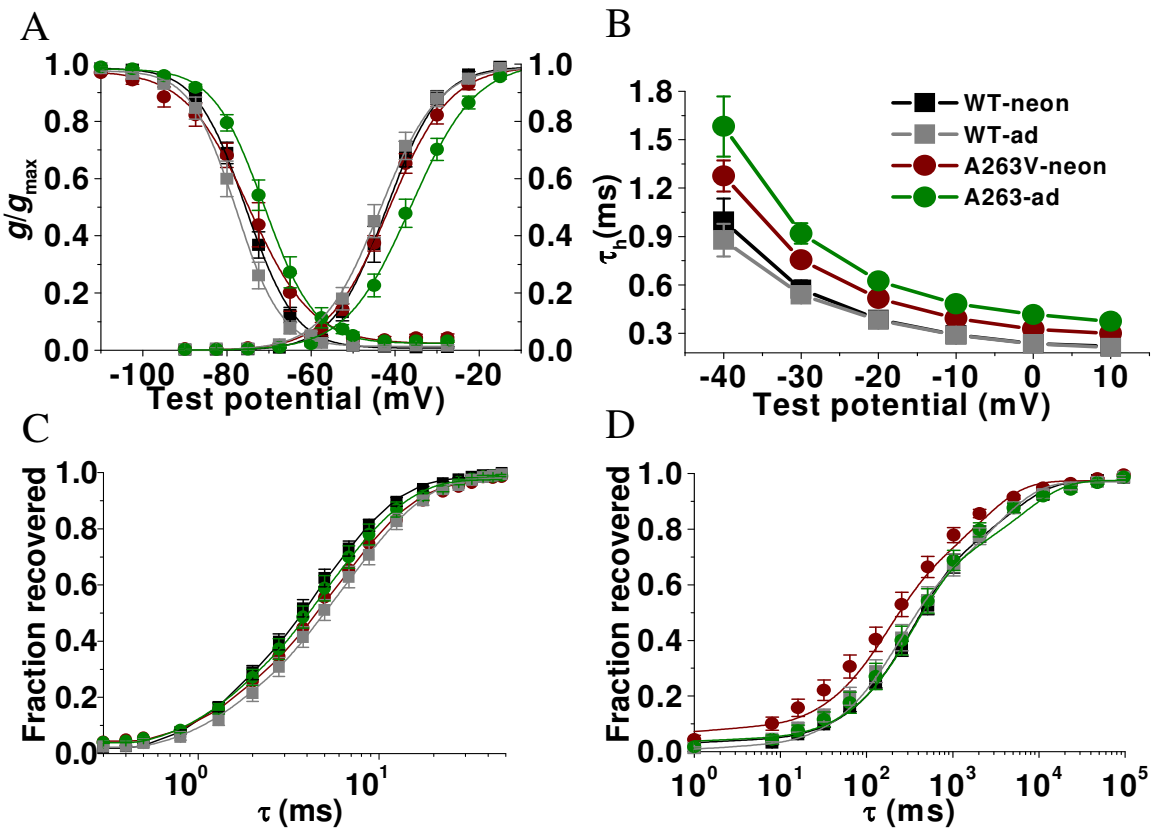

Figure 4.9: Electrophysiological properties of A263V mutant channel. *A:* voltage dependence of steady-state sodium channel activation. *B*: voltage dependence of steady-state sodium channel inactivation. Values of membrane potential for half-maximal activation, inactivation and slope factors are shown in Table 4.3. *C*: voltage dependence of fast inactivation time constants for WT and A263V mutant channels. *D*: recovery from fast inactivation at a membrane potential of -100 mV. The inset shows the voltage dependence of τ_{rec}. *E*: recovery from slow inactivation at a membrane potential of -120 mV.

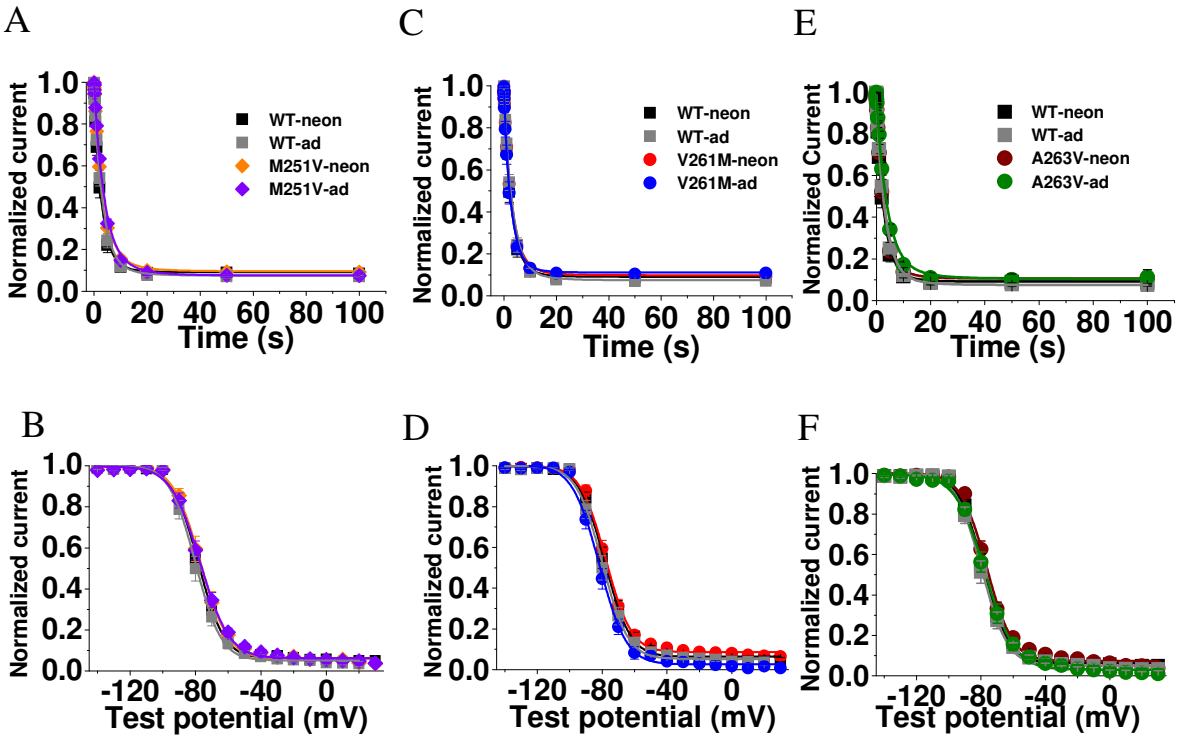

Figure 4.10: Entry into and voltage dependence of slow inactivation of the three mutant channels. *A*: M252V mutant channels entry into slow inactivation at 0 mV. The protocol is described in the methods part. *B*: voltage dependence of slow inactivation. *C*: V261M mutant channels entry into slow inactivation at 0 mV. *D*: voltage dependence of slow inactivation. *E*: A263V mutant channels entry into slow inactivation at 0 mV. *F*: voltage dependence of slow inactivation.

5. Morphological, electrophysiological and immunocytochemical identification of primary cultured rat cortical neurons

The main aim of this part of the thesis was to characterize the morphological, electrophysiological and immunocytochemical features of primary cultured rat cortical neurons to use them later as a neuronal expression system for mutations. Cultured cortical neurons were held at around -70 mV in the current clamp mode after the whole cell configuration was obtained. Action potentials were evoked by stepwise somatic current injection (duration: 500-2000 ms). The threshold was defined as the membrane potential at which, dV/dt equals 50 Vs^{-1}. The width of the spike was measured at half maximal spike amplitude, which was defined as the peak relative to the holding potential.

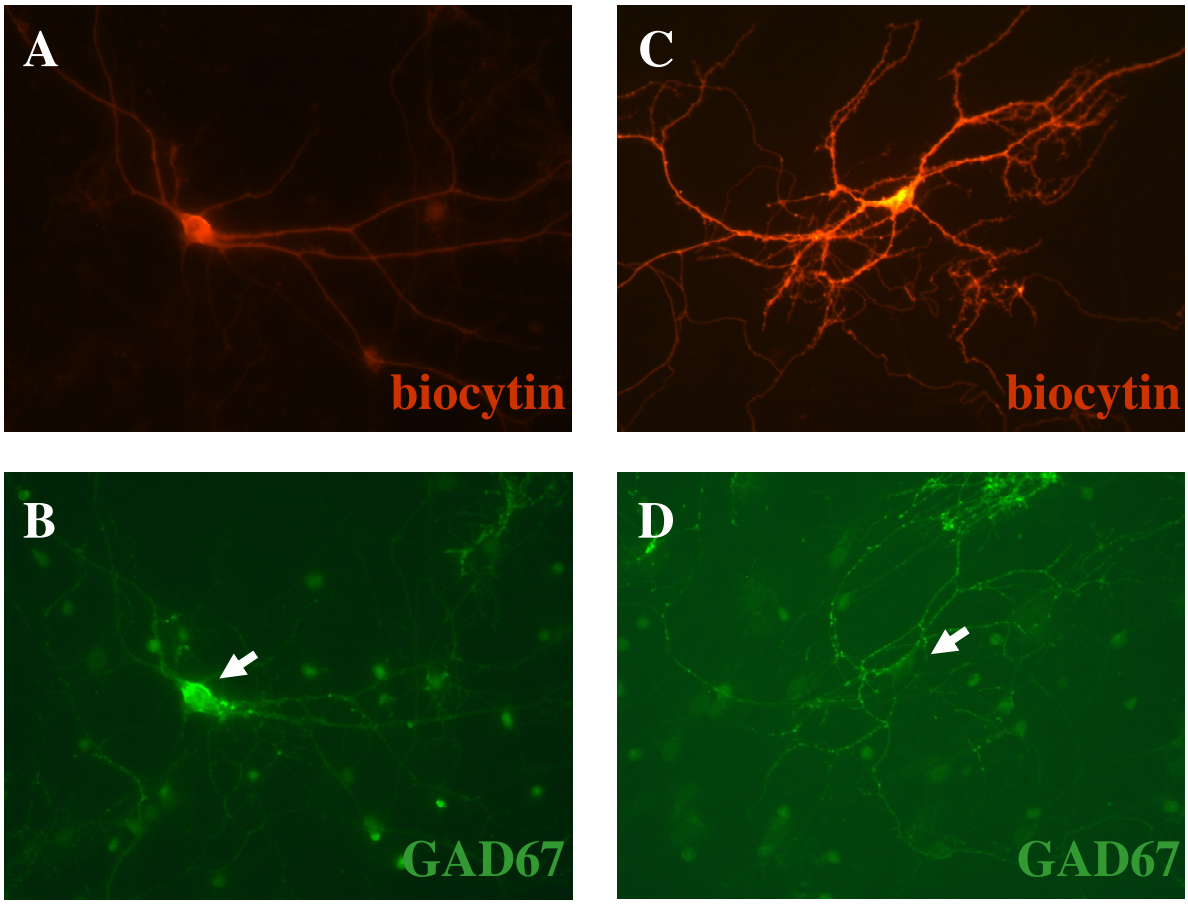

Figure 5.1: Morphological reconstruction of measured neurons and identification of their immunoreaction for GAD_{67}. *A, B*: biocytin labeled GAD_{67} immunoreaction positive neuron (arrow in *B*). *C, D*: biocytin labeled GAD_{67} immunoreaction negative neuron (arrow in *D*).

During the recordings, neurons were labeled with biocytin added to the pipette solution and later stained with a monoclonal antibody against GAD_{67}. The neurons, which were specifically stained by this antibody, were considered as inhibitory neurons (Fig. 5.1). In total, 22 primary cultured rat cortical neurons from DIV (days *in vivo*) 14 to 28 were successfully recorded and immunocytochemically stained.

5.1. Morphological diversity of measured cortical neurons

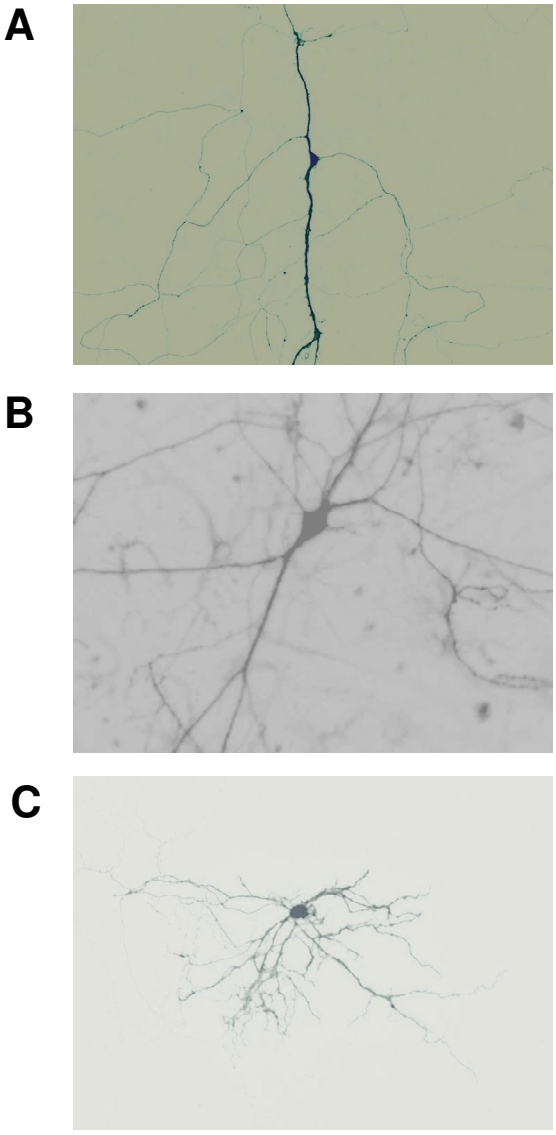

According to the reconstruction of the neurons we recorded from, we identified 3 morphological classes: pyramidal cells, bitufted cells and basket cells. Pyramidal cells compose approximately 80% of the neurons of the cortex. They have a triangularly shaped soma, a single apical dendrite, multiple basal dendrites, and a single axon (Fig. 5.2 A). Pyramidal cells release glutamate as their neurotransmitter, making them the major excitatory component of the cortex. Bitufted cells have spindle or ovoid somata and bitufted dendrites. They give rise to primary dendrites emerging on opposite poles and exhibited a distinct axonal arborization (Fig. 5.2 B). Basket cells have a basket-like appearance, aspiny and multipolar dendrites and an expansive axonal arborization (Fig. 5.2 C). About 50% of all inhibitory interneurons are basket cells.

Figure 5.2: Three morphological classes of cortical neurons.
A: pyramidal cell. *B*: bitufted cell. *C*: basket cell.

5.2. Immunocytochemical identification of cortical neurons

Cultured cortical neurons, which have been chosen for recordings, were identified as being excitatory or inhibitory using immunocytochemistry. GAD is an enzyme that catalyzes the decarboxylation of glutamate to GABA and CO_2. In mammals, GAD exists in two isoforms, GAD_{67} and GAD_{65}, with molecular weights of 67 and 65, respectively. GAD_{67} and GAD_{65} are highly conserved in evolution. They share a significant homology in the remaining part of the molecule, which contains the catalytic portion of the enzyme (~78% identity, ~95% similarity). A monoclonal antibody to GAD_{67} was used in this study as a marker of inhibitory neurons. Neurons with their cell body and proximal dendrites stained by the antibody against GAD_{67} were considered as GAD_{67} positive neurons. A typical GAD_{67} staining is shown in Fig. 5.1 B. 6 of 22 measured neurons were GAD_{67} positive neurons.

5.3. Electrophysiological properties of cultured cortical neurons

Electrophysiological properties of neurons divided by their immunoreaction with the GAD_{67} antibody are demonstrated in Tab. 5.1. There were no significant difference found in resting potential, input resistant, threshold, rate-of-rise and spike width between GAD_{67} positive neurons and GAD_{67} negative neurons.

Cultured cortical neurons were divided into three main physiological classes with regard to their firing patterns in response to depolarizing current injections. Five regular spiking neurons were observed, all of them were GAD_{67} negative, so that these were identified as excitatory neurons.

A typical GAD_{67} negative, regular spiking neuron is shown in Fig. 5.3. This neuron was recorded at DIV22, had a resting potential of -65 mV and an input resistance of 190.04 MΩ. When a small depolarizing current pulse (0.1 nA) was injected into this neuron, only an electrotonic, subthreshold depolarization was generated. A series of regular spiking was evoked by a somatic current injection of 0.26 nA (Fig. 5.3 B). Using the membrane potential at which dV/dt reaches 50 Vs^{-1} to estimate the action potential threshold, this neuron had a threshold of -29 mV under these recording conditions at room temperature.

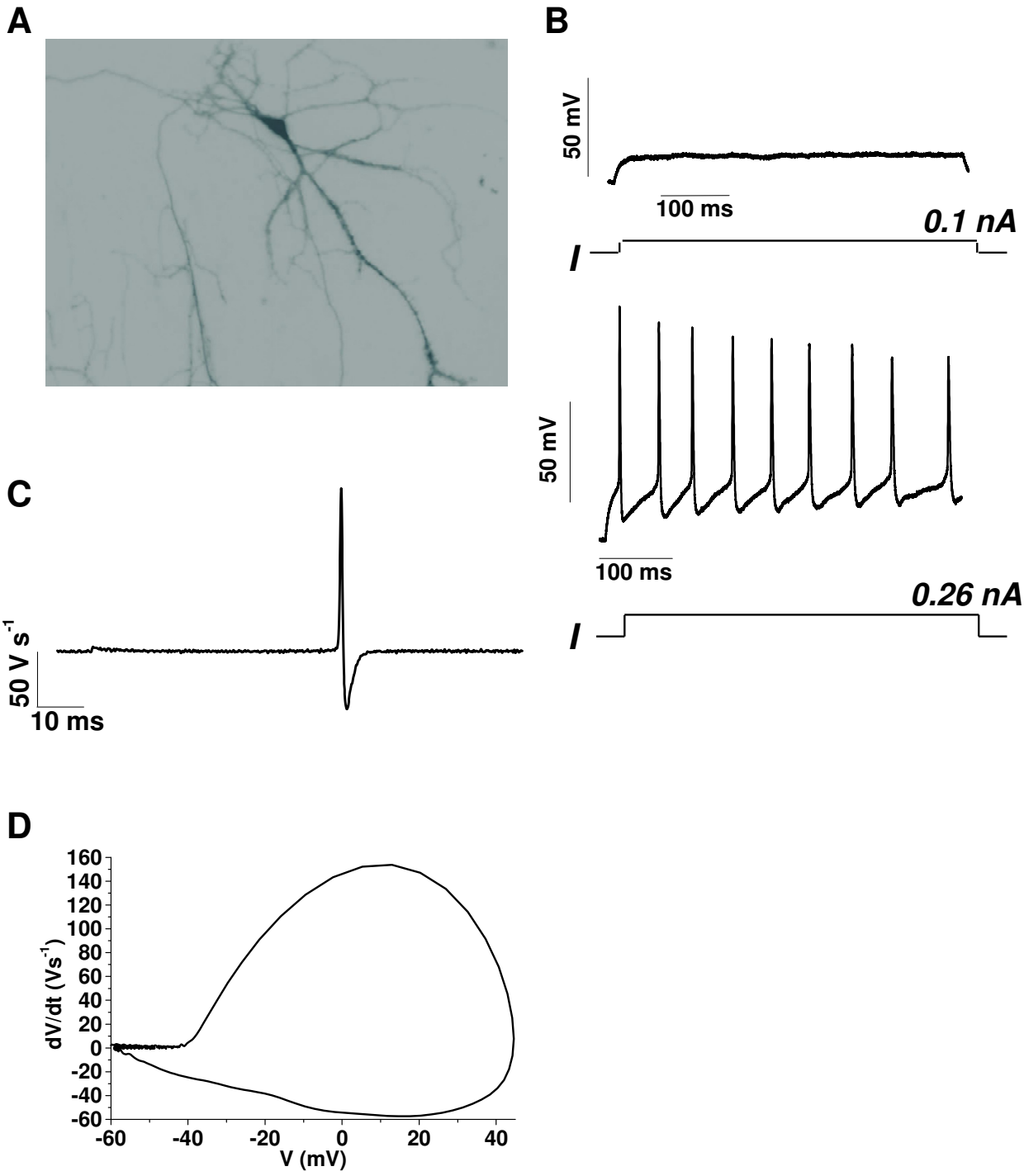

Figure 5.3: A GAD_{67} negative DIV22 cortical pyramidal neuron. A: reconstruction of the GAD_{67} negative cortical neuron. *B*: electrophysiological responses to 0.1 or 0.26 nA somatic current injection. *C*: first derivative of the first AP. *D*: Phase plane plot.

Table 5.1: Electrophysiological properties of recorded cortical neurons

	RP (mV)	R_{input} (mΩ)	Threshold (mV)	Rate-of-rise ($V\ s^{-1}$)	Spike width (ms)
GAD67+ neurons (n=6)	-51.6±2.6	383.1±201.7	-33.6±2.3	120.9±6.7	1.7±0.2
GAD67- neurons (n=16)	-54.0±2.8	201.1±42.3	-29.7±2.6	135.7±13.4	1.8±0.2

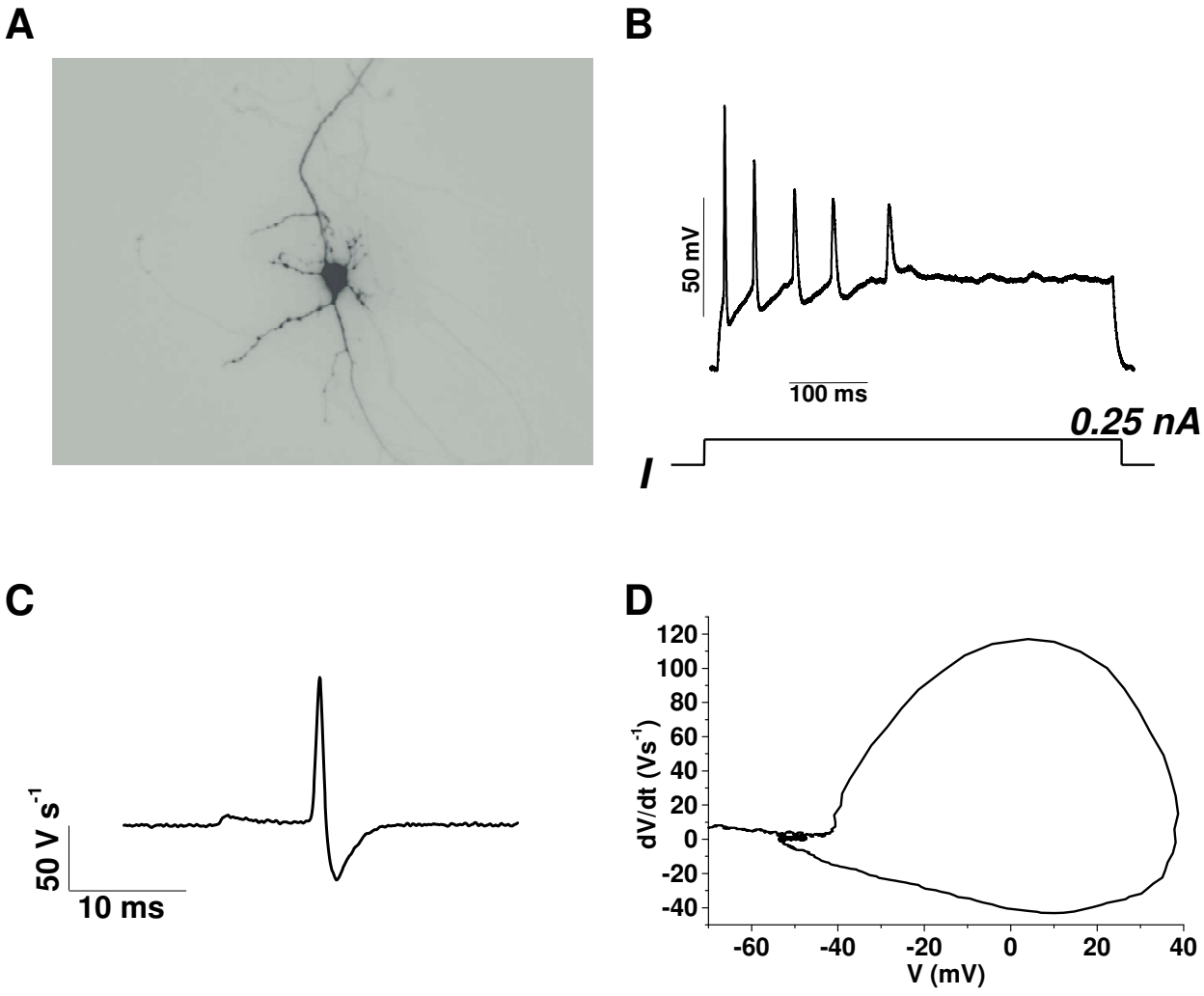

Figure 5.4: An accommodating spiking GAD_{67} positive cortical basket neuron. *A*: reconstruction of the GAD_{67} positive cortical neuron. *B*: AP evoked by 0.25 nA somatic current injection. *C*: first derivative of the first AP. *D*: Phase plane plot.

The average resting potential of the GAD_{67} negative neurons was -54.0±2.8 mV, the input resistance was 201±42 MΩ, the action potential threshold was -29.7±2.6 mV, the rate-of-rise was 135.7±13.4 Vs^{-1}, and the width of the first spike was 1.8±0.2 ms (Tab. 5.1).

Another classification of electrophysiological response is accommodating, which refers the neurons increasing their threshold for an action potential during a slowly developing or prolonged depolarization, which results in only a few action potentials are generated during developing or prolonged depolarization above the normal threshold level. Five neurons could be classified as accommodating, three of which were GAD_{67} positive. Fig. 5.4 displays an example of an accommodating spiking GAD_{67} positive neuron. The resting potential of this neuron at DIV17 was -50 mV, the input resistance was 243 MΩ, the threshold of the action potential was -30 mV, and the rate-of-rise was 109.4 mV/ms. When depolarizing current (+0.25~+3.14 nA, interval: 0.01 nA) was stepwise injected into soma, only a few action potentials were generated.

The third class of spiking pattern observed was stuttering, a subtype of fast spiking. In response to depolarizing currents, neurons fired brief bursts of action potentials intermingled with unpredictable periods of silence (‘Morse-code’-like discharges). The action potentials in a cluster hardly show any accommodation, and the silent periods between clusters vary unpredictably in duration. There were 6 stuttering neurons in this study, 3 of which were GAD_{67} positive. The neuron shown in Fig. 5.5 is a bitufted GAD_{67} positive neuron at DIV24, the resting potential was -60 mV, the input resistance was 30 MΩ the threshold was -40.2 mV, and the rate-of-rise was 125.4 mV/ms.

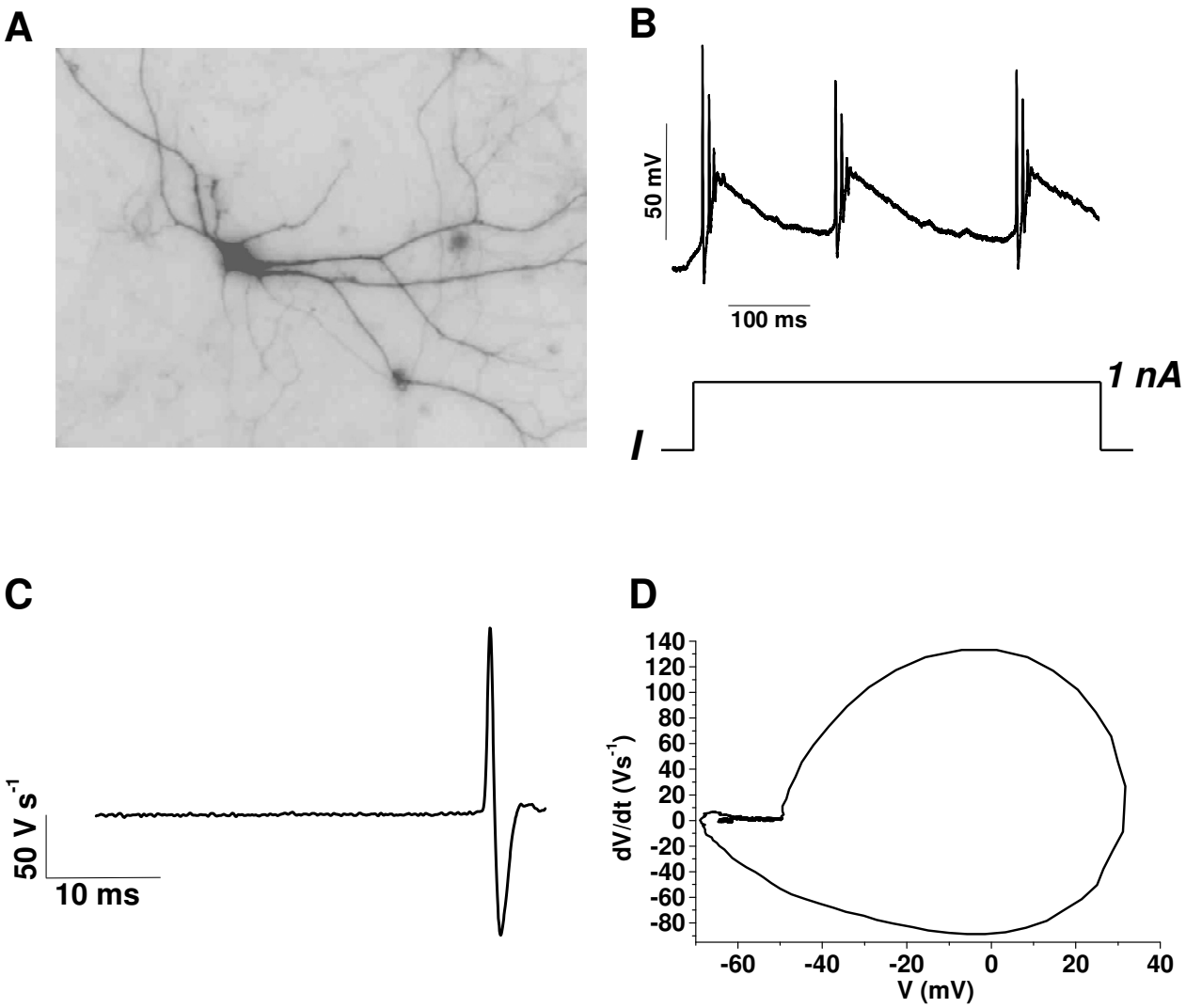

Figure 5.5: A stuttering spiking GAD_{67} positive cortical bitufted neuron at DIV 24. *A*: reconstruction of the GAD_{67} positive cortical neuron. *B*: APs evoked by 1 nA somatic current injection. *C*: first derivative of the first AP. *D*: phase plane plot

6. Discussion

6.1. Functional consequences of a GEFS+ causing *SCN1A* mutation

R1648H was one of the two first identified *SCN1A* mutations related to GEFS+. This mutation is located in a functionally important position, the S4 voltage sensor of domain 4. Functional studies on this mutation have been done in different expression systems. In our group, Alekov et al. did engineer this mutation into the human *SCN4A* cDNA and express α subunit alone in tsA-201 cells. Under this condition, defects such as a slowed inactivation, an accelerated recovery from fast inactivation and a stabilized slow inactivation were observed (Alekov et al., 2000). When it was introduced into the rat *SCN1A* cDNA and expressed in *Xenopus* oocyte, the only prominent effect was an accelerated recovery from fast inactivation with and without the β1 subunit (Spampanato et al., 2001). However, when R1648H was introduced in the human clone and expressed in mammalian tsA-201 cells with β1 and β2 subunits, it demonstrated an enhanced persistent current as the major defect besides an acceleration of recovery from fast inactivation (Lossin et al., 2002). Thus, the R1648H mutation showed different effects in various channel backgrounds and heterologous expression systems. The variability in the investigating conditions of these 3 studies may explain the discrepancies of the results. Here we performed a functional study on the human *SCN1A* WT and R1648H mutant channels in the tsA-201 cell line, which has been proved as a reliable expression system for functional studies on sodium channels. Our main aim was to investigate the role of β subunits in functional modulations of *SCN1A* WT and R1648H mutant channels, since co-expression of the β-subunit might be the key for the observed differences.

Results of the present study showed that when co-expressed with the auxiliary β subunits, the R1648H mutant channels have a slower fast inactivation time course at depolarized potentials, increased recovery rate from fast inactivation and a 2-fold enhanced persistent current, compared with the WT channels. These findings are in line with results by Alekov et al. (2000) and Spampanato et al. (2001) concerning the defects caused by R1648H mutation, such as slowed fast inactivation and accelerated recovery from fast inactivation. However, the 2-fold enhanced persistent current was only detected by Lossin et al. (2002) and in the present study with and without β subunits, in which the R1648H mutation was investigated in the human channel. This indicates that indeed the functional properties of

sodium channels can be gene-sensitive, even if the changes are in highly conserved and functionally important regions, and must be related to the background of the human channel.

The single-channel experiment and a modal gating model provided further evidences for understanding the mechanism responsible for the mutant channel behavior and for its consequences in neurons. In the single-channel analysis, the R1648H mutant exhibited a marked increased probability of late reopenings and a subfraction of channels with prolonged open times, which consequently promotes a persistent sodium current (Vanoye et al., 2005). The theoretical Markovian model of $Na_v1.1$ revealed that the R1648H mutation may disrupt the repolarization of the neuronal action potential by altering the duration or the morphology of the action potential (Clancy and Kass, 2004). The gain-of-function caused by the R1648H mutation could result in neuronal hyperexcitability by shortening both the period of depolarization needed to elicit an action potential and the refractory period after an action potential, which could explain the seizures occurring in patients.

6.2. Differential modulating effects of β subunits on *SCN1A* WT and R1648H mutant channel function

Brain sodium channels isolated from mammalian neurons are heterotrimeric protein complexes which are composed of α, β1, and β2 subunits (Catterall et al. 1992).The β subunits are not essential for channel gating, but they have been shown to modulate channel kinetics and regulate the cell surface expression of α subunits (Isom et al., 1995 cell; Isom et al. 1995 j.Biol. Chem). Brain β1 subunits can affect gating kinetics and produce an increase in sodium current amplitude which is consistent with an increase in the level of channel expression (Patton et al. 1994, Qu et al. 1995). The β2 subunit could expand the plasma membrane surface area, leading to increases in cell capacitance (Isom et al., 1995). Nevertheless, the modulation of R1648H mutant channel function by β subunits has not been investigated so far.

6.2.1. Modulation of *SCN1A* WT channel gating by β subunits

Our results revealed that the β1 subunit steepened the voltage dependence of steady-state channel activation and inactivation, and accelerated the fast inactivation time course. These findings were similar to previous functional studies examining the effects of the β1-subunit on different sodium channels in various expression systems (McClatchey et al., 1993; Bennett et al., 1993; Patton et al., 1994).

In contrast to the β1 subunit, the β2 subunit did not demonstrate any modulation effect on $Na_v1.1$ WT channel gating in our study. However, the β2 subunit has been described before to shift the voltage dependence of steady-state inactivation in a hyperpolarizing direction and to accelerate the fast inactivation time course of the rat brain sodium channel ($Na_v1.2a$), when expressed in *Xenopus* oocytes (Isom et al, 1995). Two other previous studies also showed modulating effects of the β2 subunit on sodium channel gating. Co-expression of β1, β2, and β3 subunits with rat $Na_v1.2a$ α subunits in tsA-201 cells shifted the voltage dependences of steady-state sodium channel activation and inactivation to more depolarized potentials (Qu et al., 2001). A loss of β2 subunits caused a negative shift in the voltage dependence of steady-state inactivation as observed in hippocampal neurons dissociated from β2 knock-out mice (Chen et al., 2002). Although both $Na_v1.1$ and $Na_v1.2$ channels are abundantly expressed in the adult central nervous system, they have a differential subcellular expression profile. $Na_v1.1$ is predominantly localized in parvalbumin-positive (PV) interneuons; it is clustered at their axon initial segments, whereas $Na_v1.2$ is expressed in the axon initial segment of principle excitatory neurons (Ogiwara et al., 2007). By studying functions of these two sodium channel isoforms in tsA-201 cells, subtle but significant differences were found in the kinetics of channel gating (our unpublished results). Hence, we speculated that the interaction may also vary between these two sodium channel α subunits with the auxiliary β subunits.

6.2.2. Attenuation of α-β1 interaction by the R1648H mutation

Modulations of the R1648H mutant channel by β subunits were perfectly different from those displayed in WT channels. The voltage dependencies of steady-state activation and inactivation were altered by the β1 subunit in a similar manner as in the WT channel,

whereas the effect on the fast inactivation time course by the β1 subunit was diminished. β1 is non-covalently associated with α subunits and its interaction sites with the α subunit were suggested by structure-function experiments to be located in the extracellular Ig domain (McCormick et al., 1998). A discontinuous epitope formed by I S5-S6 and IV SS2-S6 that are close to each other in the three-dimensional structure of the sodium channel has been suggested by experiments as an interaction site of α subunits with the β1 subunit (Makita et al., 1996 and Qu et al., 1999). A mutation, D1790G, which locates in the carboxyl-terminal domain of $Na_v1.5$ α subunits, has been shown to result in the disruption of α-β1 subunit interactions (An et al. 1998). Another GEFS+ mutation, D1866Y, which also locates in the carboxyl-terminal domain of $Na_v1.1$ has demonstrated the decreased modulation of the α subunit by β1 subunit as well (Spampanato et al. 2004). These results suggest that the interaction site of α and β1 may be at both intracellular and extracellular sites. The partial disruption of the β1 function in R1648H mutant channels found in our study indicated an IV S4 mutation in sodium channel α subunits may indirectly affect the interaction between the α subunit and β1 as well.

6.2.3. The β2 subunit modulates R1648H channel functions

β2 subunits are components of neuronal sodium channels and form a disulfide bond to the α subunit (Wollner et al. 1987; Messner and Catterall, 1985). In contrast to the lack of an effect on $Na_v1.1$ WT channel function, the β2 subunit alone modulated R1648H mutant channel gating. It shifted the voltage dependences of steady-state activation and inactivation in a depolarizing direction in a similar manner as the β1 subunit. We speculate that the R1648H mutation may alter the interaction between the α and β2 subunits, which may compensate the loss of modulation of the β1 subunit.

6.2.4. Co-expression of both β1 and β2 subunits partially repair defects caused by the R1648H mutation

Our results provide evidence for a reparation of defects caused by the R1648H mutation on $Na_v1.1$ channel gating when both β1 and β2 subunits are co-expressed together. Under

these conditions, the fast inactivation time course, and the recovery from fast inactivation were significantly accelerated; the level of the persistent sodium current was slightly reduced. These modulations of sodium channel functions by the two β subunits result in less difference in the physiological properties between WT and R1648H mutant channels. Modulatary effects on the fast inactivation time course and the recovery from fast inactivation indicate a functional relevance of β subunits in sodium channel fast inactivation. As found in single channel analysis, the enhanced persistent current caused by R1648H results predominantly from late reopenings of the mutant channel (Rhodes et al., 2005); therefore we assumed that the reduction of the persistent current by co-expressing both β subunits may be due to the stabilization of fast inactivation, which decrease the number of available sodium channels for reopenings. The reduction of the modulation on the fast inactivation time course by β1 subunit alone in the R1648H mutant channel and the complementary effects caused by co-expressing both β1 and β2 subunits suggest that cooperation between β subunits may shift the R1648H mutant channel gating to a more normal behavior.

In summary, we showed in the present study that the R1648H mutation may partially affect the interactions between the sodium channel α subunit and the β1 or β2 subunit, and that co-expression of both β subunits had a different, stabilizing effect on mutational changes than both β subunits alone. Such effects are probably best explained by indirect effects on the protein conformation. Modulations of the voltage dependence and kinetics of sodium channel gating by β1 and β2 subunits may be complementary, and may result in a partial repair of the defects caused by R1648H mutation.

6.3. Comparison of neonatal and adult splice variants of $Na_v1.2$ channels

Alternative splicing is a major mechanism for modulating the expression of genes. It expands the spectrum of distinct functional protein isoforms, from a finite gene pool (Cáceres and Kornblihtt, 2002; Lipscombe, 2005). Developmentally regulated alternative splicing has been reported in *SCN1A*, 2A, 3A, 8A, 9A and 11A in rats and humans (Heinzen et al., 2007; Gustafson et al., 1993; Plummer and Meisler, 1999; Raymond et al., 2004, Sarao et al., 1991). In $hNa_v1.2$, exons 6N (N for neonatal) and 6A (A for adult) (Kasai et al., 2001) are developmentally regulated and differ in a single amino acid at

position 209 (Asparagine in 6N and Aspartic acid in 6A). This residue is predicted to be located in the extracellular loop between the S3 and S4 segments of domain I, and introduces a negative change in the adult isoform during splicing, which suggesting a potential alteration in permeability, gating and the interaction between the α and β subunits (Guy and Conti, 1990; Green and Andersen, 1991; Sarao et al., 1991). However, a previous functional study of both splice variants in the oocyte expression system did not show any differences secondary to this amino acid change (Auld et al., 1990). Another study done in tsA-201 cells has shown a slower inactivation, a right shift of the voltage dependence of inactivation, a faster recovery from fast inactivation and a reduction in run down in response to high frequency stimulation for the adult isoform (Xu et al., 2007). The various results indicated the high sensitivity of sodium channel propertied to the cell milieu.

Our results in tsA-201 cells showed that when only α subunits were expressed, the adult splice form of $Na_v1.2$ channels showed a slower inactivation, a depolarizing shift in the voltage dependence of slow inactivation and a more slow entry into slow inactivation state, compared with the neonatal splice form. These observations are in agreement with the findings present in a previous study (Xu et al., 2007) and indicated a higher excitability for adult channels. However, co-expression with the auxiliary β subunits modified neonatal and adult channel functions in a different manner resulting in minimization of the gating differences between neonatal and adult channels. This suggests small probably indirect effects on the interactions between α and β subunits for neonatal and adult channels.

6.4. Functional consequences of three novel BFNIS mutations in *SCN2A*

6.4.1. The mutants in domain I S5 affect sodium channel inactivation

There are at least two distinct kinetic modes of voltage-gated sodium channel inactivation, termed fast and slow. Fast inactivation is mediated by a “ball-and-chain” or “hinged lid” mechanism, in which the inactivating particle (IFM in the cytoplasmic linker between domain III and IV) occludes the pore by binding to the its docking site, which may include the cytoplasmic linkers connecting S4-S5 in domains III and IV and the cytoplasmic end of the S6 in domain IV (Rohl et al., 1999; Goldin, 2003; Ulbricht, 2005). Slow inactivation, however, is a separate process, which may result from a structural rearrangement of the

pore. Sodium channel fast inactivation is mediated by the III-IV linker, and can be modulated by the carboxyterminus of the channel (Deschenes et al., 2001; Mantegazza et al., 2001). S4-S5 loops in domain III and IV have been proved to be involved in fast inactivation of sodium channels in a cooperative manner (Mitrovic et al., 1996; Tang et al., 1996; Smith et al., 1997; Lerche et al., 1997; McPhee et al., 1998; Tang et al., 1998; Alekov et al., 2001; Popa et al., 2004). Many regions of the sodium channel, including the pore, IV S4 (Mitrovic et al., 2000), II S5-S6 (Vilin et al., 2001) and II S6 (O'Reilly et al., 2001) have been shown to be important for the process of slow inactivation.

Detailed functional study on the role of S5 in sodium channel inactivation has not been done to date. Naturally occurring mutations are a powerful tool to study the association between the protein structure and function. We investigated the functional defects caused by three novel *SCN2A* mutations associated with BFNIS in recombinant human *SCN2A* neonatal or adult isoforms co-expressed heterologously in tsA-201 cells with the auxiliary β subunits. They are the first identified *SCN2A* mutations localized in S5 segment of domain I, belonging to the pore region of sodium channels. Our results demonstrated pronounced defects on sodium channel inactivation caused by all three BFNIS mutations, M252V, V261M and A263V, which are located in S5 segment of domain I. These mutations exhibited an enhanced persistent sodium current and an accelerated recovery from fast and slow inactivation. V261M and A263V mutations additionally showed a slower time course of fast inactivation and an alteration in the voltage dependences of steady-state activation and inactivation. Results of a previous functional study in a *SCN4A* mutation related to hyperkalaemic periodic paralysis, located in the transmembrane segment S5 in the domain IV, has shown a disruption of channel inactivation as well (Bendahhou et al., 1999). The defects in sodium channel inactivation caused by these mutations revealed a prominent role of the S5 segment in sodium channel inactivation. We hypothesize that the mutations may induce structural changes of the S4-S5 linker or the pore region in general which may alter the conformation of the receptor site for the inactivation particle IFM.

6.4.2. All mutations predict an increase in neuronal excitability

The functional analysis of the three *SCN2A* mutations, M252V, V261M and A263V, demonstrated exclusively gain-of-function defects. Significantly enhanced persistent sodium current was observed for all three mutant channels. A 2-fold increase in persistent current has been reported to be responsible for progressive seizures of hippocampal origin in the Q54 transgenic mice, in which the GAL879-8811QQQ mutation of *SCN2A* was expressed (Kearney et al., 2001). This mutation was located in the S4-S5 linker of domain II. The enhanced persistent sodium current after a prolonged depolarizing pulse may increase neuronal hyperexcitability by shifting the membrane potential towards threshold for action potential generation, amplifying the spike afterhyperpolarization and increasing the regularity of repetitive firing (Vervaeke et al. 2006). Such a neuronal hyperexcitability may explain the increased seizure susceptibility of the patients.

Other gating defects such as an accelerated recovery from fast inactivation (caused by V261M) and from slow inactivation (all three mutations) could shorten the refractory period after an action potential. A slower fast inactivation time course (observed for V261M and A263V mutant channels) could increase the Na^+ inward current. The altered voltage-dependence of steady-state activation and inactivation may increase the number of available channels and increase the window current. All these gain-of-function defects lead to an increase of neuronal excitability in different ways and likely contribute to an increase in seizure susceptibility in BFNIS.

Previous functional studies of other BFNIS mutations in transfected tsA-201 cells and primary cultured neocortical neurons also showed gain-of-function defects predicting a neuronal hyperexcitability, which is in agreement with our results (Scalmani et al. 2006; Xu et al. 2007).

6.4.3. Remission of seizures during development

In BFNIS, afebrile seizures occur usually before 4 months of age and usually resolve spontaneously within the first year of life. The mechanism of seizure remission during development is not understood. Our results showed a specific effect of the M252V

mutation in the background of the neonatal compared to the adult isoform. The hyperexcitability caused by this mutation in the neonatal isoform could increase seizure susceptibility in very young children, whereas the lack of defect in the adult isoform may provide explanation as to why the patient does not have seizures beyond the first year of life. However, the V261M and A263V mutations displayed more pronounced effects in the adult isoform clearly suggesting other mechanisms which have to be responsible for the remission of seizures.

In the cerebral cortex and hippocampus, $Na_v1.2$ and $Na_v1.6$ channels are both mainly localized in axon initial segments (AIS) and nodes of Ranvier (Westenbroek et al., 1989; Gong et al., 1999). In situ hybridization experiments revealed stronger expression level of these two sodium channel isoforms in the excitatory pyramidal neurons than in non-pyramidal cells (Whitaker et al., 2000). In addition, $Na_v1.2$ and $Na_v1.6$ have distinct distributions, since $Na_v1.2$ channels are expressed along non-myelinated axons (Westenbroek et al. 1989; Gong et al., 1999; Boiko et al., 2001), whereas $Na_v1.6$ channels are clustered at the AIS and nodes of Ranvier in myelinated axons (Caldwell et al., 2000). More importantly with regard to BFNIS pathophysiology, $Na_v1.2$ channels are replaced by $Na_v1.6$ channels at mature nodes of Ranvier in myelinated axons during development in the optic nerve (Boiko et al., 2001; Kaplan et al., 2001). These observations suggest that the developmental expression pattern of sodium channels in developing myelinated fibers may alter neuronal excitability. We assumed that the replacement of $Na_v1.2$ by $Na_v1.6$ in axons may eliminate the effects of BFNIS mutations on the excitability of myelinated fibers, hence resulting in the spontaneous remission of seizures.

To further investigate the age-dependence of distributions of $Na_v1.2$ and $Na_v1.6$ in the central nervous system, we performed an immunohistochemical study in the mouse brain during development by using specific antibodies against these two sodium channel isoforms combined with an antibody against axon initial segment (AIS): Ankyrin G (Results shown in Figure 6.1 the experiments were performed by other lab members.). Interestingly, our results demonstrated an early expression of $Na_v1.2$ in AIS, their downregulation during development and a virtual absence after postnatal day 15 (P15).In contrast, there was a lack of expression of $Na_v1.6$ in the early stage and an increased expression level in the AIS after P15. The substitution of $Na_v1.2$ by $Na_v1.6$ in the AIS of principal neurons in the hippocampus and cortex in other brain regions provides a perfect

explanation for the remission of seizures in BFNIS patients, since the observed gain-of-function defects may not have an impact on the excitability of principal neurons in later stages of development.

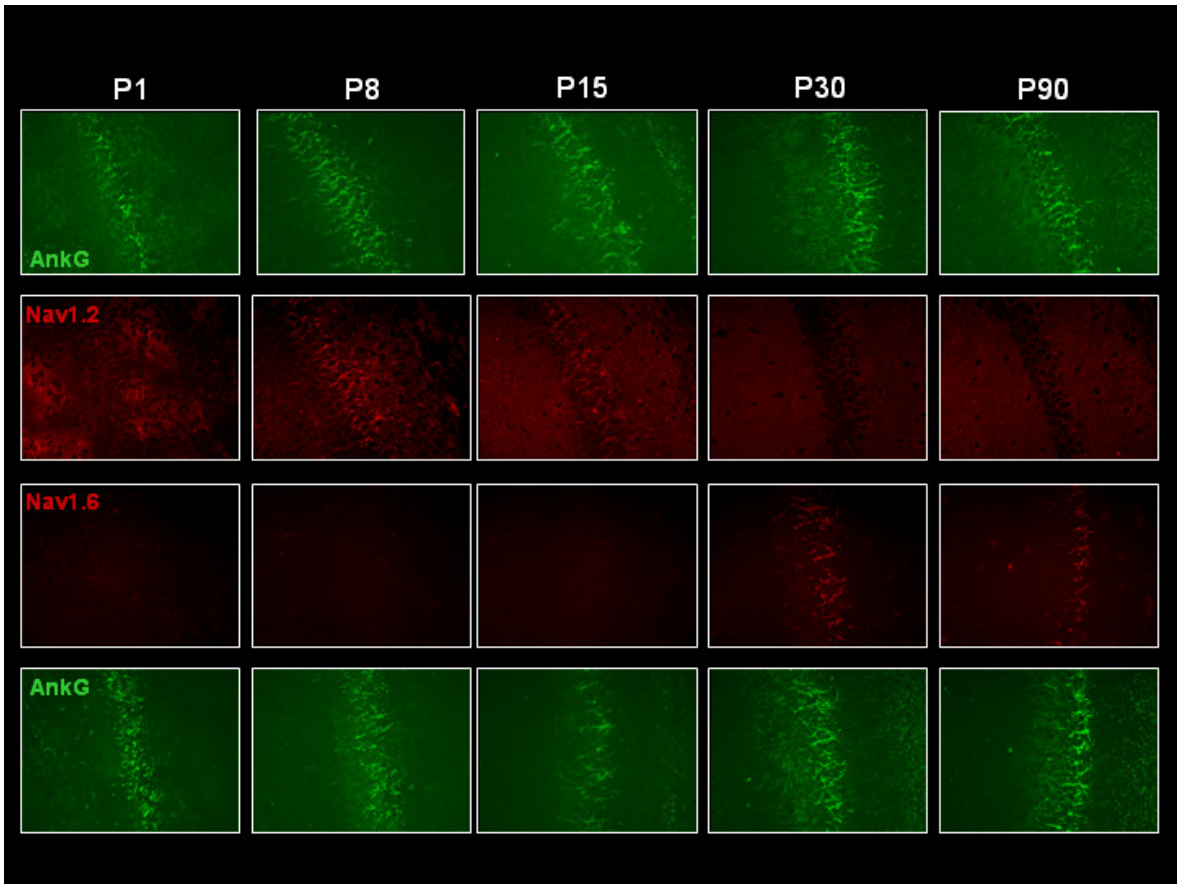

Figure 6.1: Immunohistochemical staining of $Na_v1.2$ and $Na_v1.6$ in mouse hippocampus during development.

6.5. Classification of cortical neurons

In the present study we established a method for investigating the electrophysiological features of different types of primary cortical neurons. 0.2% Biocytin added to the intracellular solution for identification of neurons we recorded from was proved to be not toxic and efficient. A sketchy morphological classification divided the neurons into three classes: 1) pyramidal cells, which are the excitatory neurons. Most of the cortical neurons (70-80%) belong to this class (DeFelipe and Farinas, 1992). However, due to our selection during experiment, only 14% (n=3) of the measured neurons in this study were pyramidal

neurons. 2) bitufted cells and 3) basket cells, which both are supposed to be GAD_{67} positive inhibitory neurons. These neurons represented a great part of the recorded cells, although some of them were GAD_{67} negative. 28% (n=6) of the measured neurons were GAD_{67} positive. Our results indicated that it is necessary to identify the inhibitory neurons not only considering their morphology in culture, but also their electrophysiological properties.

The action potential patterns of the recorded cortical neurons can be classified into three groups: 1) regular spiking (RS) 2) accommodating (AC) and 3) stuttering (STUT). All five regular spiking neurons in the present study were GAD_{67} negative including all three pyramidal, i.e. principal neurons. That is in agreement to the observation in a previous study, suggesting that the physiology of pyramidal neurons was relatively uniform (Connors and Gutnich, 1990). The other RS cells can be spiny stellate cells, which presume also excitatory synaptic function. They have high spine densities and small size (Lund, 1984). About half of the AC and STUT cells were GAD_{67} positive, showing that these were inhibitory neurons. Our results displayed a relative complex electrophysiological-morphological-functional relationship. Different expression patterns of ion channels of each type of neuron may contribute to the observed electrophysiological diversity (Martina et al., 1998; Toledo-Rodriguez et al., 2004).

This pilot study on primary cultured cortical neurons established cell labeling, current clamp and immunocytochemistry on these cells. These results will be used for later expression of mutant and WT ion channels in neurons to study their influences on firing properties.

Summary

Brain voltage-gated sodium channels are complexes of a pore-forming α subunit and auxiliary β1 and β2 subunits with modulatory effects. They play critical roles in initiation and generation of action potentials. Genetic defects of these channels have been identified in various human diseases including myotonia, cardiac arrhythmic and idiopathic epilepsy, the latter being the topic of this thesis.

A mutation R1648H in the *SCN1A* gene encoding the $Na_v1.1$ channel causes a relatively benign childhood seizure syndrome, generalized epilepsy with febrile seizures plus (GEFS+). Functional characterization of this mutation with β1 and β2 subunits in mammalian tsA-201 cells demonstrated a destabilized fast inactivation by slowing the fast inactivation time course, accelerating recovery from fast inactivation, and a 2-fold enhanced persistent sodium current. These gain-of-function effects caused by this mutation predict an increase neuronal excitability that could explain the occurrence of seizures.

The modulations of channel gating by β subunits in $Na_v1.1$ WT and R1648H channels are different. The β1 subunit modified the gating of WT channels by steepening the voltage dependence of activation and inactivation, and accelerating the fast inactivation time course. In contrast, the β2 subunit alone did not show a modulatory effect on WT channel gating. For the R1648H channel, our results indicated that the interaction between the α and β1 subunit partially disrupted by the mutation, since the acceleration of the fast inactivation time course, which is normally observed by β1 subunit, was lost. Co-expression of β1 and β2 subunits together accelerated fast inactivation and recovery from fast inactivation diminishing the defects caused by the R1648H mutation. Our results thus revealed an important role of both β subunits in modifying both WT and mutant channel gaiting.

Benign familial neonatal-infantile seizures (BFNIS) is characterized by afebrile seizures occurring almost exclusively during the first days to months of life. It is associated with mutations in *SCN2A* encoding the $Na_v1.2$ channel. Three novel BFNIS mutations in the S5 segment of domain I of $Na_v1.2$ were functional investigated in the background of the neonatal and adult splice variants of $Na_v1.2$ with co-expression of both β1 and β2 subunits

in tsA-201 cells. We identified subtle changes in channel gating leading to a gain-of-function, such as an enhanced persistent sodium current, an slowed fast inactivation time course, an accelerated recovery from fast and slow inactivation, and an altered voltage dependence of steady-state activation and inactivation leading to an increased window current. All these gain-of-function effects predict neuronal hyperexcitability, which can explain the seizures.

The gating defects caused by the M252V mutation appeared only in the background of the neonatal splice variant but not for the adult one, which could be a mechanism for the resolution of seizures during development. However, the other two mutations showed defects in the adult splice variant as well, which were even somewhat more pronounced compared to those seen in the background of the neonatal splice forms. Therefore, the mechanism of seizure resolution must be more general. We assumed that the replacement of $Na_v1.2$ by $Na_v1.6$ at the AIS during development, which was shown by other collaborators in the lab during this thesis, is the key mechanism responsible for the spontaneous remission of BFNIS.

Finally, electrophysiological and immunocytochemical investigations in primary cultured rat cortical neurons and demonstrated various classes of cortical neuron established stable experimental system for further studies in cultured neurons in particular for the functional expression of ion channel mutations such as those studied here.

References

Alekov, A., M. M. Rahman*, et al.* A sodium channel mutation causing epilepsy in man exhibits subtle defects in fast inactivation and activation in vitro. J Physiol, v.529 Pt 3, Dec 15, p.533-9. 2000.

Alekov, A. K., M. M. Rahman*, et al.* Enhanced inactivation and acceleration of activation of the sodium channel associated with epilepsy in man. Eur J Neurosci, v.13, n.11, Jun, p.2171-6. 2001.

An, R. H., X. L. Wang*, et al.* Novel LQT-3 mutation affects Na+ channel activity through interactions between alpha- and beta1-subunits. Circ Res, v.83, n.2, Jul 27, p.141-6. 1998.

Auld, V. J., A. L. Goldin*, et al.* A neutral amino acid change in segment IIS4 dramatically alters the gating properties of the voltage-dependent sodium channel. Proc Natl Acad Sci U S A, v.87, n.1, Jan, p.323-7. 1990.

Balser, J. R., H. B. Nuss*, et al.* External pore residue mediates slow inactivation in mu 1 rat skeletal muscle sodium channels. J Physiol, v.494 (Pt 2), Jul 15, p.431-42. 1996.

Baroudi, G., E. Carbonneau*, et al. SCN5*A mutation (T1620M) causing Brugada syndrome exhibits different phenotypes when expressed in Xenopus oocytes and mammalian cells. FEBS Lett, v.467, n.1, Feb 4, p.12-6. 2000.

Baulac, S., I. Gourfinkel-An*, et al.* A second locus for familial generalized epilepsy with febrile seizures plus maps to chromosome 2q21-q33. Am J Hum Genet, v.65, n.4, Oct, p.1078-85. 1999.

Belcher, S. M., C. A. Zerillo*, et al.* Cloning of a sodium channel alpha subunit from rabbit Schwann cells. Proc Natl Acad Sci U S A, v.92, n.24, Nov 21, p.11034-8. 1995.

Bendahhou, S., T. R. Cummins*, et al.* Activation and inactivation of the voltage-gated sodium channel: role of segment S5 revealed by a novel hyperkalaemic periodic paralysis

mutation. J Neurosci, v.19, n.12, Jun 15, p.4762-71. 1999.

Bennett, P. B., Jr., N. Makita, *et al.* A molecular basis for gating mode transitions in human skeletal muscle Na+ channels. FEBS Lett, v.326, n.1-3, Jul 12, p.21-4. 1993.

Berkovic, S. F., S. E. Heron, *et al.* Benign familial neonatal-infantile seizures: characterization of a new sodium channelopathy. Ann Neurol, v.55, n.4, Apr, p.550-7. 2004.

Boiko, T., M. N. Rasband, *et al.* Compact myelin dictates the differential targeting of two sodium channel isoforms in the same axon. Neuron, v.30, n.1, Apr, p.91-104. 2001.

Caceres, J. F. e A. R. Kornblihtt. Alternative splicing: multiple control mechanisms and involvement in human disease. Trends Genet, v.18, n.4, Apr, p.186-93. 2002.

Caldwell, J. H., K. L. Schaller, *et al.* Sodium channel Na(v)1.6 is localized at nodes of ranvier, dendrites, and synapses. Proc Natl Acad Sci U S A, v.97, n.10, May 9, p.5616-20. 2000.

Caraballo, R., S. Pavek, *et al.* Linkage of benign familial infantile convulsions to chromosome 16p12-q12 suggests allelism to the infantile convulsions and choreoathetosis syndrome. Am J Hum Genet, v.68, n.3, Mar, p.788-94. 2001.

Catterall, W. A. Cellular and molecular biology of voltage-gated sodium channels. Physiol Rev, v.72, n.4 Suppl, Oct, p.S15-48. 1992.

Catterall, W. A. From ionic currents to molecular mechanisms: the structure and function of voltage-gated sodium channels. Neuron, v.26, n.1, Apr, p.13-25. 2000.

Cauli, B., E. Audinat, *et al.* Molecular and physiological diversity of cortical nonpyramidal cells. J Neurosci, v.17, n.10, May 15, p.3894-906. 1997.

Chahine, M., A. L. George, Jr., *et al.* Sodium channel mutations in paramyotonia congenita uncouple inactivation from activation. Neuron, v.12, n.2, Feb, p.281-94. 1994.

Chen, C. e S. C. Cannon. Modulation of Na+ channel inactivation by the beta 1 subunit: a deletion analysis. Pflugers Arch, v.431, n.2, Dec, p.186-95. 1995.

Chen, N. e M. T. Lucero. Transient and persistent tetrodotoxin-sensitive sodium currents in squid olfactory receptor neurons. J Comp Physiol [A], v.184, n.1, Jan, p.63-72. 1999.

Chen, C., V. Bharucha*, et al.* Reduced sodium channel density, altered voltage dependence of inactivation, and increased susceptibility to seizures in mice lacking sodium channel beta 2-subunits. Proc Natl Acad Sci U S A, v.99, n.26, Dec 24, p.17072-7. 2002.

Chen, Y. H., T. J. Dale*, et al.* Cloning, distribution and functional analysis of the type III sodium channel from human brain. Eur J Neurosci, v.12, n.12, Dec, p.4281-9. 2000.

Chevrie, J. J. e J. Aicardi. Convulsive disorders in the first year of life: neurological and mental outcome and mortality. Epilepsia, v.19, n.1, Feb, p.67-74. 1978.

Clancy, C. E. e R. S. Kass. Theoretical investigation of the neuronal Na+ channel *SCN*1A: abnormal gating and epilepsy. Biophys J, v.86, n.4, Apr, p.2606-14. 2004.

Connors, B. W. e M. J. Gutnick. Intrinsic firing patterns of diverse neocortical neurons. Trends Neurosci, v.13, n.3, Mar, p.99-104. 1990.

Cummins, T. R. e F. J. Sigworth. Impaired slow inactivation in mutant sodium channels. Biophys J, v.71, n.1, Jul, p.227-36. 1996.

Cummins, T. R., F. Aglieco*, et al.* Nav1.3 sodium channels: rapid repriming and slow closed-state inactivation display quantitative differences after expression in a mammalian cell line and in spinal sensory neurons. J Neurosci, v.21, n.16, Aug 15, p.5952-61. 2001.

Defelipe, J. Neocortical neuronal diversity: chemical heterogeneity revealed by colocalization studies of classic neurotransmitters, neuropeptides, calcium-binding proteins, and cell surface molecules. Cereb Cortex, v.3, n.4, Jul-Aug, p.273-89. 1993.

Defelipe, J. e I. Farinas. The pyramidal neuron of the cerebral cortex: morphological and chemical characteristics of the synaptic inputs. Prog Neurobiol, v.39, n.6, Dec, p.563-607. 1992.

Deschenes, I., E. Trottier, *et al.* Implication of the C-terminal region of the alpha-subunit of voltage-gated sodium channels in fast inactivation. J Membr Biol, v.183, n.2, Sep 15, p.103-14. 2001.

Dietrich, P. S., J. G. Mcgivern, *et al.* Functional analysis of a voltage-gated sodium channel and its splice variant from rat dorsal root ganglia. J Neurochem, v.70, n.6, Jun, p.2262-72. 1998.

Eaholtz, G., T. Scheuer, *et al.* Restoration of inactivation and block of open sodium channels by an inactivation gate peptide. Neuron, v.12, n.5, May, p.1041-8. 1994.

Ellerkmann, R. K., V. Riazanski, *et al.* Slow recovery from inactivation regulates the availability of voltage-dependent Na(+) channels in hippocampal granule cells, hilar neurons and basket cells. J Physiol, v.532, n.Pt 2, Apr 15, p.385-97. 2001.

Escayg, A., B. T. Macdonald, *et al.* Mutations of *SCN1A*, encoding a neuronal sodium channel, in two families with GEFS+2. Nat Genet, v.24, n.4, Apr, p.343-5. 2000.

Goldin, A. L., R. L. Barchi, *et al.* Nomenclature of voltage-gated sodium channels. Neuron, v.28, n.2, Nov, p.365-8. 2000.

Goldin, A. L. Mechanisms of sodium channel inactivation. Curr Opin Neurobiol, v.13, n.3, Jun, p.284-90. 2003.

Gong, B., K. J. Rhodes, *et al.* Type I and type II Na(+) channel alpha-subunit polypeptides exhibit distinct spatial and temporal patterning, and association with auxiliary subunits in rat brain. J Comp Neurol, v.412, n.2, Sep 20, p.342-52. 1999.

Green, W. N. e O. S. Andersen. Surface charges and ion channel function. Annu Rev Physiol, v.53, p.341-59. 1991.

Guipponi, M., F. Rivier*, et al.* Linkage mapping of benign familial infantile convulsions (BFIC) to chromosome 19q. Hum Mol Genet, v.6, n.3, Mar, p.473-7. 1997.

Gustafson, T. A., E. C. Clevinger*, et al.* Mutually exclusive exon splicing of type III brain sodium channel alpha subunit RNA generates developmentally regulated isoforms in rat brain. J Biol Chem, v.268, n.25, Sep 5, p.18648-53. 1993.

Guy, H. R. e F. Conti. Pursuing the structure and function of voltage-gated channels. Trends Neurosci, v.13, n.6, Jun, p.201-6. 1990.

Hayward, L. J., R. H. Brown, Jr.*, et al.* Slow inactivation differs among mutant Na channels associated with myotonia and periodic paralysis. Biophys J, v.72, n.3, Mar, p.1204-19. 1997.

Heinzen, E. L., W. Yoon*, et al.* Nova2 interacts with a cis-acting polymorphism to influence the proportions of drug-responsive splice variants of *SCN1A*. Am J Hum Genet, v.80, n.5, May, p.876-83. 2007.

Heron, S. E., K. M. Crossland*, et al.* Sodium-channel defects in benign familial neonatal-infantile seizures. Lancet, v.360, n.9336, Sep 14, p.851-2. 2002.

Hille, B. Ion Channels of Excitable Membranes.: Sunder land, MA: Sinauer Associates Inc. 2001

Huxley, A. H. A. A quantitative description of membrane current and its application to induction and excitation in nerve. J Physiol, v.117, p.500-544. 1952.

Isom, L. L., K. S. De Jongh*, et al.* Primary structure and functional expression of the beta 1 subunit of the rat brain sodium channel. Science, v.256, n.5058, May 8, p.839-42. 1992.

Isom, L. L., D. S. Ragsdale*, et al.* Structure and function of the beta 2 subunit of brain sodium channels, a transmembrane glycoprotein with a CAM motif. Cell, v.83, n.3, Nov 3, p.433-42. 1995.

Isom, L. L., T. Scheuer, *et al.* Functional co-expression of the beta 1 and type IIA alpha subunits of sodium channels in a mammalian cell line. J Biol Chem, v.270, n.7, Feb 17, p.3306-12. 1995.

Isom, L. L. Sodium channel beta subunits: anything but auxiliary. Neuroscientist, v.7, n.1, Feb, p.42-54. 2001.

Jordan, M., A. Schallhorn, *et al.* Transfecting mammalian cells: optimization of critical parameters affecting calcium-phosphate precipitate formation. Nucleic Acids Res, v.24, n.4, Feb 15, p.596-601. 1996.

Kamiya, K., M. Kaneda, *et al.* A nonsense mutation of the sodium channel gene *SCN2A* in a patient with intractable epilepsy and mental decline. J Neurosci, v.24, n.11, Mar 17, p.2690-8. 2004.

Kaplan, M. R., M. H. Cho, *et al.* Differential control of clustering of the sodium channels Na(v)1.2 and Na(v)1.6 at developing CNS nodes of Ranvier. Neuron, v.30, n.1, Apr, p.105-19. 2001.

Kasai, N., K. Fukushima, *et al.* Genomic structures of *SCN2A* and *SCN3A* - candidate genes for deafness at the DFNA16 locus. Gene, v.264, n.1, Feb 7, p.113-22. 2001.

Kearney, J. A., N. W. Plummer, *et al.* A gain-of-function mutation in the sodium channel gene *Scn2a* results in seizures and behavioral abnormalities. Neuroscience, v.102, n.2, p.307-17. 2001.

Lehmann-Horn, F. e K. Jurkat-Rott. Voltage-gated ion channels and hereditary disease. Physiol Rev, v.79, n.4, Oct, p.1317-72. 1999.

Lerche, H., K. Jurkat-Rott, *et al.* Ion channels and epilepsy. Am J Med Genet, v.106, n.2, Summer, p.146-59. 2001.

Lerche, H., N. Mitrovic, *et al.* Paramyotonia congenita: the R1448P Na+ channel mutation

in adult human skeletal muscle. Ann Neurol, v.39, n.5, May, p.599-608. 1996.

Lerche, H., W. Peter, *et al.* Role in fast inactivation of the IV/S4-S5 loop of the human muscle Na+ channel probed by cysteine mutagenesis. J Physiol, v.505 (Pt 2), Dec 1, p.345-52. 1997.

Lerche, H., Y. G. Weber, *et al.* Ion channel defects in idiopathic epilepsies. Curr Pharm Des, v.11, n.21, p.2737-52. 2005.

Lipscombe, D. Neuronal proteins custom designed by alternative splicing. Curr Opin Neurobiol, v.15, n.3, Jun, p.358-63. 2005.

Liu, Y., M. E. Jurman, *et al.* Dynamic rearrangement of the outer mouth of a K+ channel during gating. Neuron, v.16, n.4, Apr, p.859-67. 1996.

Lossin, C., D. W. Wang, *et al.* Molecular basis of an inherited epilepsy. Neuron, v.34, n.6, Jun 13, p.877-84. 2002.

Lu, C. M. e G. B. Brown. Isolation of a human-brain sodium-channel gene encoding two isoforms of the subtype III alpha-subunit. J Mol Neurosci, v.10, n.1, Feb, p.67-70. 1998.

Lund, J. S.. Spiny stellate neurons. In: Cerebral cortex, Vol.1: Cellular components of the cerebral cortex (Peters A, Jones EG, eds), New York: Plenum Press, p.255-308.1984.

Makita, N., P. B. Bennett, *et al.* Molecular determinants of beta 1 subunit-induced gating modulation in voltage-dependent Na+ channels. J Neurosci, v.16, n.22, Nov 15, p.7117-27. 1996.

Malhotra, J. D., K. Kazen-Gillespie, *et al.* Sodium channel beta subunits mediate homophilic cell adhesion and recruit ankyrin to points of cell-cell contact. J Biol Chem, v.275, n.15, Apr 14, p.11383-8. 2000.

Mantegazza, M., F. H. Yu, *et al.* Role of the C-terminal domain in inactivation of brain and cardiac sodium channels. Proc Natl Acad Sci U S A, v.98, n.26, Dec 18, p.15348-53. 2001.

Mantegazza, M., A. Gambardella*, et al.* Identification of an Nav1.1 sodium channel (*SCN1A*) loss-of-function mutation associated with familial simple febrile seizures. Proc Natl Acad Sci U S A, v.102, n.50, Dec 13, p.18177-82. 2005.

Martina, M., J. H. Schultz*, et al.* Functional and molecular differences between voltage-gated K+ channels of fast-spiking interneurons and pyramidal neurons of rat hippocampus. J Neurosci, v.18, n.20, Oct 15, p.8111-25. 1998.

Matsumoto, A., K. Watanabe*, et al.* Long-term prognosis of convulsive disorders in the first year of life: mental and physical development and seizure persistence. Epilepsia, v.24, n.3, Jun, p.321-9. 1983.

Mcclatchey, A. I., S. C. Cannon*, et al.* The cloning and expression of a sodium channel beta 1-subunit cDNA from human brain. Hum Mol Genet, v.2, n.6, Jun, p.745-9. 1993.

Mccormick, K. A., L. L. Isom*, et al.* Molecular determinants of Na+ channel function in the extracellular domain of the beta1 subunit. J Biol Chem, v.273, n.7, Feb 13, p.3954-62. 1998.

Mccormick, K. A., J. Srinivasan*, et al.* The extracellular domain of the beta1 subunit is both necessary and sufficient for beta1-like modulation of sodium channel gating. J Biol Chem, v.274, n.46, Nov 12, p.32638-46. 1999.

Meadows, L., J. D. Malhotra*, et al.* The intracellular segment of the sodium channel beta 1 subunit is required for its efficient association with the channel alpha subunit. J Neurochem, v.76, n.6, Mar, p.1871-8. 2001.

Messner, D. J. e W. A. Catterall. The sodium channel from rat brain. Separation and characterization of subunits. J Biol Chem, v.260, n.19, Sep 5, p.10597-604. 1985.

Mickus, T., H. Jung*, et al.* Properties of slow, cumulative sodium channel inactivation in rat hippocampal CA1 pyramidal neurons. Biophys J, v.76, n.2, Feb, p.846-60. 1999.

Mickus, T., H. Y. Jung*, et al.* Slow sodium channel inactivation in CA1 pyramidal cells. Ann N Y Acad Sci, v.868, Apr 30, p.97-101. 1999.

Mitrovic, N., H. Lerche*, et al.* Role in fast inactivation of conserved amino acids in the IV/S4-S5 loop of the human muscle Na+ channel. Neurosci Lett, v.214, n.1, Aug 16, p.9-12. 1996.

Mitrovic, N., A. L. George, Jr.*, et al.* Mutant channels contribute <50% to Na+ current in paramyotonia congenita muscle. Brain, v.122 (Pt 6), Jun, p.1085-92. 1999.

Mitrovic, N., A. L. George, Jr.*, et al.* Role of domain 4 in sodium channel slow inactivation. J Gen Physiol, v.115, n.6, Jun, p.707-18. 2000.

Moulard, B., M. Guipponi*, et al.* Identification of a new locus for generalized epilepsy with febrile seizures plus (GEFS+) on chromosome 2q24-q33. Am J Hum Genet, v.65, n.5, Nov, p.1396-400. 1999.

Ogiwara, I., H. Miyamoto*, et al.* Na(v)1.1 localizes to axons of parvalbumin-positive inhibitory interneurons: a circuit basis for epileptic seizures in mice carrying an *Scn1a* gene mutation. J Neurosci, v.27, n.22, May 30, p.5903-14. 2007.

Oh, Y. e S. G. Waxman. Novel splice variants of the voltage-sensitive sodium channel alpha subunit. Neuroreport, v.9, n.7, May 11, p.1267-72. 1998.

Ong, B. H., G. F. Tomaselli*, et al.* A structural rearrangement in the sodium channel pore linked to slow inactivation and use dependence. J Gen Physiol, v.116, n.5, Nov, p.653-62. 2000.

O'reilly, J. P., S. Y. Wang*, et al.* Residue-specific effects on slow inactivation at V787 in D2-S6 of Na(v)1.4 sodium channels. Biophys J, v.81, n.4, Oct, p.2100-11. 2001.

Patton, D. E., J. W. West*, et al.* Amino acid residues required for fast Na(+)-channel inactivation: charge neutralizations and deletions in the III-IV linker. Proc Natl Acad Sci U S A, v.89, n.22, Nov 15, p.10905-9. 1992.

Patton, D. E., L. L. Isom*, et al.* The adult rat brain beta 1 subunit modifies activation and inactivation gating of multiple sodium channel alpha subunits. J Biol Chem, v.269, n.26, Jul 1, p.17649-55. 1994.

Plummer, N. W., M. W. Mcburney*, et al.* Alternative splicing of the sodium channel *SCN8A* predicts a truncated two-domain protein in fetal brain and non-neuronal cells. J Biol Chem, v.272, n.38, Sep 19, p.24008-15. 1997.

Plummer, N. W. e M. H. Meisler. Evolution and diversity of mammalian sodium channel genes. Genomics, v.57, n.2, Apr 15, p.323-31. 1999.

Popa, M. O., A. K. Alekov*, et al.* Cooperative effect of S4-S5 loops in domains D3 and D4 on fast inactivation of the Na+ channel. J Physiol, v.561, n.Pt 1, Nov 15, p.39-51. 2004.

Qu, Y., L. L. Isom*, et al.* Modulation of cardiac Na+ channel expression in Xenopus oocytes by beta 1 subunits. J Biol Chem, v.270, n.43, Oct 27, p.25696-701. 1995.

Qu, Y., J. C. Rogers*, et al.* Functional roles of the extracellular segments of the sodium channel alpha subunit in voltage-dependent gating and modulation by beta1 subunits. J Biol Chem, v.274, n.46, Nov 12, p.32647-54. 1999.

Qu, Y., R. Curtis*, et al.* Differential modulation of sodium channel gating and persistent sodium currents by the beta1, beta2, and beta3 subunits. Mol Cell Neurosci, v.18, n.5, Nov, p.570-80. 2001.

Ratcliffe, C. F., R. E. Westenbroek*, et al.* Sodium channel beta1 and beta3 subunits associate with neurofascin through their extracellular immunoglobulin-like domain. J Cell Biol, v.154, n.2, Jul 23, p.427-34. 2001.

Raymond, C. K., J. Castle*, et al.* Expression of alternatively spliced sodium channel alpha-subunit genes. Unique splicing patterns are observed in dorsal root ganglia. J Biol Chem, v.279, n.44, Oct 29, p.46234-41. 2004.

Rhodes, T. H., C. G. Vanoye*, et al.* Sodium channel dysfunction in intractable childhood

epilepsy with generalized tonic-clonic seizures. J Physiol, v.569, n.Pt 2, Dec 1, p.433-45. 2005.

Rohl, C. A., F. A. Boeckman*, et al.* Solution structure of the sodium channel inactivation gate. Biochemistry, v.38, n.3, Jan 19, p.855-61. 1999.

Sarao, R., S. K. Gupta*, et al.* Developmentally regulated alternative RNA splicing of rat brain sodium channel mRNAs. Nucleic Acids Res, v.19, n.20, Oct 25, p.5673-9. 1991.

Scalmani, P., R. Rusconi*, et al.* Effects in neocortical neurons of mutations of the Na(v)1.2 Na+ channel causing benign familial neonatal-infantile seizures. J Neurosci, v.26, n.40, Oct 4, p.10100-9. 2006.

Schaller, K. L., D. M. Krzemien*, et al.* Alternatively spliced sodium channel transcripts in brain and muscle. J Neurosci, v.12, n.4, Apr, p.1370-81. 1992.

Scheffer, I. E. e S. F. Berkovic. Generalized epilepsy with febrile seizures plus. A genetic disorder with heterogeneous clinical phenotypes. Brain, v.120 (Pt 3), Mar, p.479-90. 1997.

Scheuer, T., V. J. Auld*, et al.* Functional properties of rat brain sodium channels expressed in a somatic cell line. Science, v.247, n.4944, Feb 16, p.854-8. 1990.

Singh, R., I. E. Scheffer*, et al.* Generalized epilepsy with febrile seizures plus: a common childhood-onset genetic epilepsy syndrome. Ann Neurol, v.45, n.1, Jan, p.75-81. 1999.

Spampanato, J., A. Escayg*, et al.* Functional effects of two voltage-gated sodium channel mutations that cause generalized epilepsy with febrile seizures plus type 2. J Neurosci, v.21, n.19, Oct 1, p.7481-90. 2001.

Srinivasan, J., M. Schachner*, et al.* Interaction of voltage-gated sodium channels with the extracellular matrix molecules tenascin-C and tenascin-R. Proc Natl Acad Sci U S A, v.95, n.26, Dec 22, p.15753-7. 1998.

Spampanato, J., J. A. Kearney*, et al.* A novel epilepsy mutation in the sodium channel

SCN1A identifies a cytoplasmic domain for beta subunit interaction. J Neurosci, v.24, n.44, Nov 3, p.10022-34. 2004.

Struyk, A. F. e S. C. Cannon. Slow inactivation does not block the aqueous accessibility to the outer pore of voltage-gated Na channels. J Gen Physiol, v.120, n.4, Oct, p.509-16. 2002.

Sugawara, T., Y. Tsurubuchi*, et al.* A missense mutation of the Na+ channel alpha II subunit gene Na(v)1.2 in a patient with febrile and afebrile seizures causes channel dysfunction. Proc Natl Acad Sci U S A, v.98, n.11, May 22, p.6384-9. 2001.

Toledo-Rodriguez, M., B. Blumenfeld*, et al.* Correlation maps allow neuronal electrical properties to be predicted from single-cell gene expression profiles in rat neocortex. Cereb Cortex, v.14, n.12, Dec, p.1310-27. 2004.

Ukomadu, C., J. Zhou*, et al.* muI Na+ channels expressed transiently in human embryonic kidney cells: biochemical and biophysical properties. Neuron, v.8, n.4, Apr, p.663-76. 1992.

Ulbricht, W. Sodium channel inactivation: molecular determinants and modulation. Physiol Rev, v.85, n.4, Oct, p.1271-301. 2005.

Vanoye, C. G., C. Lossin*, et al.* Single-channel properties of human NaV1.1 and mechanism of channel dysfunction in *SCN1A*-associated epilepsy. J Gen Physiol, v.127, n.1, Jan, p.1-14. 2006.

Vassilev, P. M., T. Scheuer*, et al.* Identification of an intracellular peptide segment involved in sodium channel inactivation. Science, v.241, n.4873, Sep 23, p.1658-61. 1988.

Vassilev, P., T. Scheuer*, et al.* Inhibition of inactivation of single sodium channels by a site-directed antibody. Proc Natl Acad Sci U S A, v.86, n.20, Oct, p.8147-51. 1989.

Vervaeke, K., H. Hu*, et al.* Contrasting effects of the persistent Na+ current on neuronal excitability and spike timing. Neuron, v.49, n.2, Jan 19, p.257-70. 2006.

Vilin, Y. Y., E. Fujimoto, *et al.* A single residue differentiates between human cardiac and skeletal muscle Na+ channel slow inactivation. Biophys J, v.80, n.5, May, p.2221-30. 2001.

Wallace, R. H., D. W. Wang, *et al.* Febrile seizures and generalized epilepsy associated with a mutation in the Na+-channel beta1 subunit gene *SCN1B*. Nat Genet, v.19, n.4, Aug, p.366-70. 1998.

West, J. W., T. Scheuer, *et al.* Efficient expression of rat brain type IIA Na+ channel alpha subunits in a somatic cell line. Neuron, v.8, n.1, Jan, p.59-70. 1992.

Westenbroek, R. E., D. K. Merrick, *et al.* Differential subcellular localization of the RI and RII Na+ channel subtypes in central neurons. Neuron, v.3, n.6, Dec, p.695-704. 1989.

Whitaker, W. R., J. J. Clare, *et al.* Distribution of voltage-gated sodium channel alpha-subunit and beta-subunit mRNAs in human hippocampal formation, cortex, and cerebellum. J Comp Neurol, v.422, n.1, Jun 19, p.123-39. 2000.

Wollner, D. A., D. J. Messner, *et al.* Beta 2 subunits of sodium channels from vertebrate brain. Studies with subunit-specific antibodies. J Biol Chem, v.262, n.30, Oct 25, p.14709-15. 1987.

Xu, R., E. A. Thomas, *et al.* A childhood epilepsy mutation reveals a role for developmentally regulated splicing of a sodium channel. Mol Cell Neurosci, v.35, n.2, Jun, p.292-301. 2007.

Yu, F. H. e W. A. Catterall. Overview of the voltage-gated sodium channel family. Genome Biol, v.4, n.3, p.207. 2003.

Zhou, W. e A. L. Goldin. Use-dependent potentiation of the Nav1.6 sodium channel. Biophys J, v.87, n.6, Dec, p.3862-72. 2004.

Zimmer, T., C. Bollensdorff, *et al.* Mouse heart Na+ channels: primary structure and function of two isoforms and alternatively spliced variants. Am J Physiol Heart Circ Physiol, v.282, n.3, Mar, p.H1007-17. 2002.

Acknowledgment

This is a great opportunity to express my deepest respect and gratitude to Prof. Dr. Holger Lerche who undertook to act as my supervisor despite his many other academic and professional commitments. His wisdom, knowledge and commitment to the highest standards inspired and motivated me. His patience and understanding encouraged me during the experimental and writing work. My thanks go out to Prof. Dr. Frank Lehmann-Horn, Prof. Dr. A. C. Ludolph, Dr. Oana M. Popa, Sigrid Bail, and Astrid Bellan-Koch, who have given me support, assistance and help from various sides.

I deeply appreciate the great encouragement and bless from my dear parents, family, friends and lab colleagues in China and Germany. Thanks to the set-up I have worked with in the narrow measurement room for days and evenings.

我的每一步都和父母及家人对我的理解和支持紧紧关联，没有他们就没有我的今天。谨此向他们表达我最诚挚的感谢。

Ulm, July 2009 Yunxiang Liao